Advances in mean-field dynamo theory and applications to astrophysical turbulence

Axel Brandenburg[1,2]†

[1]Laboratory for Atmospheric and Space Physics, JILA, and Department of Astrophysical and Planetary Sciences, University of Colorado, Boulder, CO 80303, USA
[2]Nordita, KTH Royal Institute of Technology and Stockholm University, and Department of Astronomy, Stockholm University, SE-10691 Stockholm, Sweden

(Received 1 June 2018, Revision: 1.82)

Recent advances in mean-field theory are reviewed and applications to the Sun, late-type stars, accretion disks, galaxies, and the early Universe are discussed. We focus particularly on aspects of spatio-temporal nonlocality, which provided some of the main new qualitative and quantitative insights that emerged from applying the test-field method to magnetic fields of different length and timescales. We also review the status of nonlinear quenching and the relation to magnetic helicity, which is an important observational diagnostic of modern solar dynamo theory. Both solar and some stellar dynamos seem to operate in an intermediate regime that has not yet been possible to model successfully. This regime is bracketed by antisolar-like differential rotation on one end and stellar activity cycles belonging to the superactive stars on the other. The difficulty in modeling this regime may be related to shortcomings in modelling solar/stellar convection. On galactic and extragalactic length scales, the observational constraints on dynamo theory are still less stringent and more uncertain, but recent advances both in theory and observations suggest that more conclusive comparisons may soon be possible also here. The possibility of inversely cascading magnetic helicity in the early Universe is particularly exciting in explaining the lower limits of magnetic fields on cosmological length scales. This may also imply parity breaking and the presence of finite magnetic helicity of such a field throughout the entire Universe.

1. Introduction

Hydromagnetic mean-field theory has been instrumental in providing an early understanding of the oscillatory magnetic field of the Sun with its 11 year sunspot cycle and the non-oscillatory magnetic field of the Earth. This was shown by Steenbeck & Krause (1969a,b) through their numerical investigations of dynamos in spherical geometry. These were based on analytical calculations of the α effect and turbulent magnetic diffusivity a few years earlier (Steenbeck et al. 1966). Now, 50 years later, dynamo theory continues to be an important tool in many fields of astrophysics and geophysics. Mean-field theory is also an indispensable tool in predicting the outcomes of laboratory dynamos (Rädler, et al. 2002a,b,c; Forest et al. 2002; Cooper et al. 2014; Forest 2015). Even now, in the era of large-scale numerical simulations, mean-field theory provides an important reference to compare against, and to provide a framework for understanding what happens in the simulations; see, for example, section 3.4 of Rempel & Cheung (2014) for attempts in that direction. Moreover, numerical simulations have been used to calculate mean-field transport coefficients such as the α effect and turbulent magnetic diffusivity without

† Email address for correspondence: brandenb@nordita.org

facing the restrictions that analytically feasible approximations are subjected to. This has been possible with the development of the test-field method (Schrinner et al. 2005, 2007); for a review of this method, see Brandenburg et al. (2010). Unfortunately, in spite of significant progress in both numerical and analytical approaches, there is arguably still no satisfactory model of the solar dynamo. The equatorward migration of toroidal magnetic flux belts is not conclusively understood (Solanki *et al.* 2006; Miesch & Toomre 2009; Charbonneau 2010), and the spoke-like contours of constant angular velocity, as found through helioseismology (Schou et al. 1998), are not well reproduced in simulations. While simulations have been important in predicting antisolar-like differential rotation in slowly rotating stars and nonaxisymmetric global magnetic fields in rapidly rotating stars (Gastine et al. 2014; Käpylä et al. 2014; Karak et al. 2015), the parameters of the transitions from solar-like to antisolar-like differential rotation and from nonaxisymmetric to axisymmetric large-scale fields as stars spin down, are not yet well reproduced in simulations; see Table 5 of Viviani et al. (2018). The list continues toward larger length scales, from accretion disks to galactic disks, and even to scales encompassing the entire Universe, but the observational uncertainties increase in those cases, so the true extent of agreement between theory and observations is not as obvious as in the solar and stellar cases.

In this paper, we review the basic deficiencies encountered in modeling the Sun. We also highlight some outstanding questions in the applications of mean-field theory to stars with outer convection zones, to accretion disks and galaxies, and to the possibility of an inverse cascade of hydromagnetic turbulence in the early Universe. We begin by gathering some of the many building blocks of the theory. Many interesting aspects have emerged over the last 50 years—much of it became possible through a close interplay between simulations and analytic approaches. There is by now a rich repertoire of effects, and it is still not entirely clear which of them might play a role in the various applications mentioned above.

2. Building blocks used in modern mean-field theory

Mean-field theory can be applied to all the basic equations of magnetohydrodynamics: the induction equation, the momentum equation, as well as energy, continuity, and passive scalar equations. The induction equation is traditionally the best studied one, where the perhaps most remarkable effects have been discovered.

2.1. *Mean-field induction equation*

In plasmas and other electrically conducting fluids such as liquid metals, the Faraday displacement current can be omitted compared with the current density, so the Maxwell equations together with Ohm's law reduce to the induction equation in the form

$$\frac{\partial \boldsymbol{B}}{\partial t} = \boldsymbol{\nabla} \times (\boldsymbol{U} \times \boldsymbol{B} - \eta \mu_0 \boldsymbol{J}) \tag{2.1}$$

together with

$$\boldsymbol{\nabla} \times \boldsymbol{B} = \mu_0 \boldsymbol{J} \quad \text{and} \quad \boldsymbol{\nabla} \cdot \boldsymbol{B} = 0, \tag{2.2}$$

where $\boldsymbol{B}$ is the magnetic field, $\boldsymbol{U}$ is the fluid velocity, η is the magnetic diffusivity, μ_0 is the vacuum permeability, and $\boldsymbol{J}$ is the current density. At the heart of mean-field theory is a prescription for averaging, denoted by an overbar. We then decompose $\boldsymbol{U}$ and $\boldsymbol{B}$ into mean and fluctuating parts, i.e.,

$$\boldsymbol{U} = \overline{\boldsymbol{U}} + \boldsymbol{u}, \quad \boldsymbol{B} = \overline{\boldsymbol{B}} + \boldsymbol{b}. \tag{2.3}$$

We choose an averaging procedure which obeys the Reynolds rules, which state that for any two variables $F=\overline{F}+f$ and $G=\overline{G}+g$, we have (Krause & Rädler 1980)

$$\overline{\overline{F}}=\overline{F},\quad \overline{f}=0,\quad \overline{F+G}=\overline{F}+\overline{G},\quad \overline{\overline{F}\,\overline{G}}=\overline{F}\,\overline{G},\quad \overline{\overline{G}f}=\overline{G}. \tag{2.4}$$

These rules imply that

$$\overline{\boldsymbol{U}\times\boldsymbol{B}}=\overline{\boldsymbol{U}}\times\overline{\boldsymbol{B}}+\overline{\boldsymbol{u}\times\boldsymbol{b}} \tag{2.5}$$

and

$$(\boldsymbol{U}\times\boldsymbol{B})'=\overline{\boldsymbol{U}}\times\boldsymbol{b}+\boldsymbol{u}\times\overline{\boldsymbol{B}}+\boldsymbol{u}\times\boldsymbol{b}-\overline{\boldsymbol{u}\times\boldsymbol{b}}, \tag{2.6}$$

where the prime denotes the fluctuating part.† The mean-field induction equation is thus given by

$$\frac{\partial\overline{\boldsymbol{B}}}{\partial t}=\boldsymbol{\nabla}\times\left(\overline{\boldsymbol{U}}\times\overline{\boldsymbol{B}}+\overline{\boldsymbol{u}\times\boldsymbol{b}}-\eta\mu_0\overline{\boldsymbol{J}}\right) \tag{2.7}$$

together with $\boldsymbol{\nabla}\times\overline{\boldsymbol{B}}=\mu_0\overline{\boldsymbol{J}}$ and $\boldsymbol{\nabla}\cdot\overline{\boldsymbol{B}}=0$.

The next important step here is the calculation of the mean electromotive force $\overline{\boldsymbol{\mathcal{E}}}=\overline{\boldsymbol{u}\times\boldsymbol{b}}$. One often makes the assumption of an instantaneous and local response in terms of $\overline{\boldsymbol{B}}$ of the from (Krause & Rädler 1980)

$$\overline{\mathcal{E}}_i=\overline{\mathcal{E}}_i^{(0)}+\alpha_{ij}\overline{B}_j+\eta_{ijk}\overline{B}_{j,k}\qquad\text{(local \& instantaneous)}, \tag{2.8}$$

where the comma in $\overline{B}_{j,k}$ denotes partial differentiation and $\overline{\boldsymbol{\mathcal{E}}}^{(0)}$ is a nonvanishing contribution to the mean electromotive force for $\overline{\boldsymbol{B}}=\boldsymbol{0}$; see Brandenburg & Rädler (2013) for examples of terms proportional to the local angular velocity and the cross helicity $\overline{\boldsymbol{u}\cdot\boldsymbol{b}}$, which is also known as the Yoshizawa effect (Yokoi & Yoshizawa 1993; Yokoi 2013). Since the Yoshizawa effect leads to a growth even without a formal large-scale seed magnetic field, it is sometimes referred to as a turbulent battery effect (Brandenburg & Urpin 1998). It is generally caused by the presence of cross helicity, which can be generated when a mean magnetic field is aligned with the direction of gravity (Rüdiger et al. 2011). Originally, Yokoi & Yoshizawa (1993) discussed applications primarily to accretion and galactic disks, but in recent year, applications have also been discussed to solar and stellar dynamos (Pipin et al. 2011; Yokoi et al. 2016).

Let us now return to the other two terms in equation (2.8). To find expressions for α_{ij} and ϵ_{ijk}, one has to compute $\overline{\boldsymbol{\mathcal{E}}}=\overline{\boldsymbol{u}\times\boldsymbol{b}}$. We postpone the discussion of the evolution of $\boldsymbol{u}$ until § 2.4 and consider here only the evolution equation for $\boldsymbol{b}$, which is obtained by subtracting equation (2.7) from equation (2.1) and using equation (2.6). This yields

$$\frac{\partial\boldsymbol{b}}{\partial t}=\boldsymbol{\nabla}\times\left(\overline{\boldsymbol{U}}\times\boldsymbol{b}+\boldsymbol{u}\times\overline{\boldsymbol{B}}+\boldsymbol{u}\times\boldsymbol{b}-\overline{\boldsymbol{u}\times\boldsymbol{b}}-\eta\mu_0\boldsymbol{j}\right). \tag{2.9}$$

The term $\boldsymbol{u}\times\boldsymbol{b}-\overline{\boldsymbol{u}\times\boldsymbol{b}}$ is nonlinear in the fluctuations. It is important in all cases of practical interest, such as turbulent and steady flows at large magnetic Reynolds numbers (low magnetic diffusivity) and will be discussed further in § 2.4. In the second-order correlation approximation (SOCA), however, one neglects this term, which is permissible not only when η is large (small magnetic Reynolds number), but also when the correlation time is short. In those cases, the nonlinear term is overpowered either by the diffusion term, $\boldsymbol{\nabla}\times(-\eta\mu_0\boldsymbol{j})=\eta\nabla^2\boldsymbol{b}$ (for $\eta=$ const) on the right-hand side, or by the $\partial\boldsymbol{b}/\partial t$ term on the left-hand side of equation (2.9). Neglecting now also the effects of a mean flow

† In the following, we continue using the lowercase symbols $\boldsymbol{u}$ and $\boldsymbol{b}$ instead of $\boldsymbol{U}'$ and $\boldsymbol{B}'$ to denote fluctuations of $\boldsymbol{U}$ and $\boldsymbol{B}$.

($\overline{\boldsymbol{U}}=\boldsymbol{0}$) and assuming incompressibility ($\boldsymbol{\nabla}\cdot\boldsymbol{u}=0$), SOCA yields

$$\left(\frac{\partial}{\partial t}-\eta\nabla^2\right)\boldsymbol{b}=\overline{\boldsymbol{B}}\cdot\boldsymbol{\nabla}\boldsymbol{u}-\boldsymbol{u}\cdot\boldsymbol{\nabla}\overline{\boldsymbol{B}}. \tag{2.10}$$

This equation can be solved using the Green's function for the heat equation which, in Fourier space, is given by $(-\mathrm{i}\omega+\eta k^2)^{-1}$. When applied to calculating $\overline{\boldsymbol{\mathcal{E}}}$, this corresponds in the end to a multiplication by a correlation time τ (see details in Moffatt 1970, 1978; Krause & Rädler 1980). Thus, we have

$$\overline{\mathcal{E}}_i=\tau\epsilon_{ijk}\left(\overline{u_j u_{k,l}}\,\overline{B}_l-\overline{u_j u_l}\,\overline{B}_{k,l}\right)\equiv\alpha_{il}\overline{B}_l+\eta_{ikl}\overline{B}_{k,l}. \tag{2.11}$$

where $\alpha_{il}=\tau\epsilon_{ijk}\overline{u_j u_{k,l}}$ is the α tensor and $\eta_{ikl}=\tau\overline{u_j u_l}$ has a part that contributes to turbulent magnetic diffusion.

To give an explicit example, let us first discuss the isotropic idealization. In that case, α_{il} and η_{ikl} must be isotropic tensors. The only isotropic tensors of ranks two and three are δ_{il} and ϵ_{ikl}, respectively. Thus, we write $\alpha_{ij}=\alpha\delta_{ij}$ and $\eta_{ijk}=\eta_{\rm t}\epsilon_{ijk}$, where α is a pseudoscalar and $\eta_{\rm t}$ is the turbulent magnetic diffusivity. For sufficiently large magnetic Reynolds numbers (low magnetic diffusivity) the two are given approximately by what we call their reference values α_0 and $\eta_{\rm t0}$, defined through

$$\alpha_0\equiv-\tfrac{1}{3}\tau\overline{\boldsymbol{\omega}\cdot\boldsymbol{u}},\qquad\eta_{\rm t0}\equiv\tfrac{1}{3}\tau\overline{\boldsymbol{u}^2}, \tag{2.12}$$

where $\tau\approx(u_{\rm rms}k_{\rm f})^{-1}$ is the turbulent turnover time, $u_{\rm rms}=(\overline{\boldsymbol{u}^2})^{1/2}$ is the rms velocity of the fluctuations, $k_{\rm f}$ is the wavenumber of the energy-carrying eddies, and $\boldsymbol{\omega}=\boldsymbol{\nabla}\times\boldsymbol{u}$ is the fluctuating vorticity. Since $\epsilon_{ijk}\partial_k\overline{B}_j=-(\boldsymbol{\nabla}\times\overline{\boldsymbol{B}})_i$, i.e., with a minus sign, the mean electromotive force is given by $\overline{\boldsymbol{\mathcal{E}}}=\overline{\boldsymbol{\mathcal{E}}}^{(0)}+\alpha\overline{\boldsymbol{B}}-\eta_{\rm t}\mu_0\overline{\boldsymbol{J}}$. The approximations used to obtain $\alpha\approx\alpha_0$ and $\eta_{\rm t}\approx\eta_{\rm t0}$ only hold for magnetic Reynolds numbers, $R_{\rm m}=u_{\rm rms}/\eta k_{\rm f}$, that are larger then unity. For smaller $R_{\rm m}$, α and $\eta_{\rm t}$ increases linearly with $R_{\rm m}$. It must also be emphasized that Sur et al. (2008) found equation (2.12) to be valid for turbulent flows where τ is not small.

In practice, astrophysical turbulence is always driven by some kind of instability. Highly supercritical Rayleigh-Benárd convection is an example where the turbulence is inhomogeneous and therefore also anisotropic. The Bell instability (Bell 2004) is driven by a cosmic-ray current, producing anisotropic turbulence. In these cases, the anisotropy of the turbulence is characterized by one preferred direction, $\hat{\boldsymbol{e}}$. This can be used to simplify the complexity of $\overline{\boldsymbol{\mathcal{E}}}$ to

$$\overline{\boldsymbol{\mathcal{E}}}_\perp=\alpha_\perp\overline{\boldsymbol{B}}_\perp-\eta_\perp\mu_0\overline{\boldsymbol{J}}_\perp-\kappa_\perp\overline{\boldsymbol{K}}_\perp+\gamma\hat{\boldsymbol{e}}\times\overline{\boldsymbol{B}}_\perp-\delta\hat{\boldsymbol{e}}\times\mu_0\overline{\boldsymbol{J}}_\perp-\mu\hat{\boldsymbol{e}}\times\overline{\boldsymbol{K}}_\perp, \tag{2.13}$$

$$\overline{\boldsymbol{\mathcal{E}}}_\parallel=\alpha_\parallel\overline{\boldsymbol{B}}_\parallel-\eta_\parallel\mu_0\overline{\boldsymbol{J}}_\parallel-\kappa_\parallel\overline{\boldsymbol{K}}_\parallel, \tag{2.14}$$

with only nine coefficients instead of $9+27=36$ for the full rank two and rank three tensors. Here, $\overline{K}_i=\frac{1}{2}(\overline{B}_{i,j}+\overline{B}_{j,i})\hat{e}_j$ is a vector characterizing the symmetric part of $\overline{B}_{i,j}$, while $\overline{J}_i=-\frac{1}{2}\epsilon_{ijk}\overline{B}_{j,k}$ characterizes its antisymmetric part. Brandenburg et al. (2012b) have determined all these coefficients for their forced turbulence simulations using rotation, stratification, or both as preferred directions of their otherwise isotropically forced turbulence.

Instead of repeating what has been discussed and reviewed extensively in the literature (Moffatt 1978; Parker 1979; Krause & Rädler 1980; Zeldovich *et al.* 1983; Roberts & Soward 1992; Brandenburg & Subramanian 2005a), we first focus on aspects that may turn out to be rather important, namely nonlocality in space and time. Both are long known to exist (Rädler 1976), but only recently has their importance become apparent. This may be important in solving some of the long-standing problems in astrophysical

magnetism. Next, we discuss the status of α quenching and the relation to magnetic helicity fluxes, which is an important diagnostics in solar physics (Kleeorin et al. 2002, 2003).

2.2. *Nonlocality: when scale separation becomes poor*

One often makes the assumption of a separation of scales between the scale of large-scale magnetic fields and the scale of the energy-carrying eddies or fields, which are referred to as small-scale fields. In real applications, this can often not be justified very well. Think, for example, of the convective downflows extending over a major part of the convection zone, or of the possibility of giant cell convection (Miesch et al. 2008). When scale separation does indeed become poor, one cannot adopt the local and instantaneous connection used in equation (2.8), but one has to resort to the integral kernel formulation, as was explained by Rädler (1976),

$$\overline{\mathcal{E}}_i(\boldsymbol{x},t)=\overline{\mathcal{E}}_i^{(0)}+\iint\mathcal{K}_{ij}(\boldsymbol{x},\boldsymbol{x}',t,t')\,\overline{B}_j(\boldsymbol{x}',t')\,\mathrm{d}^3\boldsymbol{x}'\,\mathrm{d}t'. \tag{2.15}$$

It is convenient to retain a formulation similar to that of equation (2.8), and write

$$\overline{\mathcal{E}}_i=\overline{\mathcal{E}}_i^{(0)}+\hat{\alpha}_{ij}\circ\overline{B}_j+\hat{\eta}_{ijk}\circ\overline{B}_{j,k}\qquad\text{(nonlocal with memory)}, \tag{2.16}$$

where the symbol $\circ$ denotes a convolution and $\hat{\alpha}_{ij}$ and $\hat{\eta}_{ijk}$ are integral kernels. This all sounds troublesome, because a convolution over time requires keeping the full history of $\overline{B}_j(\boldsymbol{x}',t')$ over all past times t' at all positions $\boldsymbol{x}'$. However, there is actually a simple *approximation* which captures the *essential* effects of nonlocality in space and time. This will be explained below.

As will become clear in the next section. the importance of spatial nonlocality lies in the fact that it prevents the unphysical occurrence of small-scale structures in a mean-field dynamo. Nonlocality in time is also important, because it can lead to *new* dynamo effects of their own, as will also be explained in a moment.

Let us now discuss the term $\overline{\boldsymbol{\mathcal{E}}}^{(0)}$, whose relation to nonlocality has not previously been emphasized. Brandenburg & Rädler (2013) discussed contributions to $\overline{\mathcal{E}}_i^{(0)}$ of the form $c_\Omega\Omega_i$, where $\boldsymbol{\Omega}$ is the angular velocity and c_Ω is a dynamo coefficient proportional to the cross helicity, $\overline{\boldsymbol{u}\cdot\boldsymbol{b}}$. A similar contribution is of the form $c_\omega\omega_i$, where $\boldsymbol{\omega}$ is the local vorticity. If written in this form, it becomes plausible that this term generalizes to $c_\Omega\circ\Omega_i$ or $c_\omega\circ\omega_i$, and that it is thus no exception to the treatment as a convolution.

2.3. *A practical tool for capturing the essence of nonlocality*

A decisive step in arriving at an approximate expression for the nonlocality in space and time was the development of the test-field method for calculating turbulent transport coefficients (Schrinner et al. 2005, 2007). This is a method for calculating α effect, turbulent diffusivity, and other turbulent transport coefficients for arbitrary mean magnetic fields. It turned out that test fields of high spatial wavenumber k tend to result in transport coefficients that are decreased approximately like a Lorentzian proportional to $1/(1+k^2/k_\mathrm{f}^2)$; see Brandenburg et al. (2008c). Likewise, it was found that rapid variations in time proportional to $e^{-\mathrm{i}\omega t}$ with frequency ω lead to a reduced and modified response along with a frequency-dependent delay; see Hubbard & Brandenburg (2009). In frequency space, the corresponding response kernel was found to be of the form $1/(1-\mathrm{i}\omega\tau)$, where τ is a typical response or correlation time, namely the $\tau\approx(u_\mathrm{rms}k_\mathrm{f})^{-1}$ stated above. Thus, no new unknown physical parameters enter and everything is in principle known.

We recall that a convolution in space and time, as expressed by equations (2.15)

and (2.16), corresponds to a multiplication in wavenumber and frequency space. Furthermore, the combined k and ω dependence of our kernels was found to be proportional to $1/(1-\mathrm{i}\omega\tau+k^2/k_\mathrm{f}^2)$. This was verified empirically with the test-field method (Rheinhardt & Brandenburg 2012). Thus, we have

$$\left(1-\mathrm{i}\omega\tau+k^2/k_\mathrm{f}^2\right)\overline{\mathcal{E}}_i=\overline{\mathcal{E}}_i^{(0)}+\tilde{\alpha}_{ij}\overline{B}_j+\tilde{\eta}_{ijk}\overline{B}_{j,k}. \tag{2.17}$$

This can easily be expressed in real space as an evolution equation for $\overline{\boldsymbol{\mathcal{E}}}$ along with a diffusion term,

$$\frac{\partial\overline{\mathcal{E}}_i}{\partial t}=\frac{1}{\tau}\left(\overline{\mathcal{E}}_i^{(0)}+\alpha_{ij}^{(0)}\overline{B}_j+\eta_{ijk}^{(0)}\overline{B}_{j,k}-\overline{\mathcal{E}}_i\right)+\kappa_\mathcal{E}\nabla^2\overline{\mathcal{E}}_i, \tag{2.18}$$

where $\kappa_\mathcal{E}=(\tau k_\mathrm{f}^2)^{-1}$ is an effective diffusivity for $\overline{\boldsymbol{\mathcal{E}}}$, and $\alpha_{ij}^{(0)}$ and $\eta_{ijk}^{(0)}$ are now no longer integral kernels, but just functions of space and time (in addition of course to other parameters of the system itself). So, instead of a cumbersome convolution, we now have instead a much simpler differential equation in space and time. In other words, instead of an instantaneous and local response, as in equation (2.8), we now have an evolution equation along with a stabilizing turbulent diffusion term, which is computationally very convenient. Note that now the $\overline{\mathcal{E}}_i^{(0)}$ term is automatically treated as a convolution, too. This is, as argued above, to be expected and could be important provided the vorticity vector, which would enter this term, is space- and time-dependent.

2.4. *Tau approximation and physical reality of an evolution equation for* $\overline{\boldsymbol{\mathcal{E}}}$

The physical reality of an evolution equation for $\overline{\boldsymbol{\mathcal{E}}}$ was first proposed by Blackman & Field (2002) as a natural consequence of retaining the time derivative introduced in the τ approximation—or better τ "approach", because it is not a controlled approximation. To understand the connection with an evolution equation for $\overline{\boldsymbol{\mathcal{E}}}$, let us briefly review the essence of this approach. Unlike SOCA, where one needs only the evolution equation (2.9) for $\boldsymbol{b}$, we now also need an evolution equation for $\boldsymbol{u}$. Here we assume it to be mainly governed by the Lorentz force, $\boldsymbol{J}\times\boldsymbol{B}$, of which we only retain the term resulting from tangling of $\overline{\boldsymbol{B}}$, namely

$$\frac{\partial\boldsymbol{u}}{\partial t}=\overline{\boldsymbol{J}}\times\boldsymbol{b}+\boldsymbol{j}\times\overline{\boldsymbol{B}}+\boldsymbol{j}\times\boldsymbol{b}-\overline{\boldsymbol{j}\times\boldsymbol{b}}+\nu\nabla^2\boldsymbol{u}+..., \tag{2.19}$$

where the ellipsis indicates additional terms such as the pressure gradient and the advection term that are here omitted. Next, we calculate

$$\frac{\partial\overline{\boldsymbol{\mathcal{E}}}}{\partial t}=\overline{\boldsymbol{u}\times\dot{\boldsymbol{b}}}+\overline{\dot{\boldsymbol{u}}\times\boldsymbol{b}}, \tag{2.20}$$

where the dots on $\boldsymbol{u}$ and $\boldsymbol{b}$ indicate partial derivatives with respect to time. Thus, we have

$$\frac{\partial\overline{\mathcal{E}}_i}{\partial t}=\epsilon_{ijk}\left(\overline{u_j\overline{B}_l u_{k,l}+\overline{B}_l b_{j,l}b_k}\right)+...=\left(\alpha_{il}^{\prime\mathrm{K}}+\alpha_{il}^{\prime\mathrm{M}}\right)\overline{B}_l+...\,, \tag{2.21}$$

where $\alpha_{il}^{\prime\mathrm{K}}=\epsilon_{ijk}\overline{u_j u_{k,l}}$ and $\alpha_{il}^{\prime\mathrm{M}}=\epsilon_{ijk}\overline{b_{j,l}b_k}$ are proportional to the kinetic and magnetic α effects (the actual α effects will be without primes) and commas denote partial differentiation. Their traces are $\alpha_{ii}^{\prime\mathrm{K}}=\epsilon_{ijk}\overline{u_j u_{k,i}}=-\overline{\boldsymbol{\omega}\cdot\boldsymbol{u}}$ and $\alpha_{ii}^{\prime\mathrm{M}}=\epsilon_{ijk}\overline{b_{j,i}b_k}=\overline{\boldsymbol{j}\cdot\boldsymbol{b}}$, but the essential part for our discussion lies in the ellipsis. In the τ approach, one assumes that triple correlations resulting from the nonlinearities can be approximated by the quadratic correlation as $-\overline{\boldsymbol{\mathcal{E}}}/\tau$ on the right-hand side of equation (2.21), where τ is a relaxation time, which lent its name to this approach. This leads directly to $(1+\tau\partial_t)\overline{\boldsymbol{\mathcal{E}}}=\alpha\overline{\boldsymbol{B}}+...$,

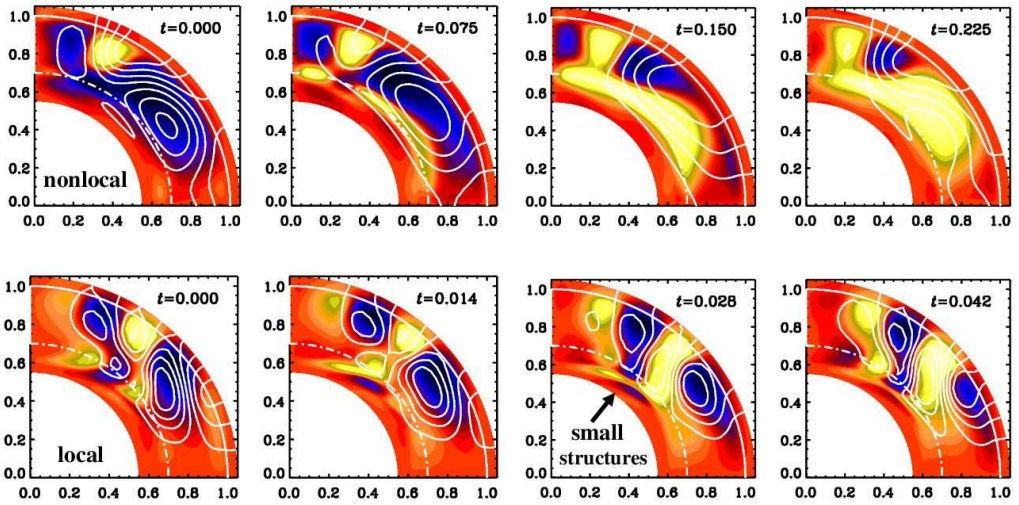

FIGURE 1. *Top*: Field lines in the meridional plane together with a color-coded representation of the toroidal field (dark/blue shades indicate negative values and light/yellow shades positive values). Evolution of the field structure for model with near-surface shear layer using the $\partial\overline{\boldsymbol{\mathcal{E}}}/\partial t$ equation. *Bottom*: same, but without the $\partial\overline{\boldsymbol{\mathcal{E}}}/\partial t$ equation. The magnetic cycle period is decreased from 0.53 to 0.11 diffusive times and the excitation conditions enhanced by a factor of five. Adapted from Brandenburg & Chatterjee (2018).

where $\alpha = \frac{1}{3}\tau(\alpha'^{\rm K}_{ii} + \alpha'^{\rm M}_{ii})$ in the isotropic case and the ellipsis denotes higher order derivatives giving rise to turbulent diffusion, etc, which are still being captured both by SOCA and the τ approach, but that were omitted for the sake of a simpler presentation.

Blackman & Field (2003) applied the idea of retaining the time derivative introduced in the τ approach to the case of passive scalar transport, where the instantaneous Fickian diffusion approximation is replaced by a telegrapher's equation. The physical reality of the telegrapher's equation in turbulent transport was subsequently confirmed using numerical simulations (Brandenburg et al. 2004). It turns the parabolic diffusion equation into a damped wave equation with a wave speed that is the turbulent rms velocity in the direction of the wave. For large turbulent diffusivities, this approach also avoids short timesteps in numerical solutions. Examples where this approach was used include cosmic ray transport in the interstellar medium (Snodin et al. 2006) and field-aligned thermal conduction in the solar corona (Rempel 2017). A particular effect of interest is that of a spiral forcing of the dynamo coefficients, which was found to result also in a shift of the mean-field spiral response by a factor of the order of $\Omega\tau$; see Chamandy et al. (2013).

The beauty of the approach of using equation (2.18) lies in the fact that there is no problem in handling spherical geometry or even nonlinearities in an *ad hoc* manner such as α quenching, as was already emphasized by Rheinhardt & Brandenburg (2012). We say here *ad hoc*, because the original convolution is linear.

In figure 1 we show a comparison of two models of Brandenburg & Chatterjee (2018) in spherical geometry with and without spatio-temporal nonlocality. This model uses solar-like differential rotation contours and turbulent transport coefficients estimated from mean-field theory. It shows that spatio-temporal nonlocality implies the absence of small structures, especially near the lower overshoot layer of the dynamo. Top and bottom panels cover half a period, so the panels on the right are similar to those on the left, except for a sign flip. The cycle period in the model with the $\partial\overline{\boldsymbol{\mathcal{E}}}/\partial t$ term included is 0.53 diffusion times, which is about five times longer than the period of

0.11 of the corresponding conventional models. For oscillatory solutions such as this one, temporal nonlocality lowers the excitation conditions for the dynamo, as was already demonstrated by Rheinhardt & Brandenburg (2012). In this example, the excitation conditions are lowered by a factor of about eight. Below, in § 2.7, we turn to the emergence of a completely new dynamo effect that occurs just owing to the presence of nonlocality in time. Before this, however, we briefly explore the essence of the test-field method that led to the new insights regarding nonlocality.

2.5. *The test-field method: a way forward*

Many of the detailed results discussed below would not have been discovered without the test-field method. We therefore briefly review in the following its basic aspects.

Analytic approaches is have demonstrated the vast multitude of different effects, but they are limited in that, for turbulent flows with finite correlation times, they are only exact at low $R_{\rm m}$. Some methods such as the τ approach are supposed to work at large $R_{\rm m}$, but they are not rigorous and always subject to numerical verification, using usually the test-field method.

In essence, the test-field method consists in solving equation (2.9) numerically, subject to given test fields $\overline{\boldsymbol{B}}^T$, where the superscript T denotes one of as many test fields as are needed to compute uniquely all elements of the α_{ij} and η_{ijk} tensors. In the following, we adopt xy averaging, denoted by an overbar, and use the two test fields

$$\overline{\boldsymbol{B}}^{T_1}=(\cos kz,0,0)\quad\text{and}\quad\overline{\boldsymbol{B}}^{T_2}=(\sin kz,0,0). \tag{2.22}$$

For each of them, we find numerically a solution that we call correspondingly $\boldsymbol{b}^{T_1}(\boldsymbol{x},t)$ and $\boldsymbol{b}^{T_2}(\boldsymbol{x},t)$. We then compute the corresponding mean electromotive force $\overline{\boldsymbol{\mathcal{E}}}^{T_1}=\overline{\boldsymbol{u}\times\boldsymbol{b}^{T_1}}$ and $\overline{\boldsymbol{\mathcal{E}}}^{T_2}=\overline{\boldsymbol{u}\times\boldsymbol{b}^{T_2}}$. Inserting this into equation (2.8) yields

$$\overline{\mathcal{E}}_i^{T_1}=\overline{\mathcal{E}}_i^{(0)}+\alpha_{i1}\cos kz-\eta_{i13}\sin kz, \tag{2.23}$$

$$\overline{\mathcal{E}}_i^{T_2}=\overline{\mathcal{E}}_i^{(0)}+\alpha_{i1}\sin kz+\eta_{i13}\cos kz. \tag{2.24}$$

Here the last index of η_{ijl} is $l=3$, because xy averages only depend on the third spatial coordinate, z. To eliminate $\overline{\mathcal{E}}_i^{(0)}$, we need solutions for the trivial test field $\overline{\boldsymbol{B}}^{T_0}=\boldsymbol{0}$. The solutions $\boldsymbol{b}^{T_0}$, and thus $\overline{\boldsymbol{\mathcal{E}}}^{(0)}$ may then well be zero, but there are also cases where they are not—for example if the cross helicity is finite; see Brandenburg & Rädler (2013). We are then left with two pairs of unknown coefficients, α_{i1} and η_{i13} for the two nontrivial cases $i=1$ and $i=2$. (The third component of xy averaged mean fields is constant because $\boldsymbol{\nabla}\cdot\overline{\boldsymbol{B}}=\overline{B}_{3,3}=0$, so $\overline{B}_3=0$ if it vanished initially.) The two pairs of unknowns are readily obtained by solving a 2×2 matrix problem with the solution

$$\begin{pmatrix}\alpha_{i1}\\ \eta_{i13}k\end{pmatrix}=\begin{pmatrix}\cos kz & \sin kz\\ -\sin kz & \cos kz\end{pmatrix}\begin{pmatrix}\overline{\mathcal{E}}_i^{T_1}-\overline{\mathcal{E}}_i^{(0)}\\ \overline{\mathcal{E}}_i^{T_2}-\overline{\mathcal{E}}_i^{(0)}\end{pmatrix}, \tag{2.25}$$

which yields altogether four coefficients: α_{11}, η_{113}, α_{21}, and η_{213}. To get the remaining four coefficients, α_{12}, η_{123}, α_{22}, and η_{223}, we need two more test fields, $\overline{\boldsymbol{B}}^{T_1}=(0,\cos kz,0)$ and $\overline{\boldsymbol{B}}^{T_2}=(0,\sin kz,0)$. Analogously to equation (2.25), this yields $(\alpha_{i2},\eta_{i23}k)$ as the corresponding solution vector.

All these coefficients are generally also time-dependent. For fluctuating fields, as is the case when $\boldsymbol{u}$ corresponds to turbulence, the coefficients are evidently also fluctuating. This can be relevant for studies of the incoherent α-shear dynamo that will be discussed in § 5.3; see Brandenburg et al. (2008a) for such applications. Another important case is

where the test fields themselves are time-dependent. In fact, this is of immediate relevance to all dynamo problems, where we expect the mean field to grow exponentially. Even for a simple turbulent decay problem, $\overline{\boldsymbol{B}}$ is time-dependent: it is exponentially decaying. Both of these cases were considered by Hubbard & Brandenburg (2009) using test fields proportional to e^{st} or $e^{-\mathrm{i}\omega t}$ with real coefficients s and ω. This allowed them to assemble the functions $\alpha_{ij}(\omega)$ and $\eta_{ij3}(\omega)$, which led them to the results that for turbulent flows, both coefficients are, to lowest order, proportional to $1/(1-\mathrm{i}\omega\tau)$ with τ being some relaxation time. The same result was obtained for test fields proportional to e^{st}.

It may be worth noting that there are a few other methods for computing α_{ij} and η_{ijl}. The simplest one is the imposed field method, which is exact in two dimensions and can then handle also fully nonlinear problems with magnetic background turbulence (Rheinhardt & Brandenburg 2010), as will be discussed in the next section. Instead of solving equation (2.9), one solves equation (2.1) in the presence of an imposed field. It was used to show that α_{xx} and α_{zz} can have opposite signs in rotating convection (Brandenburg et al. 1990). In three dimensions, however, turbulence make the mean-field non-uniform, so the actual electromotive force applies to a problem with α effect and turbulent diffusion while using just volume averages, suggesting that there is no mean current density. Thus, this method is only of limited usefulness in three dimensions.

Another method assumes that in a time-dependent turbulence simulation, $\overline{\boldsymbol{\mathcal{E}}}$, $\overline{\boldsymbol{B}}$, and $\overline{\boldsymbol{J}}$ cover all possible solutions, allowing one to obtain all the coefficients of α_{ij} and η_{ijk} after averaging. This method has even been used to determine spatial nonlocality (Brandenburg & Sokoloff 2002), but it is not fully reliable, as was later demonstrated by comparing with the test-field method (Brandenburg 2005b). Nevertheless, some success has been achieved in applications to accretion disk turbulence (Kowal et al. 2006) and convection in spherical shells (Racine et al. 2011; Simard et al. 2016). Yet another method is multiscale stability theory (Lanotte et al. 1999), which was recently shown to yield results equivalent to those of the test-field method (Andrievsky et al. 2015).

2.6. *From quasilinear to fully nonlinear test-field methods*

The test-field equations are readily available in some publicly available codes, so for example in the Pencil Code† (Brandenburg 2005b) and in Nirvana‡ (Gressel et al. 2008a; Gressel 2013). To newcomers in the field, it is always somewhat surprising that the test-field equations, i.e., equation (2.9) with $\overline{\boldsymbol{B}}$ being replaced by $\overline{\boldsymbol{B}}^T$, can be solved without the magnetic field module being included at all. The reason is that the turbulent transport coefficients characterize just properties of the flow. Thus, the number of equations to be solved is just the four or five hydrodynamic equations (either without or with energy equation included) together with the four versions of equation (2.9) for each of the four test fields—or more, if more test-fields are needed (see Warnecke et al. 2018, for a case where nine vector equations were solved). However, if the magnetic field module is invoked, the magnetic field (which is different from the test fields) can grow and backreact on the flow. Thus, one obtains turbulent transport coefficients that are being modified by the magnetic field. This method is often referred to as the quasi-kinematic method and has been used on various occasions to the magnetic quenching of α and η_{t} (Brandenburg et al. 2008b; Karak et al. 2014). The limits of applicability of this method are still being investigated. Fully nonlinear approaches have been investigated; see Courvoisier et al. (2010) and Rheinhardt & Brandenburg (2010). In those approaches, one also solves equation (2.19) for the fluctuating velocity.

† `https://github.com/pencil-code`
‡ `http://www.aip.de/Members/uziegler/nirvana-code/`

The perhaps most striking counter example where the quasi-kinematic test-field method fails is that of a magnetically forced Roberts flow. This can easily be seen by computing the α effect with the imposed field method in two dimensions, i.e., when there is no interference from turbulent diffusion or other terms. In such cases, the imposed field and fully nonlinear methods agree, while the quasi-kinematic method gives even the wrong sign of α; see Rheinhardt & Brandenburg (2010) for details. Magnetically forced flows could in principle be driven by currents flowing through wires within the flow. This is a special situation that is not encountered in astrophysics. However, Rheinhardt & Brandenburg (2010) speculated that flows exhibiting small-scale dynamo action could provide another example where the quasi-kinematic method fails, but this still needs to be demonstrated.

2.7. *Dynamo effects from memory alone: Roberts flow III*

Let us now discuss a remarkable result that has emerged by applying the test-field method to simple flow fields. The particular flow field considered here is referred to as Roberts flow III, which is one of a family of flows he studied (Roberts 1972). In Fourier space, as discussed in § 2.3, the nonlocality in time corresponds to a division by $1-\mathrm{i}\omega\tau$. This leads to an imaginary contribution in the dispersion relation that can turn a non-dynamo effect into a dynamo effect. An example is the pumping term, also known as turbulent diamagnetism (Zeldovich 1957; Rädler 1969). It corresponds to a contribution to $\overline{\boldsymbol{\mathcal{E}}}$ of the form $\boldsymbol{\gamma}\times\overline{\boldsymbol{B}}$, where $\boldsymbol{\gamma}$ is a vector that leads to advection-like transport of the mean magnetic field without actual material motion. It corresponds to a transport down the gradient of turbulent intensity. We return to this aspect in § 3.4. Note also that the $\boldsymbol{\gamma}$ term corresponds to an off-diagonal contribution to α of the form $\alpha_{ij}=-\epsilon_{ijk}\gamma_k$. Quite generally, the $\boldsymbol{\gamma}$ term implies that the dispersion relation for the complex growth rate $\lambda(k)$ takes the form

$$\lambda(k)=-\mathrm{i}\boldsymbol{k}\cdot\boldsymbol{\gamma}-(\eta+\eta_{\mathrm{t}})k^2, \tag{2.26}$$

where we have ignored other terms such as additional anisotropies, which do not enter for Roberts flow III.

Evidently, if we replace $\boldsymbol{\gamma}\to\boldsymbol{\gamma}^{(0)}/(1-\mathrm{i}\omega\tau)$, neglecting here the k^2/k_{f}^2 term from the spatial nonlocality, and assuming $\omega\tau\ll1$, then $-\mathrm{i}\boldsymbol{k}\cdot\boldsymbol{\gamma}\approx-\mathrm{i}\boldsymbol{k}\cdot\boldsymbol{\gamma}^{(0)}+\omega\tau\boldsymbol{k}\cdot\boldsymbol{\gamma}^{(0)}$. Here, $\omega=\mathrm{i}\lambda$ is a complex frequency and is used interchangeably with $\mathrm{i}\lambda$. Thus, there can be growth resulting from the second term if $\omega\tau\boldsymbol{k}\cdot\boldsymbol{\gamma}^{(0)}>\eta_{\mathrm{t}}k^2$. Such solutions are always oscillatory and show migratory dynamo waves in the direction of $\boldsymbol{\gamma}^{(0)}$.

Solutions of the type discussed above have been found in direct numerical simulations of Roberts flow III (Rheinhardt et al. 2014). We now discuss the basic properties of one of their solutions in more detail. This flow is given by (Roberts 1972)

$$\boldsymbol{u}=u_0\begin{pmatrix}\sin k_0x\,\cos k_0y\\-\cos k_0x\,\sin k_0y\\\frac{1}{2}\cos2k_0x+\cos2k_0y\end{pmatrix}\qquad\text{(Roberts flow III)},\tag{2.27}$$

where u_0 is an amplitude factor and k_0 is the wavenumber of the flow. Both parameters enter in the definition of the magnetic Reynolds number, $R_{\mathrm{m}}=u_0/\eta k_0$. Rheinhardt et al. (2014) found that dynamo action with a mean field proportional to $\exp[\mathrm{i}(kz-\omega t)]$ is possible when $k/k_0\lesssim0.78$. In the limit $k\to0$, there is large-scale dynamo action when $R_{\mathrm{m}}\gtrsim2.9$. The mean field is oscillatory with a frequency that is at onset about $\omega\approx0.037\,u_0k_0$.

The dynamo solution for Roberts flow III is beyond the validity of SOCA, in which the $\boldsymbol{u}\times\boldsymbol{b}-\overline{\boldsymbol{u}\times\boldsymbol{b}}$ term in equation (2.6) is neglected. In fact, within the limitations of SOCA, which is only valid for small R_{m}, no mean-field dynamo can be obtained for Roberts

flow III. This is because, in the mean-field formalism, the γ term emerges quadratically in $R_{\rm m}$, suggesting that it is a higher-order effect. Rheinhardt et al. (2014) discussed in detail a particular example where $R_{\rm m}=6$ and $k/k_0=0.4$. The growth rate was found to be $0.047\,u_0k_0$ and the frequency was $0.29\,u_0k_0$. In Fourier space, the turbulent magnetic diffusivity kernel was found to be $\eta_{\rm t}(k,\omega)=(0.21+0.03{\rm i})\,u_0/k_0$, which has only a small imaginary part corresponding to a weak memory effect, and $\gamma(k,\omega)=(0.73+0.27{\rm i})\,u_0$, which has a significant imaginary part corresponding to a strong memory effect. It is this term that is responsible for the positive growth rate. These complex coefficients match the dispersion relation given by equation (2.26) and reproduce the correct complex growth rate.

Describing spatio-temporal nonlocality with an evolution equation for $\overline{\boldsymbol{\mathcal{E}}}$ is an approximation that is inaccurate for two reasons. First, in equation (2.17) there are in general higher powers of k and ω, and second, the k and ω dependencies of $\tilde{\alpha}_{ij}$ and $\tilde{\eta}_{ijk}$ in equation (2.17) are usually not the same; see Rheinhardt et al. (2014) for details. The main point of using such an approximation is to do better than just neglecting spatio-temporal nonlocality altogether, as is still done in the vast majority of astrophysical applications. The differences are substantial, as was already demonstrated in figure 1. We see this again in the present example where the simple evolution equation (2.18) for $\overline{\boldsymbol{\mathcal{E}}}$ reproduces thus a qualitatively new dynamo effect.

2.8. *Other Roberts flows and generalizations*

In his original paper, Roberts (1972) discussed altogether four flows. All the Roberts flows are two-dimensional with the same flow vectors in the horizontal (x,y) directions, but different xy patterns in the z direction. His flow II is closely related to flow III discussed above; see Rheinhardt et al. (2014) for details. It also leads to dynamo waves resulting from the off-diagonal terms α_{xy} and α_{yx} of the α tensor with dynamo action owing to the memory term. The only difference is that here $\alpha_{yx}=\alpha_{xy}$ while for flow III we had $\alpha_{yx}=-\alpha_{xy}=\gamma$.

Another interesting and very different example is Roberts flow IV, which is given by

$$\boldsymbol{u}=u_0\begin{pmatrix}\sin k_0x\,\cos k_0y\\-\cos k_0x\,\sin k_0y\\0\end{pmatrix}\qquad\text{(Roberts flow IV)}.\tag{2.28}$$

It also produces large-scale magnetic fields that "survive" horizontal averaging, but in this case the governing dispersion relation is just of the form

$$\lambda(k)=-[\eta+\eta_{\rm t}(k)]k^2,\tag{2.29}$$

where $\eta_{\rm t}(k)$ was found to be sufficiently negative for $k\lesssim0.8\,k_0$, but positive (corresponding to decay) for larger values of k (Devlen et al. 2013). Thus, on small length scales, the solution is always stable.

For completeness, let us mention that negative turbulent diffusivities can also be found for some compressible flows. However, in all those cases the destabilizing effect is never strong enough to overcome the microphysical value, i.e., $\eta_{\rm t}+\eta$ is still positive (Rädler et al. 2011).

The most famous Roberts flow is his flow I, because it is helical. Moreover, its helicity is maximal with $\overline{\boldsymbol{\omega}\cdot\boldsymbol{u}}=k_0\,u_0^2$. The flow is given by

$$\boldsymbol{u}=u_0\begin{pmatrix}\sin(k_0x+\varphi_x)\,\cos(k_0y+\varphi_y)\\-\cos(k_0x+\varphi_x)\,\sin(k_0y+\varphi_y)\\0\end{pmatrix}\quad\text{(Roberts flow I for }\varphi_x=\varphi_y=0),\tag{2.30}$$

where $\varphi_x = \varphi_y = 0$ will be assumed at first. This flow leads to a standard α effect dynamo with a dispersion relation that is the same as for isotropic turbulence (Moffatt 1970), namely

$$\lambda(k) = \pm|\alpha \boldsymbol{k}| - [\eta + \eta_{\rm t}]k^2, \tag{2.31}$$

where dynamo action is only possible for the upper sign. We return to α effect dynamos further below, but before doing so, let us briefly discuss an interesting feature that arises when generalizing this flow to the case with time-dependent phases, as done by Galloway & Proctor (1992), who assumed

$$\varphi_x = \epsilon \cos \omega t, \qquad \varphi_y = \epsilon \sin \omega t, \tag{2.32}$$

where ϵ and ω are additional parameters characterizing what is now generally referred to as the Galloway–Proctor flow. One normally considers a version of this flow that is rotated by 45°, which allows one to fit two larger cells into the domain than the four cells in equation (2.30). This flow is a time-dependent generalization of Roberts flow I. This time-dependence is of particular interest in that it allows the dynamo to become "fast", which means that it can maintain a finite growth rate in the limit of large magnetic Reynolds numbers, $R_{\rm m} = u_{\rm rms}/\eta k_{\rm f} \gg 1$.

Numerical investigations of the Galloway–Proctor flow revealed the occurrence of an unexpected pumping effect, i.e., $\boldsymbol{\gamma} \neq \boldsymbol{0}$ (Courvoisier et al. 2006). This is because, owing to the circular polarization of this flow, the symmetry between $\boldsymbol{z}$ and $-\boldsymbol{z}$ is broken (Rädler & Brandenburg 2009). Remarkably, such a γ effect does not emerge in the SOCA approximation which neglects the $\boldsymbol{u} \times \boldsymbol{b} - \overline{\boldsymbol{u} \times \boldsymbol{b}}$ term in equation (2.6). Numerical computations of γ with the test-field method showed that, indeed, for $R_{\rm m} \to 0$, one has $\gamma \to 0$. Furthermore, as $R_{\rm m} \to 0$, we have $|\gamma| \propto R_{\rm m}^5$, which is a rather steep dependence. Analogously to the γ effect discussed in § 2.7, where $|\gamma|$ increases quadratically with $R_{\rm m}$, this again suggests that this effect can only be described with a higher-order approximation in $R_{\rm m}$ that is here higher than fourth order. Indeed, as shown by Rädler & Brandenburg (2009), a fourth-order approximation still does not capture this effect.

2.9. *Horizontal averaging is not always suitable*

Discontent with the use of horizontal averaging was expressed in the work of Gent et al. (2013a,b), who used averaging over a Gaussian kernel as an alternative. Ultimately, the usefulness of a particular averaging procedure can only be judged at the end, when we know the answer, what kind of large-scale field can be generated. The averaging procedure should be able to capture the expected class of large-scale fields. As an example, let us mention here a result of Devlen et al. (2013), who did not find a negative eddy diffusivity dynamo for the Taylor-Green flow. This was indeed true for horizontal averaging, but not for vertical (z) averaging, in which case the mean fields are two-dimensional. Such solutions were found by Andrievsky et al. (2015), who presented several examples where the field survives z averaging, but not xy averaging. A related example was found by Bhat et al. (2016b) using shearing box accretion disk simulations with a shear flow $u_y = Sx$ and $S = $ const. They reported the emergence of different large-scale fields, depending on whether they employed xy or yz averaging.

The advantage of any of the averages discussed so far is that they obey the Reynolds rules are still being obeyed. A practical example is azimuthal averaging in a sphere. However, such averaging fails to describe all kinds of nonaxisymmetric large-scale fields, such as dominant $m = 1$ solutions, where m is the azimuthal order. Such solutions were found for rapidly rotating stars; see Viviani et al. (2018) for a recent simulations.

2.10. *Quenching of α: self-inflicted anisotropy*

As the magnetic field grows and its energy density becomes comparable to the kinetic energy, the Lorentz force in the momentum equation begins to become important. This tends to decrease α and $\eta_{\rm t}$ in such a way as to saturate the dynamo. Assuming that our mean fields correspond to just planar averaging over the periodic x and y directions, they no longer depend on x and y. It is therefore clear that $\overline{\boldsymbol{B}}$ is just a function of z and t. Moreover, since $0=\boldsymbol{\nabla}\cdot\overline{\boldsymbol{B}}=\overline{B}_{z,z}$, we have $\overline{B}_z=$ const and, unless $\overline{B}_z$ is initially finite, it must vanish at all later times. For a dynamo driven essentially by an α effect, the $\overline{\boldsymbol{B}}$ with only x and y components must be an eigenfunction of the curl operator. This applies to all dynamos driven by a helical flow, such as the laminar Roberts flow I, and also to three-dimensional helical turbulence, for example. In a periodic domain $0<z<L_z$, the eigenfunction is given by

$$\overline{\boldsymbol{B}}=\begin{pmatrix}\sin(k_1z+\varphi)\\ \cos(k_1z+\varphi)\\ 0\end{pmatrix}, \tag{2.33}$$

where $k_1=\pm2\pi/L_z$ is the smallest wavenumber of the field in the z direction and φ is an arbitrary phase which is only determined by the initial conditions. Note that $\boldsymbol{\nabla}\times\overline{\boldsymbol{B}}=k_1\overline{\boldsymbol{B}}$ is indeed an eigenfunction of the curl operator. The eigenvalue k_1 is positive (negative) if α is positive (negative).

Once the magnetic field reaches equipartition strength with the flow, which we now assume to be driven by a forcing term in the momentum equation, the magnetic field saturates owing to the action of the Lorentz force in this momentum equation. The resulting changes to the flow begin to affect the α tensor, which then inevitably attains an anisotropy proportional to $\overline{B}_i\overline{B}_j/\overline{\boldsymbol{B}}^2$ (Roberts 1993). Thus, even if the α tensor was initially isotropic (which is here the case in the xy plane), it would, at saturation, be of the form

$$\boldsymbol{\alpha}=\alpha_0(\overline{B})\begin{pmatrix}1&0&0\\0&1&0\\0&0&0\end{pmatrix}-\alpha_1(\overline{B})\begin{pmatrix}\sin^2k_1z&\sin k_1z\cos k_1z&0\\ \sin k_1z\cos k_1z&\cos^2k_1z&0\\0&0&0\end{pmatrix}, \tag{2.34}$$

where we have assumed $\varphi=0$ for simplicity and $\overline{B}\equiv|\overline{\boldsymbol{B}}|$. Note that $\alpha\overline{\boldsymbol{B}}=(\alpha_0-\alpha_1)\overline{\boldsymbol{B}}$. This form of $\boldsymbol{\alpha}$ with $\alpha_1(\overline{B})$ having the opposite sign of $\alpha_0(\overline{B})$ was confirmed by numerical simulations using the test-field method (Brandenburg et al. 2008b). Certain aspects of it were also verified with the imposed field method where one neglects the $\boldsymbol{\eta}$ tensor and simply measures $\overline{\boldsymbol{\mathcal{E}}}=\langle\boldsymbol{u}\times\boldsymbol{b}\rangle$ in a simulation and computes then α_{ij} from $\overline{\mathcal{E}}_i/\overline{B}_j$ (Hubbard et al. 2009).

2.11. *An insightful experiment with an independent induction equation*

Cattaneo & Tobias (2009) were the first to study the nature of solutions to an independent induction equation,

$$\frac{\partial\boldsymbol{Z}}{\partial t}=\boldsymbol{\nabla}\times(\boldsymbol{U}\times\boldsymbol{Z}-\eta\boldsymbol{\nabla}\times\boldsymbol{Z}), \tag{2.35}$$

with a new vector field $\boldsymbol{Z}$ instead of $\boldsymbol{B}$, but with the same quenched velocity field $\boldsymbol{U}(\boldsymbol{B})$, which is the solution to the momentum equation with the usual Lorentz force $\boldsymbol{J}\times\boldsymbol{B}$. The result was surprising in that the dynamo did not saturate by "relaxing the system to a state close to marginality or by suppressing the chaotic stretching in the flow" (Cattaneo & Tobias 2009). They argued further "that this process is very subtle and not in concord with any of the previously suggested theories." Indeed, the naive expectation would be $\boldsymbol{Z}\propto\boldsymbol{B}$, i.e., a field proportional to the one that led to the now saturated dynamo, whose

flow we used in equation (2.35). However, the growth rate of such a $\overline{\boldsymbol{Z}}$ would be exactly zero. In other words, we have

$$\alpha\overline{\boldsymbol{Z}}=\alpha_0\overline{\boldsymbol{Z}},\quad\text{while}\quad\alpha\overline{\boldsymbol{B}}=(\alpha_0-\alpha_1)\overline{\boldsymbol{B}}. \tag{2.36}$$

Thus, if there is another solution that could actually grow under the influence of the velocity field $\boldsymbol{U}(\boldsymbol{B})$, it would be the more preferred solution to equation (2.35). Given that $\boldsymbol{U}(\boldsymbol{B})$ is helical, we expect nontrivial horizontally averaged fields $\overline{\boldsymbol{Z}}$ to be a solution of the associated mean-field problem of equation (2.35), but with the α tensor given still by equation (2.34), i.e., with $\overline{\boldsymbol{B}}$ rather than $\overline{\boldsymbol{Z}}$. Given that $\alpha_1(\overline{B})$ and $\alpha_0(\overline{B})$ have opposite signs, an essential contribution to the quenching comes from the second term. Therefore, solutions $\overline{\boldsymbol{Z}}$ that belong to the nullspace of the matrix $\overline{B}_i\overline{B}_j$ would not be quenched by this term. This is indeed what Tilgner & Brandenburg (2008) found; their $\overline{\boldsymbol{Z}}$ was a 90° phase-shifted version of $\overline{\boldsymbol{B}}$, i.e., $\overline{\boldsymbol{Z}}(z)=\overline{\boldsymbol{B}}(z+\pi/2k_1)$. Indeed,

$$\begin{pmatrix}\sin^2 k_1z & \sin k_1z\cos k_1z & 0\\ \sin k_1z\cos k_1z & \cos^2 k_1z & 0\\ 0 & 0 & 0\end{pmatrix}\begin{pmatrix}\cos k_1z\\ -\sin k_1z\\ 0\end{pmatrix}=\boldsymbol{0}, \tag{2.37}$$

so this $\overline{\boldsymbol{Z}}$ is not being quenched by this second term in equation (2.34). Thus, $|\overline{\boldsymbol{Z}}|$ continues to grow exponentially. Some quenching might still occur because of a change of $\alpha_0(\overline{B})$, but in the experiments of Tilgner & Brandenburg (2008), this effect was small. This is remarkable, but perfectly understandable behavior in the evolution of $|\overline{\boldsymbol{Z}}|$ provides another independent verification of the quenching expression given by equation (2.34).

2.12. *Catastrophic quenching*

Early work with the imposed field method using a uniform magnetic field $\boldsymbol{B}_0=$ const resulted in an α effect whose value seemed to be quenched in an $R_{\rm m}$-dependent fashion. Blackman & Field (2000a) called this *catastrophic* quenching, because α would be catastrophically small in the astrophysically relevant case of large $R_{\rm m}$. This was first suggested by Vainshtein & Cattaneo (1992) and confirmed numerically by Cattaneo & Hughes (1996). This result irritated the astrophysics community for some time. Indeed, it seemed a bit like a crisis to all of mean-field theory and, maybe, we would not have had this special edition of the Journal of Plasma Physics (JPP) if this quenching was really as catastrophic as it seemed!

The solution to the catastrophic quenching problem was another highlight of dynamo theory and has its roots in an early finding by Pouquet et al. (1976). They realized that, in the nonlinear case at sufficiently large $R_{\rm m}$, the α effect has a new contribution which is not just proportional to the mean kinetic helicity density $\overline{\boldsymbol{\omega}\cdot\boldsymbol{u}}$, as stated in the beginning in equation (2.12), but there is a term proportional to the mean current helicity density from the fluctuating fields $\overline{\boldsymbol{j}\cdot\boldsymbol{b}}$, where $\boldsymbol{j}=\boldsymbol{\nabla}\times\boldsymbol{b}/\mu_0$ is the small-scale current density. This term emerges naturally from the $\dot{\boldsymbol{u}}\times\boldsymbol{b}$ term in equation (2.20) when using the τ approximation; see § 2.4. Thus, we have (Pouquet et al. 1976)

$$\alpha_0=-\tfrac{1}{3}\tau\left(\overline{\boldsymbol{\omega}\cdot\boldsymbol{u}}-\overline{\boldsymbol{j}\cdot\boldsymbol{b}}/\overline{\rho}\right), \tag{2.38}$$

where $\overline{\rho}$ is the mean fluid density. However, if the small-scale magnetic field is still approximately statistically isotropic, the small-scale current helicity, $\overline{\boldsymbol{j}\cdot\boldsymbol{b}}$, must be approximately $k_{\rm f}^2\,\overline{\boldsymbol{a}\cdot\boldsymbol{b}}/\mu_0$, where $\boldsymbol{a}$ is the magnetic vector potential of the small-scale field, $\boldsymbol{b}=\boldsymbol{\nabla}\times\boldsymbol{a}$. Interestingly, $\overline{\boldsymbol{a}\cdot\boldsymbol{b}}$ is constrained, on the one hand, by $\overline{\boldsymbol{A}\cdot\boldsymbol{B}}$, i.e., the mean magnetic helicity density of the total field, which obeys a conservation equation, and on the other hand by $\overline{\boldsymbol{A}}\cdot\overline{\boldsymbol{B}}$, which is the result of the mean-field dynamo problem (Hubbard

& Brandenburg 2012), i.e.,

$$\frac{\partial}{\partial t}\overline{\boldsymbol{A}}\cdot\overline{\boldsymbol{B}}=2\overline{\boldsymbol{\mathcal{E}}}\cdot\overline{\boldsymbol{B}}-2\eta\mu_0\overline{\boldsymbol{J}}\cdot\overline{\boldsymbol{B}}-\boldsymbol{\nabla}\cdot(\overline{\boldsymbol{F}}_{\rm m}-\overline{\boldsymbol{\mathcal{E}}}\times\overline{\boldsymbol{A}}),\tag{2.39}$$

where $\overline{\boldsymbol{F}}_{\rm m}$ is the magnetic helicity flux from the large-scale field and $\overline{\boldsymbol{E}}=\eta\mu_0\overline{\boldsymbol{J}}-\overline{\boldsymbol{U}}\times\overline{\boldsymbol{B}}$ is the mean electric field without the $\overline{\boldsymbol{\mathcal{E}}}$ term. Thus, $\overline{\boldsymbol{a}\cdot\boldsymbol{b}}$ must obey the equation (Kleeorin & Ruzmaikin 1982; Kleeorin et al. 2000)

$$\frac{\partial}{\partial t}\overline{\boldsymbol{a}\cdot\boldsymbol{b}}=-2\overline{\boldsymbol{\mathcal{E}}}\cdot\overline{\boldsymbol{B}}-2\eta\mu_0\overline{\boldsymbol{j}\cdot\boldsymbol{b}}-\boldsymbol{\nabla}\cdot(\overline{\boldsymbol{F}}_{\rm f}+\overline{\boldsymbol{\mathcal{E}}}\times\overline{\boldsymbol{A}}),\tag{2.40}$$

so that the sum of equations (2.39) and (2.40) is equal to

$$\frac{\partial}{\partial t}\overline{\boldsymbol{A}\cdot\boldsymbol{B}}=-2\eta\mu_0\overline{\boldsymbol{J}\cdot\boldsymbol{B}}-\boldsymbol{\nabla}\cdot\overline{\boldsymbol{F}}_{\rm tot},\tag{2.41}$$

where $\overline{\boldsymbol{F}}_{\rm tot}=\overline{\boldsymbol{F}}_{\rm m}+\overline{\boldsymbol{F}}_{\rm f}$ is the sum of magnetic helicity fluxes from the mean and fluctuating fields, respectively. Equation (2.40) can easily be formulated as an evolution equation for α, or at least its magnetic contribution, as was first done by Kleeorin & Ruzmaikin (1982).

A few additional comments are here in order. First, analogous to the pair of terms $\pm2\overline{\boldsymbol{\mathcal{E}}}\cdot\overline{\boldsymbol{B}}$ in equations (2.39) and (2.40), we have isolated the pair $\mp\overline{\boldsymbol{\mathcal{E}}}\times\overline{\boldsymbol{A}}$ underneath the corresponding flux divergence terms. This was first done by Hubbard & Brandenburg (2012), who found these to give important contributions, especially to the flux in the equation for the small-scale magnetic helicity. This term complements a corresponding term of opposite in the equation for the large-scale magnetic helicity, but it does not contribute to the total magnetic helicity flux. Second, it can be advantageous to solve directly the equation for the total magnetic helicity flux, as was also done by Hubbard & Brandenburg (2012). This ensures that mutually canceling terms do not contribute "accidently" (as a result of inaccurate approximations) to the total magnetic helicity flux. This approach has been adopted by Pipin et al. (2013a,b) and Pipin & Kosovichev (2013, 2016) to model the solar dynamo; see also Pipin (2015, 2017).

The approach described above is therefore often referred to as "dynamical" quenching. This is not an alternative to the "algebraic" quenching, which describes the functional dependencies of $\alpha_0(\overline{B})$ and $\alpha_1(\overline{B})$ in equation (2.34), but it is an additional contribution to $\alpha_0(\overline{B})$, and in principle also additional anisotropic contributions (Rogachevskii & Kleeorin 2007; Pipin 2008). It provides a feedback from the growing or evolving $\overline{\boldsymbol{A}}\cdot\overline{\boldsymbol{B}}$ that is necessary to obey the total magnetic helicity equation (2.41).

As pointed out by Rädler & Rheinhardt (2007), dynamical quenching has not been derived rigorously within mean-field theory, and must rather be regarded as a heuristic approach. In other words, dynamical quenching does not emerge in the traditional approach of solving for the fluctuations and in that way computing α. Indeed, one should expect that the magnetic helicity equation would automatically be obeyed if one solved the equations for the fluctuations by avoiding questionable approximations. At present, however, dynamical quenching is the only known approach that describes correctly the resistively slow saturation of α^2 dynamos in triply-periodic domains (Field & Blackman 2002; Blackman & Brandenburg 2002; Subramanian 2002) found by Brandenburg (2001), as will be discussed in § 2.13.

The aforementioned simulations were done with helically forced turbulence, which led, at late times, to the development of a large-scale magnetic field of Beltrami type; see equation (2.33) for one such example, where the wavevector of the mean field points in

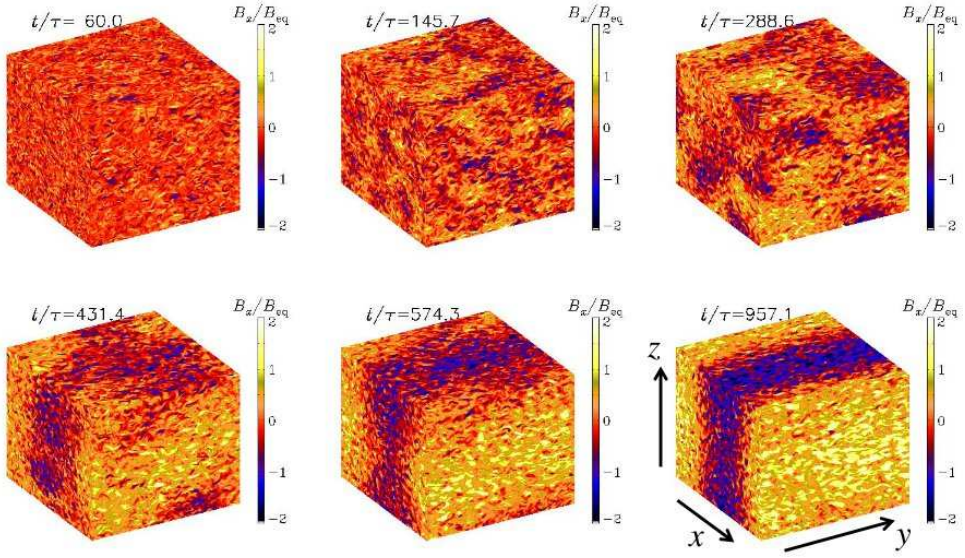

FIGURE 2. Visualizations of $B_x/B_{\rm eq}$ on the periphery of the domain at six times during the late saturation stage of the dynamo when a large-scale field is gradually building up. The small-scale field has reached its final value after $t/\tau \approx 100$ turnover times. The diffusive time is here about 7000 times the turnover time. The maximum field strength is about twice $B_{\rm eq}$.

the z direction. In figure 2 we show an example of the approach to such a Beltrami field, which has here a wavevector pointing in the x direction.

The evolution equation for α can also be written in implicit form with the time derivative of α on the right-hand side as (Brandenburg 2008)

$$\alpha = \frac{\alpha_{\rm K} + R_{\rm m}\left[\eta_{\rm t}\mu_0\overline{\boldsymbol{J}}\cdot\overline{\boldsymbol{B}}/B_{\rm eq}^2 - (\boldsymbol{\nabla}\cdot\overline{\boldsymbol{F}}_{\rm f})/(2B_{\rm eq}^2) - (\partial\alpha/\partial t)/(2\eta_{\rm t}k_{\rm f}^2)\right]}{1 + R_{\rm m}\overline{\boldsymbol{B}}^2/B_{\rm eq}^2}, \tag{2.42}$$

where $\alpha_{\rm K}$ is the α effect in the kinematic limit. The formulation in equation (2.42) confirms first of all the early catastrophic quenching result of Vainshtein & Cattaneo (1992) for *volume-averaged* mean fields, because those are independent of the spatial coordinates and, therefore, $\mu_0\overline{\boldsymbol{J}} = \boldsymbol{\nabla}\times\overline{\boldsymbol{B}} = \boldsymbol{0}$. The periodicity then implies $\boldsymbol{\nabla}\cdot\overline{\boldsymbol{F}}_{\rm f} = 0$. Also, they considered a stationary state, so $\partial\alpha/\partial t = 0$. Thus, all the factors of $R_{\rm m}$ in the numerator vanish and therefore we have $\alpha = \alpha_{\rm K}/(1 + R_{\rm m}\overline{\boldsymbol{B}}^2/B_{\rm eq}^2)$, as predicted by Vainshtein & Cattaneo (1992). In general, however, the presence of any of the three additional terms in the numerator multiply $R_{\rm m}$ and are therefore of the same order as those in the denominator. This should readily alleviate the threat of an $R_{\rm m}$-dependent quenching. Interestingly, equation (2.42) applies also when the dynamo is not driven by the $\alpha_{\rm K}$ term, but by the shear-current effect, for example (Brandenburg & Subramanian 2005b). Thus, somewhat paradoxically, we could say that an α effect can be quenched even if there is no α to begin with.

In the absence of magnetic helicity fluxes, i.e., when $\boldsymbol{\nabla}\cdot\overline{\boldsymbol{F}}_{\rm f} = 0$, as in the present case of homogeneous turbulence with periodic boundary conditions, the time evolution is inevitably controlled by a resistively slow term. This somewhat surprising constraint for *homogeneous* helical turbulence can be understood quite generally—even without resorting to any mean-field theory, i.e., without talking about α effect and turbulent magnetic diffusivity. This will be discussed next.

2.13. *Resistively slow saturation in homogeneous turbulence*

To describe the late saturation phase, we just invoke the magnetic helicity equation for the whole volume, which is assumed to be either periodic or embedded in a perfect conductor. Volume averages will be denoted by angle brackets. Thus, we have

$$\frac{\mathrm{d}}{\mathrm{d}t}\langle \boldsymbol{A}\cdot\boldsymbol{B}\rangle = -2\eta\mu_0\langle \boldsymbol{J}\cdot\boldsymbol{B}\rangle, \tag{2.43}$$

which is the same as equation (2.41), but without the magnetic helicity flux divergence term. (For the volume averages employed here, this would lead to a surface term, which vanishes for periodic or perfectly conducting boundaries.) This equation highlights an important result for the steady state, namely

$$\langle \boldsymbol{J}\cdot\boldsymbol{B}\rangle = 0 \qquad \text{(for any steady state in triply periodic domains)}. \tag{2.44}$$

This sounds somewhat boring, but becomes immediately interesting when realizing that mean fields and fluctuations can both be finite, i.e.,

$$\langle \boldsymbol{j}\cdot\boldsymbol{b}\rangle = -\langle \overline{\boldsymbol{J}}\cdot\overline{\boldsymbol{B}}\rangle \neq 0, \tag{2.45}$$

so that $\langle \boldsymbol{J}\cdot\boldsymbol{B}\rangle = \langle \overline{\boldsymbol{J}}\cdot\overline{\boldsymbol{B}}\rangle + \langle \boldsymbol{j}\cdot\boldsymbol{b}\rangle = 0$, as required.

To describe the approach to the stationary state given by equation (2.44), we have to retain the time derivative in equation (2.43). Writing $\langle \boldsymbol{A}\cdot\boldsymbol{B}\rangle = \langle \overline{\boldsymbol{A}}\cdot\overline{\boldsymbol{B}}\rangle + \langle \boldsymbol{a}\cdot\boldsymbol{b}\rangle$, and assuming that in the late saturation phase, the quadratic correlations of the fluctuations are already constant and only the correlations of mean fields are not, we can omit the time derivative of $\langle \boldsymbol{a}\cdot\boldsymbol{b}\rangle$. Furthermore, we assume magnetic fields with positive (negative) magnetic helicity at small scales, i.e.,

$$\mu_0\langle \boldsymbol{j}\cdot\boldsymbol{b}\rangle \approx \pm k_\mathrm{f}\langle \boldsymbol{b}^2\rangle \approx k_\mathrm{f}^2\langle \boldsymbol{a}\cdot\boldsymbol{b}\rangle, \tag{2.46}$$

and that $\langle \boldsymbol{b}^2\rangle \approx \mu_0\langle \rho\boldsymbol{u}^2\rangle \equiv B_\mathrm{eq}^2$, which is the square of the equipartition value. Furthermore, owing to equation (2.33), we have

$$\overline{\boldsymbol{J}}\cdot\overline{\boldsymbol{B}} = \mp k_1\overline{\boldsymbol{B}}^2 = k_1^2\,\overline{\boldsymbol{A}}\cdot\overline{\boldsymbol{B}}, \tag{2.47}$$

which is, for pure modes with wavenumber k_1, constant in space. However, this relation is no longer exact for a superposition of modes. Thus, with these provisions, equation (2.43) becomes (Brandenburg 2001)

$$\frac{\mathrm{d}}{\mathrm{d}t}\langle \overline{\boldsymbol{B}}^2\rangle = 2\eta k_1 k_\mathrm{f} B_\mathrm{eq}^2 - 2\eta k_1^2\langle \overline{\boldsymbol{B}}^2\rangle, \tag{2.48}$$

with the solution

$$\langle \overline{\boldsymbol{B}}^2\rangle = B_\mathrm{eq}^2\frac{k_\mathrm{f}}{k_1}\left[1 - e^{-2\eta k_1^2(t-t_\mathrm{sat})}\right]. \tag{2.49}$$

This agrees with the slow saturation behavior seen first in the simulations of Brandenburg (2001); see figure 3. Here t_sat is the time when the slow saturation phase commences; see the crossing of the green dashed line with the abscissa. Interestingly, instead of waiting until full saturation is accomplished, one can obtain the saturation value already much earlier simply by differentiating the simulation data to compute (Candelaresi & Brandenburg 2013)

$$B_\mathrm{sat}^2 \approx \langle \overline{\boldsymbol{B}}^2\rangle + \tau_\mathrm{diff}\frac{\mathrm{d}}{\mathrm{d}t}\langle \overline{\boldsymbol{B}}^2\rangle. \tag{2.50}$$

Note that the inverse time constant $\tau_\mathrm{diff}^{-1} = 2\eta k_1^2$ in the exponent of equation (2.49) is fixed by the microphysics and does not involve the turbulent magnetic diffusivity. This

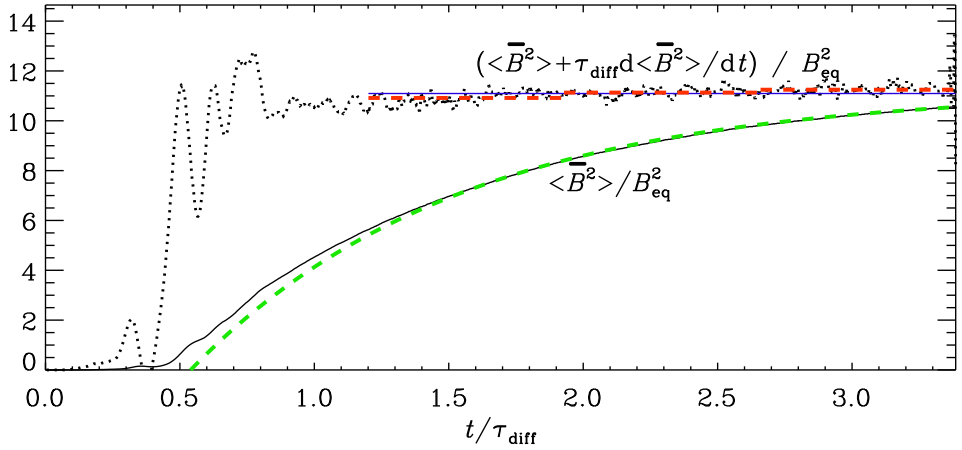

FIGURE 3. Evolution of the normalized $\langle\overline{\boldsymbol{B}}^2\rangle$ and that of $\langle\overline{\boldsymbol{B}}^2\rangle+\tau_{\rm diff}{\rm d}\langle\overline{\boldsymbol{B}}^2\rangle/{\rm d}t$ (dotted), compared with its average in the interval $1.2\le t/\tau_{\rm diff}\le 3.5$ (horizontal blue solid line), as well as averages over three subintervals (horizontal red dashed lines). The green dashed line corresponds to equation (2.49) with $t_{\rm sat}/\tau_{\rm diff}=0.54$.

is therefore still in some sense catastrophic, so real astrophysical dynamos do not work like this, and this is because of magnetic helicity fluxes. To demonstrate this in a really convincing way requires simulations at magnetic Reynolds numbers well in excess of 1000 (Del Sordo et al. 2013). We discuss magnetic helicity fluxes next.

2.14. *Magnetic helicity fluxes*

The most important contribution to the magnetic helicity flux is a turbulent diffusive flux proportional to the negative gradient of the magnetic helicity density (Hubbard & Brandenburg 2010), i.e.,

$$\overline{\boldsymbol{F}}_{\rm f}=-\kappa_h\boldsymbol{\nabla}\overline{\boldsymbol{a}\cdot\boldsymbol{b}}. \tag{2.51}$$

Such a formulation raises immediately the question of the gauge dependence of magnetic helicity. This turns out to be less of an issue than originally anticipated. A first step in this realization comes from the work of Subramanian & Brandenburg (2006), who showed that the magnetic helicity density can be expressed in terms of a density of linkages, provided the correlation scale is much smaller than the mean field or system scale. In reality, of course, a broad range of length scales will be excited, and this can be described by the (shell-integrated) magnetic helicity spectrum, $H_{\rm M}(k)$, which is normalized such that $\int H_{\rm M}(k)\,{\rm d}k=\langle\boldsymbol{A}\cdot\boldsymbol{B}\rangle$. For a review discussing also spectra such as these, see Brandenburg & Nordlund (2011).

Magnetic helicity spectra have been obtained from solar observations (Zhang et al. 2014, 2016; Brandenburg et al. 2017c) and even for the solar wind (Matthaeus & Goldstein 1982; Brandenburg et al. 2011b), as will be discussed below. Such spectra are automatically gauge-invariant owing to the implicit assumption that, by taking a Fourier transform, one assumes a periodic domain. Clearly, this is unrealistic on the largest scales, but this only affects the magnetic helicity spectra at the smallest wavenumbers. At all other wavenumbers, the spectrum should be a physically meaningful quantity and the same in any gauge.

Measurements of magnetic helicity fluxes have been performed by Hubbard & Brandenburg (2010) for an α^2 dynamo embedded in a poorly conducting halo and by Del Sordo et al. (2013) for a dynamo with a wind so one can compare turbulent–diffusive

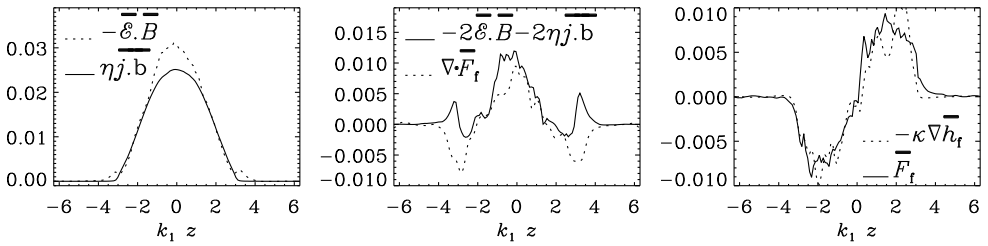

FIGURE 4. Time-averaged profiles of $\langle\overline{\boldsymbol{\mathcal{E}}}\cdot\overline{\boldsymbol{B}}\rangle$ and $\eta\langle\boldsymbol{j}\cdot\boldsymbol{b}\rangle$ (left panel), the difference between these terms compared with the magnetic helicity flux divergence of small-scale fields $\langle\boldsymbol{\nabla}\cdot\overline{\boldsymbol{F}}_{\rm f}\rangle$ (middle panel), and the flux itself compared with the Fickian diffusion ansatz (right-hand panel). The fluxes are in given in units of $\eta_{\rm t0}B_{\rm eq}^2$ and the flux divergence is given in units of $k_1\eta_{\rm t0}B_{\rm eq}^2$.

and advective fluxes. Mitra et al. (2010b) have explicitly demonstrated the gauge independence of the small-scale magnetic helicity flux. In all those cases, it was found that the magnetic helicity flux divergence is comparable to the Spitzer magnetic helicity production, $2\eta\mu_0\overline{\boldsymbol{j}\cdot\boldsymbol{b}}$. In figure 4, we show time-averaged profiles of $\langle\overline{\boldsymbol{\mathcal{E}}}\cdot\overline{\boldsymbol{B}}\rangle$ and $\eta\langle\boldsymbol{j}\cdot\boldsymbol{b}\rangle$, as well as the difference between these two terms compared with the magnetic helicity flux divergence of small-scale fields, $\langle\boldsymbol{\nabla}\cdot\overline{\boldsymbol{F}}_{\rm f}\rangle$, and the flux itself compared with the Fickian diffusion ansatz for the model of Hubbard & Brandenburg (2010) at $R_{\rm m}\approx270$. We see that the magnetic helicity flux divergence of small-scale fields is still less than the magnetic helicity production by the mean electromotive. Thus, the magnetic helicity flux divergence is still subdominant. It can therefore not yet alleviate the resistively slow saturation of the dynamo. One might hope that this will change at are larger values of $R_{\rm m}$. As of now, however, it has still not been possible to demonstrate this convincingly.

Most of the dynamo simulations to date are not yet in the asymptotic regime where $R_{\rm m}$ is large enough to alleviate resistively slow saturation. It would be important to demonstrate more thoroughly to what extent those dynamo are in the asymptotic regime, and that

$$|\boldsymbol{\nabla}\cdot\overline{\boldsymbol{F}}_{\rm f}|\approx|2\overline{\boldsymbol{\mathcal{E}}}\cdot\overline{\boldsymbol{B}}|\gg|2\eta\mu_0\overline{\boldsymbol{j}\cdot\boldsymbol{b}}|, \tag{2.52}$$

as one should expect. Let us emphasize here that, unlike the flux divergence $\boldsymbol{\nabla}\cdot\overline{\boldsymbol{F}}_{\rm f}$, the actual helicity fluxes can always be gauged such that they vanish across an impenetrable boundary by adopting the gauge $\boldsymbol{U}\cdot\boldsymbol{A}=0$ (Candelaresi et al. 2011). In that case, the magnetic helicity density evolves just like a passive scaler, i.e.,

$$\frac{\partial}{\partial t}\boldsymbol{A}\cdot\boldsymbol{B}=-\boldsymbol{\nabla}\cdot[(\boldsymbol{A}\cdot\boldsymbol{B})\,\boldsymbol{U}], \tag{2.53}$$

where the flux contribution $(\boldsymbol{U}\cdot\boldsymbol{A})\,\boldsymbol{B}$ vanishes; see Hubbard & Brandenburg (2011).

2.15. *Oscillatory α^2 dynamo: an exactly solvable model for continued investigations*

Much of the work on catastrophic quenching and resistively slow saturation has come from studies in periodic domains, where no helicity fluxes are possible. To go beyond this limitation, we need to focus on inhomogeneous conditions and possibly also inhomogeneous turbulence. A particularly simple system that has not yet been studied in this regard is the α^2 dynamo between a perfectly conducting boundary on one side ($A_x=A_y=A_{z,z}=0$ in the Weyl gauge) and a vertical field condition ($A_{x,z}=A_{y,z}=A_z=0$) on the other. Such dynamos have oscillatory solutions that can be written in closed form as (Brandenburg 2017)

$$\mathcal{A}(z,t)\equiv A_x+{\rm i}A_y=A_0\,\left(e^{{\rm i}k_+z}-e^{{\rm i}k_-z}\right)e^{-{\rm i}\omega t}, \tag{2.54}$$

where the wavenumbers k_+ and k_- are complex so as to satisfy the vacuum boundary condition $\partial\mathcal{A}/\partial z = 0$ at $k_0 z = \pi/2$, with k_0 being the lowest wavenumber of the decay mode in this model, and A_0 is an amplitude factor. The two wavenumbers obey the constraint relation $(k_+ + k_-)\eta_{\rm T} + \alpha = 0$ with $\eta_{\rm T}$ being the total (turbulent and microphysical) magnetic diffusivity, and are given by

$$k_+/k_0 \approx 0.10161896 - 0.51915398\,{\rm i}, \tag{2.55}$$

$$k_-/k_0 \approx -2.6522693 + 0.51915398\,{\rm i}. \tag{2.56}$$

at the first critical complex eigenvalue defined by the marginal value of α and the frequency ω with

$$\alpha k_0 + {\rm i}\omega \approx (2.5506504 - 1.4296921\,{\rm i})\,\eta_{\rm T} k_0^2. \tag{2.57}$$

Equation (2.54) automatically obeys the perfect conductor boundary condition $\mathcal{A} = 0$ at $z = 0$. These solutions display dynamo waves traveling away from the perfect conductor boundary toward the vacuum boundary. This is reminiscent of the work of Parker (1971b), who found that for oscillatory $\alpha\Omega$ dynamos, boundary conditions can introduce behaviors that are not obtained for infinite domains. Subsequently, Worledge et al. (1997) and Tobias et al. (1997) found that the antisymmetry condition at the equator plays the role of an absorbing boundary that led to localized wall modes. Later, Tobias et al. (1998a) showed that boundary conditions can play a decisive role in determining the migration direction of traveling waves.

Oscillatory α^2 dynamos have been studied numerically in strongly stratified domains (Jabbari et al. 2016b), but the question of magnetic helicity fluxes has not yet been addressed. This model may be an ideal target to re-address the question of magnetic helicity fluxes. This model would be an improvement over previous studies where the vertical field boundary condition has been used on both ends of the domain; see Gruzinov & Diamond (1994, 1995, 1996) and Brandenburg & Dobler (2001).

A particularly simple mean-field model with nontrivial helicity fluxes was presented by Brandenburg et al. (2009) for a variant of the model presented above. It revealed for the first time that the magnetic helicity density in the outer parts of the domain, i.e., in the halo, are reversed. Its significance was not fully appreciated until later when it was actually observed in the solar wind (Brandenburg et al. 2011b). Before going into details, let us first discuss what is know about magnetic helicity in the Sun.

3. The solar dynamo

The measurement of solar magnetic helicity has always been concerned with the gauge dependence and topological nature of magnetic helicity. This led to the development of the relative magnetic helicity (Berger & Field 1984; Finn & Antonsen 1985), a gauge-invariant formulation of the magnetic helicity in a given open domain obtained by making reference to a potential field obeying the same boundary conditions on the periphery of the domain. In the following, however, we focus on magnetic helicity spectra and discuss their significance and advantages over the full volume integrated quantity.

3.1. *Magnetic helicity spectra*

It has long been speculated that astrophysical dynamos might be in some way magnetically driven, i.e., driven by a magnetic instability such magnetobuoyancy or the magneto-rotational instability. This motivated the study of dynamos with a forcing term in the induction equation, as was first done by Pouquet et al. (1976). Although this reasoning may not apply in practice, such models do have the interesting property that they have

the same sign of magnetic helicity at all length scales (Park & Blackman 2012b). By contrast, kinetically driven dynamos result in a bihelical spectrum with opposite signs of magnetic helicity at large and small length scales (Brandenburg 2001; Blackman & Brandenburg 2003). Thus, from a dynamo-point-of-view, the important question concerns the spectrum of magnetic helicity, and, in particular, the possibility of different signs of magnetic helicity at different scales or wavenumbers. It is therefore not enough to obtain the magnetic helicity of the total field, $\langle \boldsymbol{A} \cdot \boldsymbol{B} \rangle = \int H_{\rm M}(k)\,{\rm d}k$, but the detailed scale dependence through $H_{\rm M}(k)$. For a particular active region on the solar surface, AR 11158, the equivalence between the two approaches has been demonstrated; see Zhang et al. (2014). They estimated the total magnetic helicity density of the active region AR 11158 by multiplying the total magnetic helicity density, $\int H_{\rm M}(k)\,{\rm d}k$, with the volume spanned by the surface area of the magnetogram of $186 \times 186\,{\rm Mm}^2$ and an assumed height of 100 Mm. In this way, they found a total magnetic helicity of $10^{43}\,{\rm Mx}^2$, which agrees with the value found by several groups (Vemareddy et al. 2012; Liu & Schuck 2012; Jing et al. 2012; Tziotziou et al. 2013). We recall that $1\,{\rm Mx} = 1\,{\rm G\,cm}^2$ is the unit of magnetic flux. The linkage of flux tubes is proportional to the product of the two fluxes of two interlinked flux tubes and thus has the unit ${\rm Mx}^2$.

The work done so far has shown that at the solar surface the magnetic helicity density is negative in the northern hemisphere and peaks at $k \approx 0.06\,{\rm Mm}^{-1}$, which corresponds to a scale of about 100 Mm; see Brandenburg et al. (2017c). Surprisingly, there is no evidence for a sign reversal, as was expected based on theoretical models (Blackman & Brandenburg 2003) and as was also seen in the active region AR 11515, which was exceptionally helical (Lim et al. 2012; Wang et al. 2014; Zhang et al. 2016). A positive sign of magnetic helicity has also been seen in the mean-field computations of Pipin & Pevtsov (2014). The work of Brandenburg et al. (2017c) was preliminary in the sense that one should really perform an analogous analysis using spherical harmonics, but this has not yet been done and the two-scale formalism has not yet been developed for that case. Also, they only analyzed three Carrington rotations of the Sun. By analyzing a much larger sample, Singh et al. (2018) found many other Carrington rotations for which the spectrum is bihelical. However, the energy contained in the large-scale contribution with opposite sign of magnetic helicity is rather weak.

3.2. *Magnetic helicity in the solar wind*

To compute magnetic helicity from a time series of the magnetic field vector in the solar wind, $\boldsymbol{B}(t)$, one first adopts the Taylor hypothesis, i.e., $\boldsymbol{B}(r) = \boldsymbol{B}(r_0 - u_r t)$, where r is the radial coordinate and $u_r \approx 800\,{\rm km\,s}^{-1}$ is the solar wind speed in the r direction at high solar latitudes. Next, one makes use of the isotropic representation of the Fourier-transformed two-point correlation tensor (Moffatt 1978; Matthaeus & Goldstein 1982)

$$\langle \hat{B}_i(\boldsymbol{k}) \hat{B}_j^*(\boldsymbol{k}') \rangle = \left[\left(\delta_{ij} - \hat{k}_i \hat{k}_j \right) 2\mu_0 E_{\rm M}(k) - {\rm i} k_l \epsilon_{ijl} H_{\rm M}(k) \right] \frac{\delta^3(\boldsymbol{k} - \boldsymbol{k}')}{8\pi k^2} \tag{3.1}$$

where $E_{\rm K}(k)$ and $H_{\rm M}(k)$ are again the magnetic energy and magnetic helicity spectra. Matthaeus & Goldstein (1982) analyzed Voyager data, but Voyager 1 and 2 were close to the ecliptic in the data analyzed, so the helicity fluctuated around zero. The work of Brandenburg et al. (2011b) used data from *Ulysses*, which flew over the poles of the Sun. They showed that $H_{\rm M}(k)$ changes sign at the ecliptic, as expected, but it is positive at small scales; see figure 5. Thus, we see that the sign of magnetic helicity is the other way around than what is expected in the dynamo interior and at found at the solar surface.

Simple numerical models of Warnecke et al. (2011, 2012) and Brandenburg et al. (2017a) confirm the sign change of magnetic helicity between the dynamo interior and

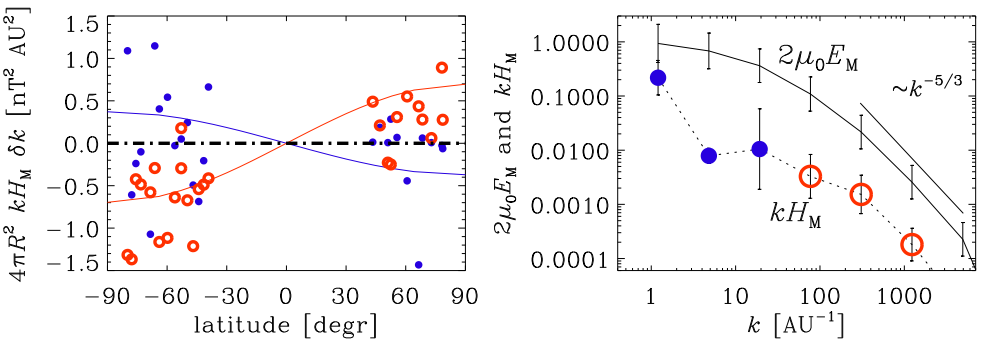

FIGURE 5. *Left*: Latitudinal dependence of spectral magnetic helicity for $k = 300\,\mathrm{AU}^{-1} \approx 2\times10^{-3}\,\mathrm{Mm}^{-1}$ (open red symbols) and $k = 1.2\,\mathrm{AU}^{-1} \approx 10^{-5}\,\mathrm{Mm}^{-1}$ (filled blue symbols). *Right*: magnetic helicity spectrum for heliocentric distances above 2.8 AU for the northern hemisphere, where filled blue symbols denote negative values and open red ones positive values.

the halo. Thus, for the Sun, we expect a similar sign change to occur somewhere above the surface, and perhaps already within the corona. This question can hopefully soon be addressed observationally, possibly with the help of the Faraday rotation technique developed in Brandenburg & Stepanov (2014) and applied to the solar corona in Brandenburg et al. (2017a) or with NASA's *Parker Solar Probe* or with ESA's *Solar Orbiter*.

Realistic corona simulations by Bourdin et al. (2013) have now shown that this magnetic helicity reversal occurs when the magnetic plasma beta drops below unity Bourdin et al. (2018), i.e., when the plasma becomes dominated by magnetic pressure compared with the gas pressure. Brandenburg et al. (2011b) explained this reversal by a subdominance of the α effect compared with turbulent diffusion. An alternative explanation was offered by Warnecke et al. (2012), who argued that a turbulent-diffusive magnetic helicity flux down the gradient of the local magnetic helicity density can result in its sign change, because, unlike temperature, magnetic helicity density is not sign-definite. Whether any of these explanations is right needs to be seen.

3.3. *The solar dynamo dilemma*

The solar dynamo dilemma was posed by Parker (1987) in response to the then emerging helioseismological result that the Sun's internal angular velocity, $\Omega(r,\theta)$, increases outward, i.e., $\partial\Omega/\partial r > 0$, where r is radius and θ colatitude. This was found to be the case in the bulk of the convection zone and especially in the lower overshoot layer, also known as the tachocline. The Parker–Yoshimura rule for the migration direction of $\alpha\Omega$ dynamo waves states that waves migrate in the direction

$$\boldsymbol{\xi}_{\rm migration} = -\alpha\hat{\boldsymbol{\phi}}\times\boldsymbol{\nabla}\Omega, \tag{3.2}$$

where $\hat{\boldsymbol{\phi}}$ is the unit vector in the azimuthal direction. It was based on the original paper of Parker (1955a) and generalized in a coordinate-independent way by Yoshimura (1975). Indeed, already the first global and fully selfconsistent convective dynamo simulations of Gilman (1983) and Glatzmaier (1985) showed poleward migration and this has been confirmed in subsequent simulations; see, e.g., Käpylä et al. (2010). Not surprisingly, corresponding mean-field dynamos with selfconsistently generated differential rotation driven by the Λ effect (Rüdiger 1980, 1989; Rüdiger & Hollerbach 2004) with magnetically modulated convective energy fluxes (Brandenburg et al. 1992a) also confirmed this somewhat disappointing result.

Several possible solutions out of the solar dilemma have been proposed; see the reviews by Solanki *et al.* (2006), Miesch & Toomre (2009), and Charbonneau (2010). Choudhuri et al. (1995) have shown that the Sun's meridional circulation can turn the dynamo wave around and produce equatorward migration owing to the local circulation speed at the bottom of the convection zone where it is believed to point equatorward. This type of model is now referred to as Babcock–Leighton flux transport dynamo (Dikpati & Charbonneau 1999), but it can only work if the turbulent magnetic diffusivity η_t is low enough. This is already a problem, because η_t should be more than ten times smaller than what is expected from mixing length theory (Krivodubskii 1984). Furthermore, the induction zones of α effect and differential rotation must be non-overlapping. This is also not really borne out by simulations. Indeed, when the induction zones are non-overlapping, meridional circulation was always found to lead to a suppression of the dynamo, i.e., the dynamo becomes harder to excite (Rädler 1986a). Another approach is to adopt a dynamo that attains its equatorward migration from the near-surface shear layer. This is a layer in the top 40 Mm of the Sun, where $\partial\Omega/\partial r < 0$, which causes equatorward migrating dynamo waves when α is positive in the northern hemisphere (Brandenburg 2005a). Such a dynamo model has been developed by Pipin & Kosovichev (2011); Pipin (2017).

Cameron & Schüssler (2017) have presented an updated version of the one-dimensional phenomenological dynamo model of Leighton (1969) by including a number of effects such as the evolution of the radially integrated toroidal magnetic field, the latitudinal variation of the surface angular velocity, turbulent downward pumping, and some other features. Using surface magnetic field observations, Cameron & Schüssler (2015) showed that the emerged magnetic flux at the solar surface controls the net toroidal magnetic flux generated in each hemisphere. This allowed Cameron et al. (2018) to compute maps of poloidal and toroidal magnetic fields of the global solar dynamo.

Global simulations continue to have a hard time reproducing not only the near-surface shear layer with $\partial\Omega/\partial r < 0$, but also the approximately spoke-like angular velocity contours throughout the deeper parts of the convection zone and of course the equatorward migration of the sunspot belts. Whether or not they are explicable in terms of the Parker–Yoshimura rule needs to be seen.

The butterfly diagram derived from the simulations of Käpylä et al. (2012, 2013) look convincing, but here an equatorward dynamo wave results from a local minimum of the differential rotation at mid-latitudes (Warnecke et al. 2014). Another possibility was proposed by Augustson et al. (2015), who also found equatorward migration. They argued this to be the result of nonlinearity. More detailed analysis would be needed to clarify the true reason behind equatorward migration in those models. Furthermore. the angular velocities of all these models exceed that of the Sun by at least a factor of three (Brown et al. 2011), although simulations with the EULAG code (Ghizaru et al. 2010; Racine et al. 2011) seem to produce cyclic solutions already at the solar angular velocity. Larger angular velocities were also used by Käpylä et al. (2013) and Käpylä et al. (2017a), who compared differences in the parameters used in the models of different groups.

All the global simulations have certain shortcomings that we need to be aware of when assessing their overall validity. Firstly, the differential rotation of the near-surface shear layer is not yet well developed, although the recent simulations of Hotta et al. (2014, 2015, 2016) at very high resolution could be promising. Second, the contours of constant angular velocity are still distinctly cylindrical and not spoke-like, as found from helioseismology (Schou et al. 1998). Whether this mismatch in the angular velocity contours between simulations and observations implies also a problem for the solar dynamo remains an open question, however. Not only the contours of angular velocity are distinctly cylindrical in

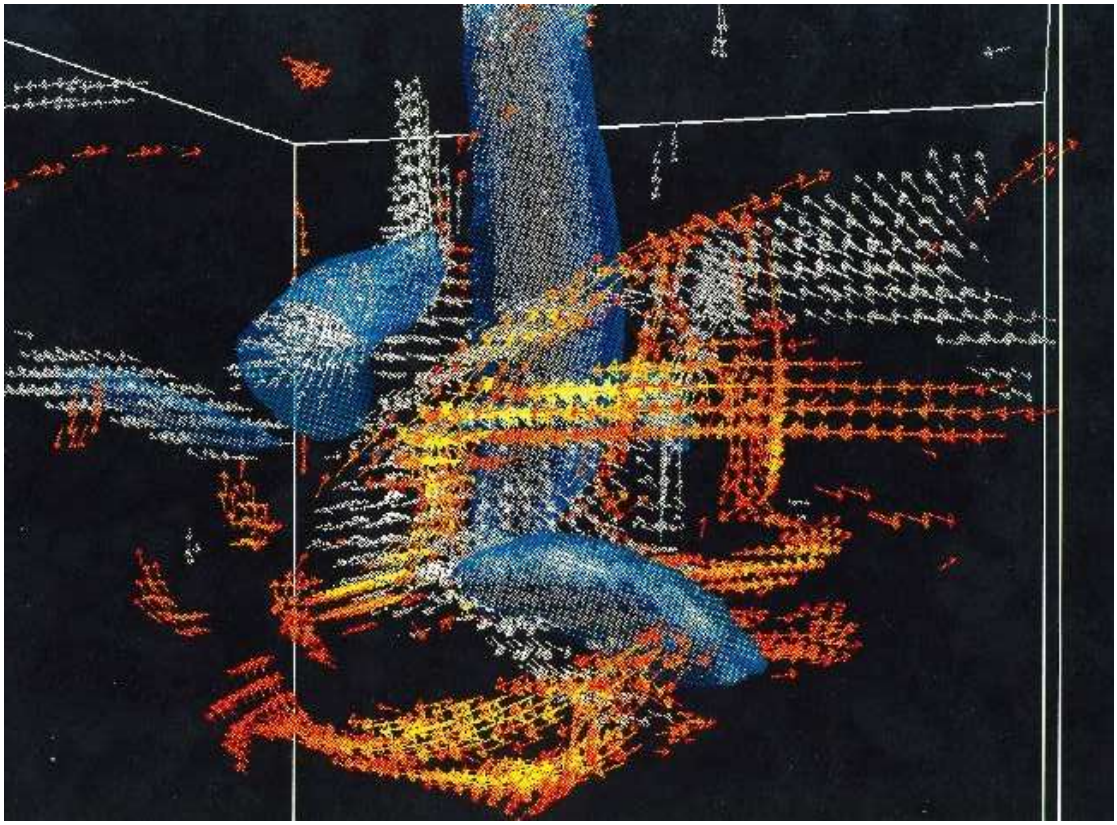

FIGURE 6. Vorticity vectors $\boldsymbol{\omega}$ (from gray to white as $|\boldsymbol{\omega}|$ increases) and magnetic field vectors $\boldsymbol{B}$ (from red to yellow as $|\boldsymbol{B}|$ increases). Only vectors whose strength exceeds a threshold of three times the rms value are plotted. An isosurface of constant pressure fluctuation is shown in blue and it is seen to encompass some of the vortex tubes, especially the one around the cyclonic down draft descending from the middle of the domain. Magnetic flux tubes are seen to be wrapped around the spinning downdraft and are being pushed down, which is the effect of downward pumping Adapted from Brandenburg & Tuominen (1991).

simulations, but also the streamlines of meridional circulation do not correspond to a single or double cell, as seen in some helioseismic inversions (Zhao et al. 2013). This might not be a problem for the dynamo that is shaped by the near-surface shear layer, but it would be a problem for the flux transport dynamo models.

3.4. *Downward pumping versus turbulent diamagnetism*

Downward pumping was clearly seen in the numerical dynamo simulations of turbulent convection; see figure 6 of an early review on this by Brandenburg & Tuominen (1991) and the work of Nordlund et al. (1992) and Brandenburg et al. (1996). Tobias et al. (1998b) and Tobias et al. (2001) quantified many aspects of pumping in dedicated numerical experiments.

The simulations mentioned above were not very deep, so τ does not change significantly between top and bottom of the domain. Therefore, the difference between

$$\gamma = \begin{cases} -\frac{1}{6}\tau\boldsymbol{\nabla}\overline{\boldsymbol{u}^2} & \text{(if } \tau \text{ is outside the gradient),} \\ -\frac{1}{2}\boldsymbol{\nabla}(\frac{1}{3}\tau\overline{\boldsymbol{u}^2}) \equiv -\frac{1}{2}\boldsymbol{\nabla}\eta_{\rm t0} & \text{(if } \tau \text{ is under the gradient),} \end{cases} \tag{3.3}$$

is not yet significant. Theoretically, it is not clear which of the two formulations is the correct one. The former version was obtained by Rädler (1969), but a variation of τ was not explicitly considered. The latter version was obtained by Roberts & Soward (1975). Near the surface of the Sun, $\eta_{\rm t0}$ increases with depth (Krivodubskii 1984), so $\gamma=-\frac{1}{2}\boldsymbol{\nabla}\eta_{\rm t}$ would point upward, but $\overline{\boldsymbol{u}^2}$ decreases with depth, so $\gamma=-\frac{1}{6}\tau\boldsymbol{\nabla}\overline{\boldsymbol{u}^2}$ would point downward, which would be in agreement with the simulations.

This question has implications on whether or not the γ effect can be understood as turbulent diamagnetism, because we could then write

$$-\boldsymbol{\gamma}\times\overline{\boldsymbol{B}}-\eta_{\rm t}\mu_0\overline{\boldsymbol{J}}=-\eta_{\rm t}^{1/2}\,\boldsymbol{\nabla}\times\left(\eta_{\rm t}^{1/2}\,\overline{\boldsymbol{B}}\right), \tag{3.4}$$

where $\eta_{\rm t}^{1/2}$ would play the role of both a renormalized magnetic diffusivity and a renormalized magnetic permeability.

Mean-field simulations have long shown a significant effect of pumping the migration of the dynamo wave (Kitchatinov 1991; Brandenburg et al. 1992b). Significant equatorward pumping near the surface and poleward pumping deeper down was recently found in global test-field calculations (Warnecke et al. 2018). This is obviously contrary to what is expected from flux-transport dynamos, but one should remember that none of the global convective dynamo simulations have ever reproduced features of flux-transport dynamos, nor have they reproduced features of the solar dynamo for that matter.

There is also topological pumping (Drobyshevskij & Yuferev 1974). It has been applied to convection, where the up- and downflows tend to occupy distinct regions in each horizontal plane. The effective pumping velocity depends only on the vertical flow in horizontally connected regions, which we refer to as flow lanes. For example near the surface we have horizontally connected downflow lanes, so pumping would be downward. In the deeper layers, however, the downdrafts are isolated and the upwellings are horizontally connected, so topological pumping would here be upward. Numerical simulations have confirmed this effect (Arter 1983) and have been applied to what is known as the fountain flow in galaxies (Brandenburg et al. 1995).

As seen above, many of the turbulent transport coefficients have both kinetic and magnetic contributions. For example, the α effect has both kinetic and current helicities, and the turbulent pumping effect also has two contributions, namely $\gamma=-\frac{1}{6}\tau\boldsymbol{\nabla}(\overline{\boldsymbol{u}^2}-\overline{\boldsymbol{b}^2}/\mu_0\rho_0)$, but the turbulent magnetic diffusivity has only one, i.e., $\eta_{\rm t}=\frac{1}{3}\tau\overline{\boldsymbol{u}^2}$. This was been shown by Rädler, et al. (2003); see also Brandenburg & Subramanian (2005a) for a review. However, one should be aware that this result is a consequence of the second order correlation approximation and the assumption of isotropy, and has not yet been confirmed with the test-field method. It is simply another one of the open question in mean-field theory.

3.5. *Contributions to the α effect*

There is a related uncertainty regarding the α effect. In the original derivation of Steenbeck et al. (1966), α was proportional to the gradient of $\ln\rho u_{\rm rms}$. The α effect also depends on the angular velocity, so the full expression can then be written in the form

$$\alpha=\ell^2\boldsymbol{\Omega}\cdot\boldsymbol{\nabla}\ln(\rho^\sigma u_{\rm rms}), \tag{3.5}$$

where ℓ is the correlation length of the turbulence and σ is an exponent that characterize the importance of density stratification relative to velocity stratification. Rüdiger & Kitchatinov (1993) confirmed $\sigma=1$ for rapid rotation, but found $\sigma=3/2$ for slow rotation. Recent work using the test-field method now shows that $\sigma=1/2$ for forced turbulence and convection with strong density stratification, while for supernova-driven

turbulence $\sigma = 1/3$ was found Brandenburg et al. (2013). In any case, contrary to the earlier scaling, σ is always less than unity.

We clearly see that at the equator, the rotation and stratification vectors are at right angles to each other, so $\alpha = 0$. It is important to realize, however, that a nonvanishing α is in principle also possible at the equator if α is the result of an instabilities, whose eigenfunctions are helical. The sign of the helicity and the α effect depends then on the initial conditions. This has been demonstrated both for the magnetobuoyancy instability (Chatterjee et al. 2011) and for the Tayler instability (Gellert et al. 2011; Bonanno et al. 2012). Even though the growth rates are the same for both signs of helicity, only one sign will survive in the nonlinear regime owing to what is called mutual antagonism in the related application of spontaneous chiral symmetry breaking leading finite handedness of biomolecules at the origin of life (Frank 1953).

The presence of α in a system affects also the turbulent magnetic diffusivity. This was not theoretically expected, but it is easy to see that such a term is theoretically possible. Brandenburg et al. (2017d) showed that, for intermediate values of $R_{\rm m}$, $\eta_{\rm t}$ *decreases* by almost a factor of two. This may not be very much in view of other uncertainties known astrophysical turbulence, but it can be important enough to make a difference in theoretical studies, where reasonably accurate estimates of turbulent diffusivity are now available.

3.6. *Buoyant flux tubes*

The notion of flux tubes was quite popular since Parker's other early work of 1955, when he argued that bipolar regions at the solar surface can be explained by flux tubes piercing the surface. This appeared quite plausible, given that the anticipated depth of those flux tubes was expected to be about 20 Mm (Parker 1955b). In that case, the depth of flux tubes and the separation of bipolar regions would be comparable, but in subsequent years, Parker (1975) argued for a storage depth of magnetic flux tubes of about 200 Mm, which is the bottom of the convection zone. This makes the flux tube picture much harder to accept, because flux tubes not only expand during their ascent, but their dynamics is rather complicated and by no means as simple as that of a garden hose sweeping through the air and then piercing the roof of a tent. This was demonstrated in numerous simulations (Fan 2001, 2008, 2009; Hood et al. 2009; Syntelis et al. 2015).

Some success of the flux tube picture has however been noted. In some of those cases, the magnetic flux tubes are analogous to the vortex tubes seen in the direct numerical simulations of She et al. (1990). The meshpoint resolution of 96^3 used at the time was moderate by nowadays standards. In figure 7 we reproduce a snapshot from a dynamo simulation where a cooling layer was included at the top. One sees buoyant flux tubes having reached the surface in various places. However, saying that these are the tubes that make a sunspot pair would be rather optimistic, because those magnetic tubes are analogues to the vortex tubes in turbulence and have radii comparable to the resistive length (Brandenburg et al. 1995), so they only look solar-like because those simulations did not yet have large resolution.

There are more recent simulations displaying flux tubes, but those were displayed differently; not as vectors whose strengths exceeds a certain threshold, but as field lines integrated along any local field vector—regardless of its strength (Nelson et al. 2013, 2014; Nelson & Miesch 2014). Therefore, it is not obvious that such visualizations automatically imply any agreement with Parker's original picture.

One more point is in order here. The idea about flux tube storage mention by Parker (1975) is an aspect that has not been verified or is seen in simulations; see the simulations of Guerrero & Käpylä (2011) for an attempt to amplify magnetic flux at the bottom of the

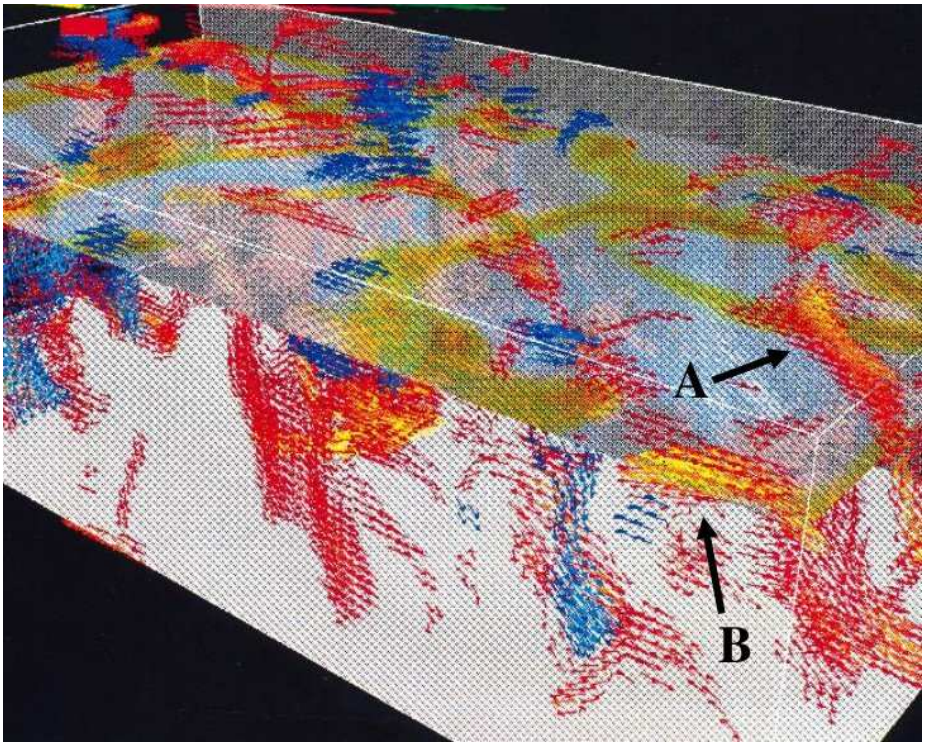

FIGURE 7. Magnetic field vectors (red to yellow) and vorticity vectors (blue) for a convectively driven dynamo in an elongated domain with a radiative cooling layer above a surface marked with a transparent visualization of temperature. Note the appearance of flux tubes crossing the surface (see the positions marked with A and B).

convection zone. And important ingredient of flux transport dynamos is the induction effect at the surface that is supposedly caused by the decay of tilted active regions (Babcock 1961; Leighton 1969). If these effects really operate, one should be able to verify them in a dedicated simulation using the test-field method. This has not yet been done.

3.7. *Surface flux transport models*

In spite of the problems encountered in modeling the solar dynamo, there has been some success in modeling the advection of active regions using what is called the surface flux transport model (see, e.g., Hickmann et al. 2015). This is a two-dimensional model that ignores the dynamics in the vertical direction. That this actually works is remarkable and suggests that active regions just "float" at the surface. Such models are perhaps the best we have to predict the magnetic field after it disappeared on the far side of the Sun. Of course, it is not a model of the solar dynamo because it assimilates continuous input from observations.

The fact that active regions appear to *float* at the solar surface might well be consistent with them being locally maintained entities at or just beneath the surface. The one process that is known to lead to magnetic flux concentrations of that type is the negative effective magnetic pressure instability (NEMPI); see Brandenburg et al. (2016) for a review. This is a mean-field process in the momentum equations, where the Reynolds and Maxwell stresses attain a component proportional to $\overline{\boldsymbol{B}}^2/2\mu_0$, which acts effectively like a negative pressure by suppressing the turbulent pressure; see van Ballegooijen (1984) for

early ideas along similar lines of thought. Mean-field investigations started with Kleeorin et al. (1989, 1990, 1993, 1995, 1996) and Kleeorin & Rogachevskii (1994), while the first simulations of the mean-field equations were produced by Brandenburg et al. (2010, 2012a) and Kemel et al. (2012). This effect was also detected in various direct numerical simulations (Brandenburg et al. 2011a; Kemel et al. 2012, 2013). The formation of bipolar regions from NEMPI was first studied by Warnecke et al. (2013, 2016).

NEMPI has a number of properties that affect negatively its role in explaining magnetic flux concentrations in the Sun. One is rotation: already rather small Coriolis numbers well below unity suppress the instability (Losada et al. 2012, 2013). NEMPI has also not been found in convection (Käpylä et al. 2016), which is possibly due to insufficient scale separation in their simulations. However, more detailed work showed that the derivative of the effective magnetic pressure with respect to the mean magnetic field was found to have an unfavorable sign for the onset of NEMPI. Furthermore, radiation transport was found to make the onset of NEMPI oscillatory and the width of the eigenfunctions about ten times smaller (Perri & Brandenburg 2018). Even if NEMPI were excited, the flux concentrations are too weak to produce sunspots. An alternative possibility that has been discussed in the past is the suppression of the convective heat flux by magnetic fields. This could lead to a large-scale instability (Kitchatinov & Mazur 2000). Unfortunately, not enough is known about this possibility, nor has it been detected in direct numerical simulations as yet.

3.8. *The convective conundrum*

Over the past few decades, numerous simulations have demonstrated how difficult it is to reproduce the Sun (Gilman 1983; Brown et al. 2011; Nelson et al. 2013); see also Miesch & Toomre (2009) for a review. If it is true that the solar dynamo is driven by the velocity field in the Sun, one wonders what exactly is "wrong" with it. That something is not quite right is immediately evident when comparing the contours of constant angular velocity from helioseismology with those from simulations; see Thompson et al. (2003) for a review and the discussion in § 3.3.

A more subtle discrepancy is that the horizontal scales of convection are observed to be much smaller that what is seen in convection. This phenomenon was called the convective conundrum (O'Mara et al. 2016). Global convection simulations of Miesch et al. (2008) predict giant cells that are not observed. Helioseismological observations with the time-distance method predict very low velocities at those scales (Hanasoge et al. 2010, 2012, 2016), but this, in turn, could also be an artifact of excessive noise reduction (Greer et al. 2015).

From a theoretical point of view, one problem is that all global simulations of convection assume a prescribed unstable layer of about 200 Mm depth. This is not realistic and in reality the deeper layers are convecting only because of strong mixing driven by the surface motions (Spruit 1997; Brandenburg 2016; Käpylä et al. 2017b). Thus, the depth of the convection zone should be a sensitive function of the vigor of convection in the surface layers.

The deeper layers may not transport the convective flux based on a superadiabatic gradient, as assumed in standard mixing length theory (Vitense 1953), but based on another term suggested first by Deardorff (1966, 1972) in the geophysical context and applied to the solar context by Brandenburg (2016). The calculation is analogous to that presented in § 2.4, but instead of equations (2.10) and (2.19), we now have

$$\frac{\partial s}{\partial t} = -\boldsymbol{u}\cdot\boldsymbol{\nabla}\overline{S} + \dots\,, \quad \text{and} \quad \frac{\partial \boldsymbol{u}}{\partial t} = -\boldsymbol{g}s/c_p + \dots\,, \tag{3.6}$$

where $S = \overline{S} + s$ is the specific entropy separated into mean and fluctuating parts, $\boldsymbol{g}$ is gravity, and c_p is the mean specific heat at constant pressure. Computing the correlation $\overline{\boldsymbol{\mathcal{F}}} = \overline{s\boldsymbol{u}}$, which is proportional to the mean convective energy flux, we have, analogously to equation (2.20), two terms, which are now

$$\frac{\partial \overline{\boldsymbol{\mathcal{F}}}}{\partial t} = \overline{\boldsymbol{u}\dot{s}} + \overline{\dot{\boldsymbol{u}}s}. \tag{3.7}$$

The first ones leads to the usual negative gradient contribution, $-\tau\overline{u_i u_j}\nabla_j \overline{S}$, but there is a second term, $-\tau\boldsymbol{g}\overline{s^2}/c_p$, which is the Deardorff term; see Brandenburg (2016) for details. This term is always in the negative direction of gravity and proportional to the square of the specific entropy fluctuation. The enthalpy flux is thus the sum of a gradient term proportional to the usual superadiabatic gradient and a Deardorff term.

A full mean-field model of the Sun must include hydrodynamics and thermodynamics (Brandenburg et al. 1992a; Rempel 2005). Such models were considered by Tuominen & Rüdiger (1989), who found what appeared to be a new instability of the full system of equations; see Rüdiger & Spahn (1992) for its detailed investigation. However, this turned out to be essentially a Rayleigh-Benárd type instability (Tuominen et al. 1994). It could potentially be stabilized by having a turbulent viscosity and a turbulent thermal diffusivity that are large enough. Alternatively, of course, it could be stabilized by a sufficiently small or even negative superadiabatic gradient, which would naturally occur in the Deardorff-type convection discussed in § 3.8.

Global simulations using a more realistic opacity prescription result in extended subadiabatic layers (Käpylä et al. 2018). They also lead to significant latitudinal specific entropy gradients, which are known to alleviate the tendency to form cylindrical contours of constant angular velocity arising from the Taylor-Proudman theorem (Rüdiger 1989; Brandenburg et al. 1992a). Clearly, more work in that direction is needed to clarify the role and origin of these extended subadiabatic layers.

3.9. *Solar equatorward migration from an oscillatory α^2 dynamo*

Another idea that has been discussed is that the equatorward migration could be caused by an α^2 dynamo. Stefani & Gerbeth (2003) found oscillatory α^2 dynamos for a nonuniform α distribution in the radial direction. Later, Mitra et al. (2010a) found an oscillatory α^2 dynamo with equatorward migration in a model with a change of sign of α across the equator. It was therefore thought that a gradient in the kinetic helicity was the reason behind the oscillatory nature of the dynamo and thus equatorward migration. Käpylä et al. (2013) investigated the phase relation between toroidal and poloidal magnetic fields in their oscillatory convectively driven dynamo with equatorward migration and found a phase shift of $\pi/2$, which is compatible with what is expected for an oscillatory α^2 dynamo. Masada & Sano (2014) confirmed this finding for a dynamo in Cartesian geometry and reinforced the suggestion that the solar dynamo might indeed be of α^2 type. Then, Cole et al. (2016) found that the oscillatory α^2 dynamo requires highly contacting plasma at high latitudes or, alternatively, a perfectly conducting boundary condition at high latitudes, as is often assumed in spherical wedge simulations (Mitra et al. 2009). This was then confirmed through the realization that an oscillatory migratory α^2 dynamo is possible even with constant α effect provided there are two different boundary conditions on the two sides (Brandenburg 2017). With this realization, the idea of a solar α^2 dynamo now begins to sound somewhat artificial. The best use of such a model might therefore now be the application to studying magnetic helicity fluxes, as discussed in § 2.14.

4. Stellar dynamos

Cycles like the 11 year sunspot cycle are known to exist on other main sequence stars with outer convection zones. Stellar activity cycles are usually detected in the calcium H&K lines which form in chromospheric magnetic loops in emission (Wilson 1978). This was already known since the early work of Eberhard & Schwarzschild (1913). Some cycles are also seen in X-rays and in extreme ultraviolet, for example that of α Cen A (Ayres 2009, 2015). For some stars, it has also been possible to observe surface magnetic fields directly through Zeeman Doppler imaging. An example is HD 78366, where it has been possible to see a sign reversal of the magnetic field on a ~ 2 years timescale (Morgenthaler et al. 2011), which was not evident from just the times series (Brandenburg et al. 2017b). Unfortunately, Zeeman Doppler imaging requires many nights on big telescopes with high-resolution spectrographs. It them becomes prohibitive to cover many epochs, which is a serious disadvantage over the more regularly spaced light curve observations. On the other hand, neither circular nor linear polarization has been detected on α Cen A, indicating the absence of a net longitudinal magnetic field stronger than 0.2 G (Kochukhov et al. 2011), which was puzzling.

4.1. *Stellar cycle frequency, rotation, and activity*

It has been known for some time that stellar activity increases with increasing rotation rate up to a certain point above which it saturates. However, to be able to compare different stellar types with different convective turnover times ranging from $\tau = 7$ to 26 days between F7 and K7 dwarfs, it was found to be useful to normalize the rotation period by τ. Indeed, the dependence of stellar activity on rotation period $P_{\rm rot}$ is well described by $P_{\rm rot}/\tau$ (Vilhu 1984; Noyes et al. 1984a), which is referred to as the Rossby number in stellar astrophysics. Note, however, that in astrophysical fluid dynamics the inverse Rossby number or Coriolis number is defined as $2\Omega\tau$, which is larger than $\tau/P_{\rm rot}$ by a factor of 4π because of $P_{\rm rot} = 2\pi/\Omega$ and the factor of two in the Coriolis force.

Another source of discrepancy is connected with the definition of τ. In observational stellar astrophysics, one routinely uses the turnover time one pressure scale height above the bottom of the convection zone. Thus works well in the sense that the Rossby number defined in that way is found to control the chromospheric stellar activity with relatively little scatter (Noyes et al. 1984a). In theoretical models, one often uses the rms velocity based on the entire convection zone together with a rudimentary estimate of the wavenumber of the energy-carrying eddies; see Käpylä et al. (2013).

It is unclear how large the Rossby number of the Sun really is, because solar-like differential rotation is currently only obtained for somewhat faster rotation rates than what is expected based on the actual numbers. According to observations, the transition point may be at $P_{\rm rot}/\tau \approx 2$, but simulations suggest that this happens at a two times larger value angular velocity than that of the Sun.

Let us now turn to the cycle frequency. Early work of Noyes et al. (1984b) indicated that the cycle frequency, $\omega_{\rm cyc} = 2\pi/P_{\rm cyc}$, with $P_{\rm cyc}$ being the activity cycle period (not the magnetic Hale cycle period), increases with rotation frequency $\Omega = 2\pi/P_{\rm rot}$ like a power law,

$$\omega_{\rm cyc} \propto (\Omega\tau)^{\nu}, \tag{4.1}$$

with $\nu = 1.25$. Using simple dynamo models in a single mode (or one-mode) approximation, they compared three different nonlinearities (α quenching, quenching of differential rotation, and magnetic buoyancy), and found that only the magnetic buoyancy nonlinearity was within certain limits compatible with the observational result. By contrast, Kleeorin et al. (1983) found an almost perfect agreement with a linear free wave model

which maximizes the growth rate. However, this model remained unsatisfactory, because it is natural that a dynamo is nonlinearly saturated.

In another approach, Brandenburg et al. (1998) argued that both α and η_t are nonlinear functions of the modulus of the magnetic field B of the form $\propto |B|^n$ and $\propto |B|^m$, respectively. Again, their models were based on a single mode approximation. Interestingly, when such a model is solved without this restriction, it no longer reproduced the same result. Regarding magnetic buoyancy, it is important to emphasize that the modeling of this phenomenon in the one-mode approximation is necessarily *ad hoc*. In the two-dimensional models of Moss et al. (1990), magnetic buoyancy was modelled as a mean upward drift, i.e., as a $\boldsymbol{B}$-dependent γ effect. This was an idea that was communicated to the authors by K.-H. Rädler. The consequences for the cycle period are not known however. Brandenburg et al. (1998) argued therefore that the one-mode assumption might not actually be a "restriction," but a physical feature of such a model. This can qualitatively be explained by models with spatial nonlocality, where only the lowest wavenumbers contribute to $\overline{\boldsymbol{\mathcal{E}}}$ in Fourier space.

4.2. *Antiquenched stellar dynamos*

The reason for the anticipated antiquenching is easily understood when one considers the expression for the cycle frequency of an $\alpha\Omega$ dynamo (Stix 1974)

$$\omega_{\rm cyc} \approx \sqrt{\alpha\Omega'}, \tag{4.2}$$

where $\Omega' = {\rm d}\Omega/{\rm d}r$ is the radial angular velocity gradient. Assuming furthermore that $\alpha \approx \Omega\ell$ with $\ell = \ell(B)$ being an effective correlation length and $\Omega' = g\Omega/r$ with $g(B)$ being a nondimensional shear gradient, we see that $\omega_{\rm cyc}/\Omega = \sqrt{g\ell/r}$ is independent of Ω and depends only on the magnetic field, providing thereby a direct representation of α quenching.

The magnetic activity of late-type stars is usually measured by the normalized chromospheric Ca II H+K line emission, $R'_{\rm HK}$ (e.g., Vilhu 1984; Noyes et al. 1984a). Furthermore, the work of Schrijver et al. (1989) has shown that

$$R'_{\rm HK} \propto (B/B_{\rm eq})^\kappa \tag{4.3}$$

with $\kappa \approx 1/2$; see also Schrijver (1983). Therefore, measuring the slope ν in the representation of $\omega_{\rm cyc}/\Omega \propto R'^{\,\mu}_{\rm HK}$ gives us insight into the quenching dependence of $\alpha(B)$. Figure 8(a) shows the frequency ratio $\omega_{\rm cyc}/\Omega$ with two separate fits, as proposed by Brandenburg et al. (1998, 2017b). Since $\omega_{\rm cyc}/\Omega$ increases with increasing values of $R'_{\rm HK}$, i.e., since $\nu > 0$, the exponent n must also be positive. Specifically, we have $n = 2\nu\kappa \approx \nu$. Observations indicate that $\nu \approx 0.5$, and therefore also $n \approx 0.5$, but it could be somewhat larger if g increases with Ω, which is an additional complication that can be accounted for; see Brandenburg (1998b) and Brandenburg et al. (1998) for details.

The exponent m is constrained by the balance between the destabilizing contribution, which, for an $\alpha\Omega$ dynamo, is again proportional to $\sqrt{\alpha\Omega'} \propto |B|^{n/2}$, and the dissipating contribution proportional $\eta_t/L^2 \propto \tau^{-1} \propto |B|^m$. Since τ enters in the expression for the Rossby number, $P_{\rm rot}/\tau$, which is proportional to $R'^{\,\mu}_{\rm HK}$ with $\mu \approx 1$ (Brandenburg et al. 1998), we have $m = (\nu + 1/\mu)\,\kappa \approx 0.75$.

As is clear from the explanations above, theoretical models reproduce a growing $\omega_{\rm cyc}/\Omega$ ratio with increasing $|B/B_{\rm eq}|$ only with antiquenching and nonlocality. However, this does not happen in the usual mean-field dynamo models. Also, three-dimensional global convective dynamo simulations (Strugarek et al. 2017; Warnecke 2017) do not reproduce this trend, which is why they argue that the correct representation has actually a negative slope in the $\omega_{\rm cyc}/\Omega$ versus $R'_{\rm HK}$ diagram, as shown in figure 8(b). To resolve this conflict,

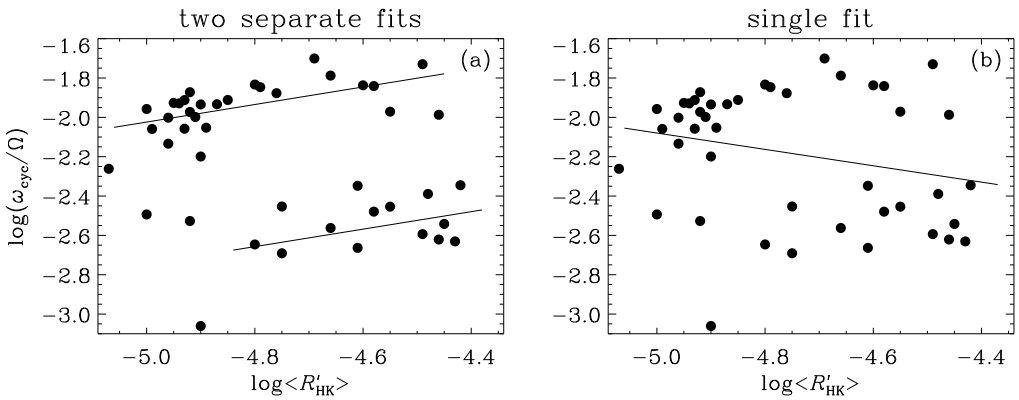

FIGURE 8. Cycle to rotation frequency ratios for all primary and secondary cycles versus $R'_{\rm HK}$ discussed in Brandenburg et al. (2017b) along with their two separate fits for long and short cycles (left) compared with the same frequency ratios and a general single fit through all cycle ratios (right).

more accurate cycle data are needed to be able to tell whether the correct slope in figure 8 is positive or negative. This uncertainty is caused by the fact that there is no agreement whether there are two distinct branches with a positive slope and not just one with a negative slope.

Böhm-Vitense (2007) plotted not the $\omega_{\rm cyc}/\Omega$ ratio, but $\omega_{\rm cyc}$ versus Ω and found an approximately linear slope, which would suggest that the $\omega_{\rm cyc}/\Omega$ ratio would actually be constant, i.e., $\nu = 0$ instead of $\nu = 0.5$, as found from almost the same data. She also suggested that the two branches could correspond to two dynamos operating simultaneously at two different locations. Evidence for different dynamo modes in a convection simulation was presented by Käpylä et al. (2016); Beaudoin (2016). This interpretation was also adopted by Brandenburg et al. (2017b), who found that many stars with ages younger than 2.3 Gyr might exhibit both short and long cycles. In fact, they examined altogether 11 stars with double cycles. They also computed cycle periods based on the observed $R'_{\rm HK}$ and $P_{\rm rot}$ values that would be expected if the cycle periods would fall exactly onto each of the two branches. In some cases, it became clear that secondary periods could not have been observed because the cadence was too long or the time series was not long enough. The stars on the two branches with larger and shorter cycle periods have traditionally also been referred to as active and inactive branch stars. This interpretation can be justified by noting that longer (shorter) cycle periods are more (less) pronounced when $R'_{\rm HK}$ is larger.

In addition to the two branches discussed above, there is also another branch for superactive stars, where $\omega_{\rm cyc}/\Omega$ does indeed decline with increasing activity. All the convectively driven dynamo simulations in spherical shells seem to reproduce this branch qualitatively rather well. Indeed, one could argue that none of those models reflects the Sun and that it really operates in a different regime than what has been studied in spherical shell models so far, where one mainly sees a declining trend. However, looking again at figure 7 of Warnecke (2017), there is a short interval between the stars with antisolar-like differential rotation (his $\log {\rm Co} = 0.2$) and the declining branch (his $\log {\rm Co} = 0.7$), where the data points are compatible with an increasing trend, albeit with more noise.

A recent reanalysis of the Mt. Wilson data by (Olspert et al. 2018) now suggests that many of the double cycles may not be real. This conclusion was also reached recently by Boro-Saikia et al. (2018). Furthermore, the active branch no longer exhibit any signifi-

cant slope, and the disappearance of the multiple cycles between the branches appears spurious. Their method represents a marked methodological improvement of stellar cycle detection and will need to be looked at more seriously.

4.3. *Antisolar differential rotation*

The fact that the Sun's differential rotation is as it is, namely "solar-like" with a fast equator and slow poles is, in hindsight, somewhat surprising. Antisolar rotation has occasionally been seen in numerical simulations (Gilman 1977; Rieutord *et al.* 1994; Dobler et al. 2006) and has been associated with a dominance of meridional circulation (Kitchatinov & Rüdiger 2004). In fact, even simulations that are performed at the nominal solar rotation rate (Brown et al. 2011) have produced antisolar-like differential rotation, i.e., the equator rotates more slowly than the poles. Thus, it seems that there is something about the solar models that makes them being shifted in parameter space relative to the actual position of the Sun (Miesch et al. 2015). On the other hand, although we are able to reproduce solar-like differential rotation with a three-fold or five-fold larger Coriolis number, there are still other aspects not yet well reproduced, for example the equatorward migration of the sunspot belts or the contours of constant angular velocity.

Simulations of Karak et al. (2015) have shown that the magnetic activity increases again at low rotation rates, because the differential rotation becomes antisolar-like and that the absolute value of this differential rotation exceeds that of the solar-like value. There are now indications from the stars of the open cluster M67 that show an increasing trend for decreasing Coriolis numbers, supporting the qualitative predictions of the spherical global dynamo simulations (Giampapa et al. 2017; Brandenburg & Giampapa 2018). Unfortunately, no direct evidence for antisolar-like differential rotation on dwarfs is available as yet. With longer time series it might become possible to detect antisolar differential rotation through changes in the apparent rotation rate that would be associated with spots at different latitudes; see Reinhold & Arlt (2015) for details. So far, antisolar DR has only been observed in some K giants (Strassmeier et al. 2003; Weber et al. 2005; Kővári et al. 2015, 2017) and subgiants (Harutyunyan et al. 2016).

4.4. *Stellar surface magnetic field structure*

Mean-field models have long shown that the surface magnetic field structure does not always have to be of solar type, i.e., with a toroidal field that is antisymmetric about the equatorial plane (Roberts 1971). It could instead be symmetric about the equator, i.e., quadrupolar instead of dipolar. Yet another possibility is that the large-scale field is nonaxisymmetric, for example with a dominant azimuthal order of unity (Rädler 1973).

Early mean-field models of Roberts (1971) have demonstrated that quadrupolar mean fields are preferred when the dynamo operates in thin spherical shells. In principle, the break point where this happens should be for models that have convection zones that are somewhat thicker than that of the Sun. From that point of view, it is unclear why the Sun has an antisymmetric field and not a symmetric one. This problem is somewhat reminiscent of the problem of why the Sun has solar-like differential rotation at the solar rotation rate and not an antisolar-like, as theoretically expected. Thus, again, simulations of the solar dynamo seem to place the model in a position in parameters space that is shifted somewhat relative to what is theoretically expected. These two problems may even have a common origin, related, for example, to the convective conundrum (Lord et al. 2014; Cossette & Rast 2016; Featherstone & Hindman 2016), i.e., the lack of power at large length scales. This is possibly explained by stellar convection being dominated by thin downdrafts or threads which, in the Sun, result from the cooling near the surface

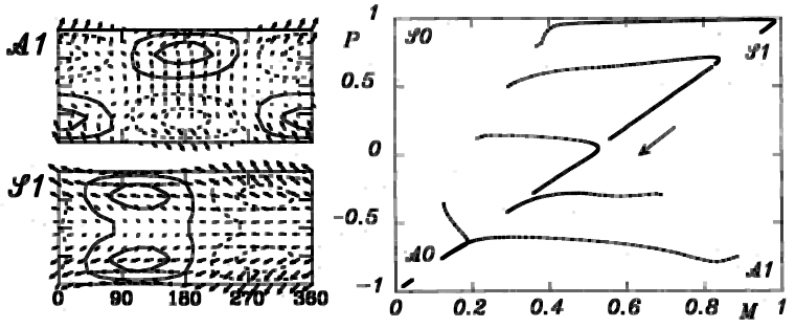

FIGURE 9. *Left*: Surface magnetic field structure of nonlinear nonaxisymmetric with an $m = 1$ azimuthal order for magnetic fields that are symmetric (S1) or antisymmetric (A1) about the equatorial plane. *Right*: Evolutionary tracks of solutions in the MP diagram. Adapted from Rädler et al. (1990).

(Spruit 1997). This leads to the phenomenon of what is called entropy rain (Brandenburg 2016), where a significant fraction of the energy is being carried by the Deardorff term.

Regarding nonaxisymmetry, we do expect rapidly rotating stars to exhibit nonaxisymmetric magnetic fields. It is conceivable that the convection can develop spontaneously a marked nonaxisymmetric modulation, as has been seen in the simulations of Browning (2008). This can lead to an α effect that is nonaxisymmetric. Such models have been studied in the context of galactic dynamos where such a modulation through the spiral arms is conceivable (Moss et al. 1991). As already discussed in § 2.9, this implies that the Reynolds rules cannot be applied. Not much is known about this case, which deserves further study.

Theoretically, nonaxisymmetric magnetic fields can also be caused by the α effect becoming anisotropic. We recall that α_{ij} is a pseudo tensor that can be constructed from products of terms proportional to gravity $\boldsymbol{g}$ (a polar vector) and angular velocity $\boldsymbol{\Omega}$ (an axial or pseudo vector). The term $\boldsymbol{g} \cdot \boldsymbol{\Omega}\, \delta_{ij}$ is particularly important because it leads to α effect dynamo action. However, there are also terms proportional to $g_i \Omega_j$ and $g_j \Omega_i$ that were already present in the early work of Steenbeck et al. (1966). These are important, because they can favor the generation of nonaxisymmetric magnetic fields (Rädler 1986a); see the left panel of figure 9 for symmetric and antisymmetric magnetic field configurations with an azimuthal order of $m = 1$. These solutions are referred to as $\mathcal{S}1$ and $\mathcal{A}1$, respectively.

For rapid rotation, higher powers of $\boldsymbol{\Omega}$ are expected, so we expect a term of the form $\boldsymbol{g} \cdot \boldsymbol{\Omega}\ \Omega_i \Omega_j$, as was obtained by Moffatt (1972) and Rüdiger (1978). This term enters with a minus sign and thus tends to cancels the component α_{zz}, where we have assumed that $\boldsymbol{\Omega}$ points in the z direction. The Roberts flow I is an example of a flow that has $\alpha_{zz} = 0$; see equation (2.34). The resulting magnetic field has only x and y components, corresponding to a global magnetic field of that of a dipole lying in the equatorial plane.

If this should be a model of the geodynamo, it is unclear why the Earth's magnetic field is then not also nonaxisymmetric, given that its Coriolis number is expected to be much larger than that of many stars.

We have the same problem also for the giant planets Jupiter and Saturn which have basically axisymmetric magnetic fields, while Uranus and Neptune are known to have nonaxisymmetric fields corresponding to a dipole lying in the equatorial plane (Rädler & Ness 1990). A possible explanation for the occurrence of asymmetric mean magnetic fields in rapid rotators could be the presence of a small but sufficient amount of differ-

ential rotation in Jupiter and Saturn which prevents the excitation of nonaxisymmetric magnetic fields (Rädler 1986b). Corresponding mean-field calculations were presented by Moss & Brandenburg (1995).

Regarding stellar magnetic fields, several stars are seen to have nonaxisymmetric magnetic fields (Rosén et al. 2016; See et al. 2016). Those are indeed rapidly rotating stars. However, the breakpoint between predominantly axisymmetric and predominantly nonaxisymmetric magnetic fields is observed to be at about 5 times the solar rotation rate (Lehtinen et al. 2016), while simulations suggest this to happen already at about 1.8 times the solar value (Viviani et al. 2018).

When the anisotropy is weak, the axisymmetric dipole solution $\mathcal{A}0$ is often the most preferred one. Nevertheless, even in that case the nonaxisymmetric $\mathcal{S}1$ solution can occur as a transient for an extended period of time, if the initial condition has a strong symmetric component. As shown in a state diagram (figure 9) of parity P ($= 1$ for symmetric and -1 for antisymmetric fields) versus nonaxisymmetry M (i.e., the fractional energy in the nonaxisymmetric components), the solution first evolves to become more symmetric with respect to the equatorial plane ($P \to 1$), but more nonaxisymmetric ($M \to 1$), until it evolves along the diagonal in the PM diagram toward the $\mathcal{A}0$ solution (Rädler et al. 1990); see the right panel of figure 9. If only axisymmetric solutions are permitted, the $\mathcal{S}0$ solution would be a stable end state (Brandenburg et al. 1989). However, as was shown by Rädler & Wiedemann (1989), this is an artifact of the restriction to axisymmetry. Fully nonaxisymmetric models demonstrate that the stellar surface field can undergo extended transients via the nnoaxisymmetric mode before the axisymmetric dipole solution is restored. This could potentially be important in understanding the nature of the secondary cycles observed in stellar dynamos; see Brandenburg et al. (2017b).

5. Accretion disk dynamos

Unlike stars, accretion disks are flat. Early simulations in the context of galactic dynamos have suggested for some time that the toroidal magnetic fields in disks should be symmetric about the midplane, i.e., quadrupolar (Ruzmaikin et al. 1988; Beck et al. 1996). This was indeed confirmed by the first simulations of magnetic fields generated by turbulence from the magnetorotational instability (Brandenburg et al. 1995).

5.1. *Unconventional sign of α*

The early simulations of Brandenburg et al. (1995) indicate that accretion disks have an α effect that is negative in the upper disk plane, which was rather unexpected. Here, α was measured simply by correlating the local value of $\overline{\boldsymbol{\mathcal{E}}}$ is the toroidal direction (corresponding to $\overline{\mathcal{E}}_y$ in their shearing box simulations) with the mean toroidal magnetic field. Similar results were later reproduced by Ziegler & Rüdiger (2000). As explained above, this method is not always reliable; see § 2.5. However, subsequent simulations with the test-field method have confirmed that the relevant $\alpha_{\phi\phi}$ is negative (Brandenburg 2005b; Gressel et al. 2008a), at least close to the midplane (Gressel et al. 2008a; Gressel 2013; Gressel & Pessah 2015).

Local mean-field models with a negative α effect in the upper disk plane predicted oscillatory magnetic fields (Brandenburg 1998a), which agrees with what is seen in the simulations of Brandenburg et al. (1995). Again, however, Gressel (2013) and Gressel & Pessah (2015) found that the sign may change in the outer parts, where they found it to be the usual one.

The theoretical explanation for an unconventional sign could be related to a dominance of a magnetic buoyancy-driven α effect. The idea is that a magnetic field that is enhanced

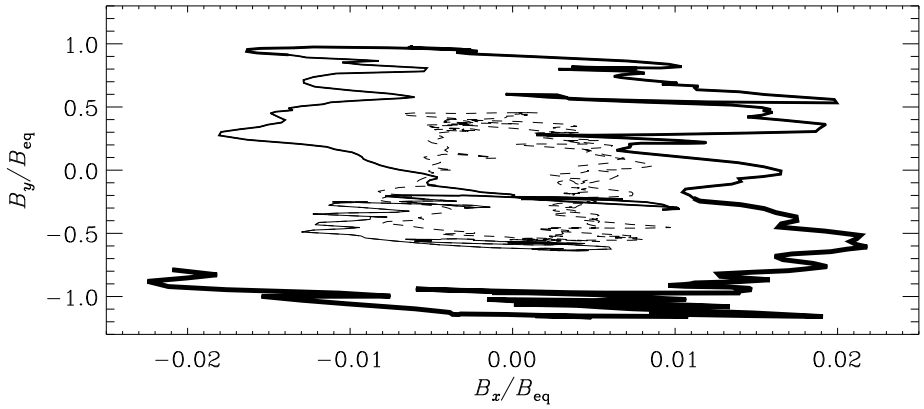

FIGURE 10. Phase plot of the averages of poloidal and toroidal fields over narrow slices in the z direction of the simulation domain. The first times are plotted as dashed lines, but the later times are solid with increasing thickness toward the end showing that a point on the curve moves forward in a clockwise direction. Overplotted are two ellipses showing $B_{y0} \propto \cos(\omega t + \phi)$ versus $B_{x0} \propto \cos\omega t$ with $\phi = 0.65\pi$, $B_{x0} = 0.035\,B_{\rm eq}$, and $B_{x0} = 1.8\,B_{\rm eq}$ (solid line) and $\phi = 0.75\pi$, $B_{x0} = 0.03\,B_{\rm eq}$, and $B_{x0} = 1.74\,B_{\rm eq}$ (dotted line).

locally in a flux tube leads not only to its rise, but also to its contraction along the tube (Brandenburg & Campbell 1997). If this effect dominates over the expansion of rising gas, it could explain the opposite sign of α. This could indeed be the right explanation (Rüdiger & Pipin 2000; Ziegler & Rüdiger 2000). Magnetically driven turbulence might also be relevant to the Sun and could cause unconventional turbulent transport (Rüdiger et al. 2001; Chatterjee et al. 2011).

5.2. *Identifying $\alpha\Omega$-type dynamo action in disk simulations*

To identify $\alpha\Omega$-type dynamo action as the main course of oscillations seen in simulations, it is advantageous to determine the phase relation between poloidal and toroidal fields (Brandenburg 2008). This is a standard tool in solar dynamo theory for inferring the sense of radial differential rotation. Mean-field theory predicts a phase shift by $3\pi/4$, which was confirmed by Brandenburg & Sokoloff (2002); see figure 10.

An alternative idea is magnetic buoyancy being the reason for migration away from the midplane (Salvesen et al. 2016). However, no detailed proposal for the phase relation from the buoyancy effect has yet been made. By comparison, the interpretation of the magnetic field migration in terms of an $\alpha\Omega$ dynamo is rather straightforward; see Gressel & Pessah (2015) for a recent analysis.

5.3. *Incoherent α–shear dynamo*

It has been suggested that the magnetic field of accretion disks could be explained by what is known as an incoherent α–shear dynamo (Vishniac & Brandenburg 1997). This type of effect is a hybrid between a fluctuation dynamo (i.e., small-scale dynamo) and a mean-field dynamo and involves fluctuations in the mean field itself. The occurrence of fluctuations in the mean field is a natural outcome of finite scale separation when the turbulent eddies are comparable to the size of the domain along the direction of averaging. This was originally proposed by Hoyng (1988) to explain irregularity of standard $\alpha\Omega$ dynamos. He discussed the occurrence of fluctuation mean fields, but not the occurrence of a new mean-field dynamo effect. The occurrence of a new dynamo effect is possible when there is also strong differential rotation together with turbulent diffusion (Vishniac & Brandenburg 1997). The verification of this mechanism was discussed in Brandenburg

et al. (2008a), who measured $\alpha(z,t)$ and found that its rms value, $\langle\alpha^2\rangle^{1/2}$, was large enough the explain to dynamo action found in their model. Unlike $\alpha\Omega$ dynamos, which rely on the presence of stratification to produce an α effect, this is not required for the incoherent α–shear dynamo effect. Yousef et al. (2008a,b) have suggested instead a mechanism which they called a shear dynamo. It is not clear, however, whether this is really a new mechanism (Proctor 2007; Heinemann et al. 2011; Mitra & Brandenburg 2012).

There is also the possibility of a dynamo effect from what is known as the shear–current effect (Rogachevskii & Kleeorin 2003, 2004). There is, however, no independent verification of this effect (Brandenburg 2005b; Rüdiger & Kitchatinov 2006; Rädler & Stepanov 2006). Sridhar & Subramanian (2009) found this term to vanish under SOCA. Subsequent work by Squire & Bhattacharjee (2016) has shown that this effect may work when there are small-scale magnetic fields, for example those produced by small-scale dynamo action. **?** have shown that the shear–current effect could, with suitably adjusted parameters, reproduce the magnetic cycles rather well. However, to find conclusive evidence for a magnetic version of this effect, as advocated by Squire & Bhattacharjee (2016), one needs to apply the fully nonlinear version of the test-field method to such simulations. It would be important to verify that this fully nonlinear method is really required in cases where the small-scale dynamo is excited. So far, however, no such evidence has been presented yet.

5.4. *Magnetic Prandtl number dependence*

At about the same time when it became clear that small-scale dynamos are harder to excite at small values of the magnetic Prandtl number, it was noticed that MRI-driven dynamos are no longer excited at small magnetic Prandtl numbers **?**. This may indeed be for the same reason. It still needs to be demonstrated then that at larger magnetic Reynolds numbers, the MRI-driven dynamos become excited again.

The assumption of periodic boundary conditions in MRI-simulations is crucial for obtaining the result that those dynamos are no longer or not that easily excited at small magnetic Prandtl numbers.

6. Galactic dynamos

The realization that interstellar space harbors magnetic fields has intrigued scientists already in the 1950s (Biermann & Schlüter 1951) and the idea of a turbulent origin was anticipated (Batchelor 1950). His early theory of what is nowadays called a small-scale dynamo was a simple one, but it turned out to be incorrect and was later superseded by the work of Kazantsev (1968); see also Rogachevskii & Kleeorin (1997) for the generalization of this theory to finite magnetic Prandtl numbers. The application of mean-field theory started with the work of Vainshtein & Ruzmaikin (1971) and Parker (1971a).

6.1. *Supernovae, the drivers of galactic turbulence*

Galactic dynamos are similar to accretion disk dynamos, in that their geometry is flat, but here, turbulence and thus an α effect can be driven by supernova explosions (Ferrière 1992a,b, 1993a,b). Those calculations showed an unexpected result in that the vertical component of the α tensor was negative in the northern hemisphere; see Ferrière (1993a). This unusual sign of α_{zz} was first found in convection simulations (Brandenburg et al. 1990). Of course, α_{zz} can only be determined when one relaxes the assumption of horizontal averaging. This was done in Brandenburg et al. (2012b), where a special test-field method for axisymmetric turbulence was adopted. However, under the physical

conditions considered (stably stratified rotating turbulence), the sign of α_{zz} was found to be the same as for the horizontal α effect; see their figure 8, where only for $R_{\rm m} \approx 40$ a negative value was found ($\alpha_{zz} = 0.002\,u_{\rm rms}/3$, which is rather small).

Simulations by **?** where the first ones that produced small-scale dynamo action in the interstellar medium. The first ones showing large-scale dynamo action were those by Gressel et al. (2008b), but that was at four times the actual rotation rate. They had larger resolutions than similar models of Korpi et al. (1999), which did not show dynamo action. The simulations of Gressel et al. (2008a) produced detailed predictions for the tensors α_{ij} and η_{ijk} using the test-field method. Contrary to the results of Ferrière (1992b), they found that turbulent pumping is directed toward the midplane, as was already assumed in Brandenburg et al. (1993). The simulations of **?** were the first to produce large-scale dynamos for the actual values of the galactic rotation rate. They also found small-scale dynamo action, but the magnetic Prandtl number was strongly varying by phase, so the interpretation is not obvious.

6.2. *Axisymmetric and bisymmetric spirals: significance of the arms*

An obvious question concerns the importance of spiral arms in making the α effect nonaxisymmetric and thus causing or facilitating nonaxisymmetric magnetic fields. The perhaps only galaxy where nonaxisymmetric magnetic fields have been detected is M81, while the magnetic field detected in many other galaxies are axisymmetric; see Beck et al. (1996). Mestel & Subramanian (1991) found that $m = 1$ modes could grow if α is assumed to be nonaxisymmetric. Chamandy et al. (2013) extended these considerations to try and explain magnetic spirals, also using the time nonlocality of mean-field dynamo theory. Simulations with a nonaxisymmetric α effect have shown that the marginal dynamo numbers for nonaxisymmetric dynamos are substantially lowered when the α effect is nonaxisymmetric (Moss et al. 1991). It is not obvious, however, that the magnetic field coincides with the gaseous arms and there are arguments that magnetic and gaseous arms are actually interlaced (Shukurov 1998).

6.3. *Significance of galactic halos*

Galaxies also have extended halos that could support dynamo action. The main difference between dynamos in the disk and in the halo is that halo dynamos behave essentially like stellar ones in that they are expected to produce a dipolar magnetic field whereas the disk dynamo is expected to produce a quadrupolar magnetic field. This can lead to interesting interactions between the two (Brandenburg et al. 1989; Schmitt & Schüssler 1989). The occurrence of mixed modes between symmetric and antisymmetric fields was first proposed by Sokoloff & Shukurov (1990) and then tested numerically by Brandenburg et al. (1992). It has also been proposed that the galactic bulge may provide another near-spherical entity that could harbor dipolar magnetic fields (Donner & Brandenburg 1990).

An important question concerns the direction of turbulent pumping. Is it directed toward the disk midplane or away from it? Brandenburg et al. (1993) discussed the possibility that it is directed toward the disk midplane, which could lead to an enhancement of the dynamo effect by making the field more concentrated. This was indeed supported by the simulations of Gressel et al. (2008a, 2013). The magnetorotational instability could also act in the galaxy (Machida et al. 2013), which may become important in the outer parts where supernova driving becomes inefficient (Korpi 2004).

6.4. *Cosmic ray driven turbulence*

In modelling the galactic dynamo, an additional energy source is provided by cosmic rays, which can inflate magnetic flux tubes and thus make them buoyant, which causes them to rise and thereby exert work on the magnetic field. This was first addressed by Parker (1992) and has been modelled numerically by Hanasz et al. (2004, 2009a) in local models and by Hanasz et al. (2009b) in global models. It has even been argued that the presence of cosmic rays helps to make the galactic dynamo "fast", i.e., independent of the microphysical resistivity. This question remains somewhat puzzling, because one would have thought that *any* turbulent dynamo would be a fast one, at least in the kinematic sense, because the kinematic values of α and η_t are thought to be independent of the microphysical value of η. Given that the cosmic ray diffusivity is very large, Snodin et al. (2006) used in their simulations a non-Fickian telegrapher's equation approach discussed in § 2.3.

In the scenario discussed above, cosmic rays inflate magnetic field structures and make them buoyant in an external gravity field. This is not the most direct way of cosmic rays driving turbulent motions. Another process is to invoke the electric current associated with the flow of protons in the cosmic rays. If there is a magnetic field with a component aligned with this current, it can drive an instability (Bell 2004). This can lead to turbulence and a slow continued build-up of magnetic field in terms of α effect. Furthermore, since the magnetic field and the current density form a pseudo-scalar, it is not surprising that their presence causes a turbulent α effect that explains the slow growth of the magnetic field after the initial exponential phase is over. Beresnyak & Li (2014) measured the anisotropy of such Bell turbulence and found $\ell^{2/3}$ and linear scalings of the perpendicular and parallel second order structure functions, as also expected for regular hydromagnetic turbulence (Goldreich & Sridhar 1995).

6.5. *Mode cleaning by nonlinearity*

Even though the kinematic dynamo may be a fast one, as discussed in § 6.4, it does not seem to be sufficiently prominent owing to the dominance of small-scale dynamo action (Beck et al. 1994). There is work suggesting that large-scale dynamos work successfully only because of nonlinearity (Cattaneo & Hughes 2009). This notion was already supported by the work of Brandenburg (2001), which showed that in the kinematic regime, no large-scale field was found and that it was only near the end of the nonlinear phase that large-scale magnetic fields became fully developed. This can also be seen by looking at figure 2.

One reason for the emergence of a large-scale field only in the nonlinear phase is the fact that there can be multiple solutions to the large-scale dynamo problem: not only can a large-scale field develop in any of the three coordinate directions, but, in a periodic domain, it can also come with any possible phase shift. Also, if the scale separation is large, the direction of the large-scale does not need to be any of the coordinate directions, and many of the intermediate directions are possible. This explains the extended time interval during which large-scale, but incoherently arranged patches of magnetic field are present; see figure 2 of § 2.12. Subramanian & Brandenburg (2014) have shown that the kinematic dynamo does operate in high Reynolds number turbulence and that one really has a new type of dynamo that has aspects of small-scale and large-scale dynamos. Interestingly, as the dynamo saturates, even the small-scale fields attain more power at intermediate length scales (Park & Blackman 2012a; Bhat et al. 2016a).

7. Early Universe

The connection between the early Universe and mean-field dynamos is not evident, because no mean fields have ever been observed and such fields are also not really expected. Instead, we expect a turbulent magnetic field. On the other hand, the possibility that a turbulent magnetic field might have helicity has frequently been discussed (Brandenburg et al. 1996; Christensson et al. 2001; Field & Carroll 2002). The most important reason is that then a turbulent magnetic field can undergo efficient inverse cascading (Pouquet et al. 1976), which significantly increases the turbulent correlation length of the magnetic field from the scale of a few centimeters at the time of the electroweak phase transition to about 10^8 cm, which, after the cosmological expansion of the Universe, would correspond to about 30 kpc, making it a strong candidate for explaining the large-scale magnetic fields in the Universe (Banerjee & Jedamzik 2004; Kahniashvili et al. 2013).

7.1. *Inversely cascading turbulent magnetic fields*

There are lower limits on the strength of a diffuse magnetic field throughout all of space of about 10^{-14} to 10^{-18} G on a scale of about 1 Mpc (Aharonian et al. 2006; Taylor et al. 2011; Dermer et al. 2011). These limits constrain the product of magnetic energy and length scale, $\langle \boldsymbol{B}^2 \rangle \xi_{\rm M}$, so the lower limit would be ten times larger if $\xi_{\rm M}$ was a hundred times smaller. On dimensional grounds, this product can also be a measure of the modulus of the magnetic helicity (Brandenburg et al. 2017e).

Simulation have shown that the magnetic energy spectra $E_{\rm M}(k,t)$ of decaying turbulence tend to display a selfsimilar behavior (Brandenburg & Kahniashvili 2017),

$$E_{\rm M}(k,t) = \xi_{\rm M}^{-\beta} \phi_{\rm M}\left(k\xi_{\rm M}(t)\right). \tag{7.1}$$

where $\xi_{\rm M}$ is the magnetic correlation length, $\phi_{\rm M}$ is a universal function for the magnetic spectra at all times, and β is an exponent that depends mostly on the physics governing the decay and, in some cases, also on the initial conditions (Olesen 1997). For example, $\beta = 0$ in the fully helical case when $\langle \boldsymbol{A} \cdot \boldsymbol{B} \rangle$ is conserved, $\beta = 1$ when $\langle \boldsymbol{A}^2 \rangle$ is conserved, $\beta = 2$ when the Saffman integral is conserved, and $\beta = 4$ when the Loitsiansky integral is conserved; see Brandenburg & Kahniashvili (2017) for details.

Assuming that $\xi_{\rm M}(t) \propto t^q$ with exponent q, we then expect the magnetic energy to decay like

$$\mathcal{E}_{\rm M}(t) = \int_0^\infty E_{\rm M}(k,t)\,{\rm d}k = \xi_{\rm M}^{-(\beta+1)} \int_0^\infty \phi_{\rm M}(k\xi_{\rm M})\,{\rm d}(k\xi_{\rm M}) \propto t^{-(\beta+1)q} \propto t^{-p}, \tag{7.2}$$

so $p = (\beta+1)q$ is the exponent on the decay of magnetic energy. Furthermore, as noted by Olesen (1997), the hydrodynamic and hydromagnetic equations are invariant under rescaling, $x \to \tilde{x}\ell$ and $t \to \tilde{t}\ell^{1/q}$, which implies corresponding rescalings for velocity $u \to \tilde{t}\ell^{1-1/q}$ and viscosity $\nu \to \tilde{\nu}\ell^{2-1/q}$. Furthermore, using the fact that the dimensions of $E(k,t)$ are given by $[E] = [x]^3[t]^{-2}$, and requiring ψ to be invariant under rescaling $E \to \tilde{E}\ell^{3-2/q} \propto \tilde{k}^\beta \ell^{-\beta}\psi$, he finds that $\beta = -3 + 2/q$. This is indeed compatible with simulations of nonhelical hydromagnetic turbulence (Zrake 2014; Brandenburg et al. 2015).

7.2. *Connection with mean-field theory*

The helical decay law has been modelled using mean-field theory for the spectra $E_{\rm M}(k,t)$ and $H_{\rm M}(k,t)$ in the form (Campanelli 2007)

$$\frac{\partial E_{\rm M}}{\partial t} = -2(\eta + \eta_{\rm t})k^2 E_{\rm M} + \alpha k^2 H_{\rm M}, \tag{7.3}$$

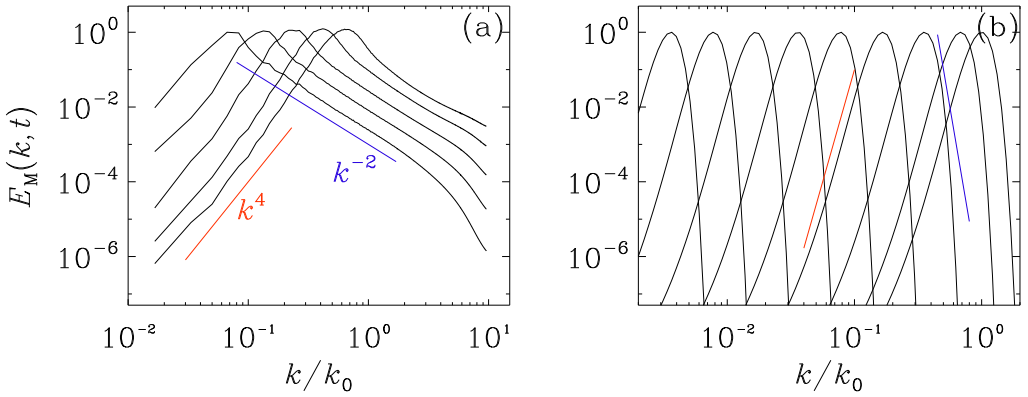

FIGURE 11. (a) Fully helical three-dimensional turbulence simulation of a decaying initially fully helical turbulent magnetic field. The velocity is driven entirely by the Lorentz force of the magnetic field. The time in units of the initial Alfvén time are 17, 50, 150, 430, and 1200. The red and blue lines are proportional to k^4 and k^{-2}, respectively. (b) Solution of (7.3) and (7.4) shown at times 1, 10^2, 10^3, ..., until 10^9. The red and blue lines are proportional to k^{12} and k^{-20}, respectively.

$$\frac{\partial H_{\rm M}}{\partial t} = -2(\eta+\eta_{\rm t})k^2 H_{\rm M} + 4\alpha E_{\rm M}, \tag{7.4}$$

where $\eta_{\rm t}$ and α are here time-dependent coefficients with $\eta_{\rm t} = \tau_{\rm d}\int E_{\rm M}\,{\rm d}k$ being the magnetic diffusivity and $\alpha = \tau_{\rm d}\int k^2 H_{\rm M}\,{\rm d}k$ is a purely magnetic contribution to the α effect. The assumption of Campanelli (2007) that $\eta_{\rm t}$ can in this case of strong magnetic fields be assumed to be proportional to the magnetic energy density needs to be verified, as it would seem to contradict the results form the second order correlation approximation in the kinematic case, as discussed at the end of § 3.4. The timescale $\tau_{\rm d}$ is assumed constant in these considerations and equal to the friction or drag time that is introduced when replacing the nonlinear term $\boldsymbol{u}\cdot\boldsymbol{\nabla}\boldsymbol{u}$ by $\boldsymbol{u}/\tau_{\rm d}$. This approximation was already used by Subramanian (1999) who referred to it as the ambipolar diffusion nonlinearity. Brandenburg & Subramanian (2000) solved their model numerically and also obtained inverse cascading.

The solutions to these equations characterize certain aspects of the helical decay law, but they do not correctly describe details of the spectra, as shown in figure 11. In particular, the model does not reproduce the k^4 subinertial range spectrum (Durrer & Caprini 2003) and also not the k^{-2} inertial range (Brandenburg et al. 2015).

7.3. *Comments on the chiral magnetic effect*

The equations have been generalized to the case where magnetic helicity can be generated through what is known as the chiral magnetic effect. This is an effect of relativistic fermions whose spin aligns with the magnetic field, leading to oppositely oriented currents from left- and right-handed fermions. At low temperatures, the spin can flip rapidly, so there is no net current, but this is not the case under relativistic conditions. In that case, when the difference in the number densities between left- and right-handed fermions, i.e., their chemical potential, is different from zero, it leads to a field-aligned current proportional to $\mu\boldsymbol{B}$. This is *formally* equivalent to an α effect, but here it is not connected with turbulence, but it is a microphysical effect (Joyce & Shaposhnikov 1997; Boyarsky et al. 2012, 2015; Rogachevskii et al. 2017; Schober et al. 2017). The total chirality is however conserved, so $\mu+\frac{1}{2}\lambda\langle\boldsymbol{A}\cdot\boldsymbol{B}\rangle = \text{const}\equiv\mu_0$, i.e., it is equal to the initial chemical potential μ_0 if the initial magnetic helicity was vanishing. This implies that a fully helical

magnetic field can be produced by exponential amplification from a weak seed magnetic field. This continues until the magnetic helicity (multiplied by $\lambda/2$) reaches the value μ_0 at later times. Similar to the simulations without the chiral magnetic effect, the difference between the two models is related to the absence of a forward cascade (Dvornikov & Semikoz 2017; Pavlović et al. 2017; Brandenburg et al. 2017e).

8. Conclusions

The applications of mean-field theory to astrophysical bodies has been far from straightforward. One might have thought that, given that so much is known about the expressions for α_{ij} and η_{ijk}, and that even the inclusion of nonlocality is now straightforward, it should not be a problem to apply the full theory to the Sun or to galaxies. This is true in theory, and some models of galactic and solar dynamos now include nonlocality in space and/or time; see Chamandy et al. (2013) and Brandenburg & Chatterjee (2018), respectively. In practice, however, success remained limited because it looked like that models for the Sun did not reproduce the Sun too well. It was therefore though that this problem could be fixed by "massaging" some of the coefficients such that the model works, but even that did not seem to lead to satisfactory results. In the wake of this type of experience, the flux transport model was developed, which was not just a small refinement of theoretically justified models, but it was completely made up by the desire to make the model work for the Sun. This remains unsatisfactory even today. The problem with this is that, given that such a flux transport dynamo has no theoretical basis, it is unclear whether such a model can be applied in a predictive manner to other stars. In that respect, it was already noted that the flux transport dynamo does not seem to be able to explain the rising branches seen in figure 8, but only a declining branch obtained by fitting one line through both branches (Jouve et al. 2010; Karak et al. 2014).

Alternatively, one may argue that the solar dynamo simply cannot be treated with mean-field theory, and that we just have to wait for numerical simulations to resolve the Sun sufficiently well in space and time to reproduce its main features such as the equatorial migration or the toroidal flux belts, spoke-like angular velocity contours, and the near-surface shear layer. While this viewpoint may turn out to be true in the end, the argument for this remains unsatisfactory simply because we clearly do see a well-defined mean field with large-scale spatial and temporal order. Therefore, there is *a priori* no reason why there should be no theory for describing such a mean field, which clearly does seem to exist. On the other hand, it is true that the full range of mean-field coefficients and effects can be rather large and too complex to be dealt with in a fully predictive manner without fudge parameters. Thus, mean-field theory might in principle still be correct, but impractical under conditions of practical interest.

This unsettled situation is obviously one of the reasons why—after all these years—mean-field theory is still a very active field of research, and thus it is the very reason for having this special issue in JPP.

I feel privileged to acknowledge Karl-Heinz Rädler for having taught me so many important aspects of dynamo theory through our joint work since we first met in Helsinki in 1986. I also thank the two referees for their detailed and constructive reports. This research was supported in part by the NSF Astronomy and Astrophysics Grants Program (grant 1615100), and the University of Colorado through its support of the George Ellery Hale visiting faculty appointment.

REFERENCES

Aharonian, F., Akhperjanian, A. G., Bazer-Bachi, A. R., et al. 2006 A low level of extragalactic background light as revealed by γ-rays from blazars. *Nature* **440**, 1018–1021.

Andrievsky, A., Brandenburg, A., Noullez, A., & Zheligovsky, V. 2015 Negative magnetic eddy diffusivities from the test-field method and multiscale stability theory. *Astrophys. J.* **811**, 135.

Arter, W. 1983 Magnetic flux transport by a convecting layer–topological, geometrical and compressible phenomena. *J. Fluid Mech.* **132**, 25–48.

Augustson, K., Brun, A. S., Miesch, M., & Toomre, J. 2015 Grand minima and equatorward propagation in a cycling stellar convective dynamo. *Astrophys. J.* **809**, 149.

Ayres, T. R. 2009 The cycles of α Centauri. *Astrophys. J.* **696**, 1931–1949.

Ayres, T. R. 2015 The far-ultraviolet ups and downs of alpha Centauri. *Astron. J.* **149**, 58.

Babcock, H. W. 1961 The topology of the Sun's magnetic field and the 22-year cycle. *Astrophys. J.* **133**, 572–587.

Banerjee, R., Jedamzik, K. 2004 Evolution of cosmic magnetic fields: From the very early Universe, to recombination, to the present. *Phys. Rev. D***70**, 123003.

Batchelor, G. K. 1950 On the spontaneous magnetic field in a conducting liquid in turbulent motion. *Proc. Roy. Soc. Lond.* **A201**, 405–416.

Beaudoin, P., Simard, C., Cossette, J.-F., & Charbonneau, P. 2016 Double Dynamo Signatures in a Global MHD Simulation and Mean-field Dynamos. *Astrophys. J.* **826**, 138.

Beck, R., Brandenburg, A., Moss, D., Shukurov, A., & Sokoloff, D. 1996 Galactic Magnetism: Recent Developments and Perspectives. *Ann. Rev. Astron. Astrophys.* **34**, 155–206.

Beck, R., Poezd, A. D., Shukurov, A., Sokoloff, D. D. 1994 Dynamos in evolving galaxies. *Astron. Astrophys.* **289**, 94–100.

Bell, A. R. 2004 Turbulent amplification of magnetic field and diffusive shock acceleration of cosmic rays. *Month. Not. Roy. Astron. Soc.* **353**, 550–558.

Beresnyak, A., & Li, H. 2014
. *Astrophys. J.* **788**, 107–Basic Bell-MHD Turbulence.

Berger, M., & Field, G. B. 1984 The topological properties of magnetic helicity. *J. Fluid Mech.* **147**, 133–148.

Bhat, P., Subramanian, K., & Brandenburg, A. 2016a A unified large/small-scale dynamo in helical turbulence. *Month. Not. Roy. Astron. Soc.* **461**, 240–247.

Bhat, P., Ebrahimi, F., & Blackman, E. G. 2016b Large-scale dynamo action precedes turbulence in shearing box simulations of the magnetorotational instability. *Month. Not. Roy. Astron. Soc.* **462**, 818–829.

Biermann, L., & Schlüter, A. 1951 Cosmic radiation and cosmic magnetic fields. II. Origin of cosmic magnetic fields. *Phys. Rev.* **82**, 863–868.

Blackman, E. G., & Brandenburg, A. 2002 Dynamic nonlinearity in large scale dynamos with shear. *Astrophys. J.* **579**, 359–373.

Blackman, E. G., & Brandenburg, A. 2003 Doubly helical coronal ejections from dynamos and their role in sustaining the solar cycle. *Astrophys. J. Lett.* **584**, L99–L102.

Blackman, E. G., & Field, G. B. 2000 Constraints on the magnitude of α in dynamo theory. *Astrophys. J.* **534**, 984–988.

Blackman, E. G., & Field, G. B. 2002 New dynamical mean-field dynamo theory and closure approach. *Phys. Rev. Lett.* **89**, 265007.

Blackman, E. G., & Field, G. B. 2003 A simple mean field approach to turbulent transport. *Phys. Fluids* **15**, L73–L76.

Böhm-Vitense, E. 2007 Chromospheric Activity in G and K Main-Sequence Stars, and What It Tells Us about Stellar Dynamos. *Astrophys. J.* **657**, 486–493.

Bonanno, A., Brandenburg, A., Del Sordo, F., & Mitra, D. 2012 Breakdown of chiral symmetry during saturation of the Tayler instability. *Phys. Rev. E***86**, 016313.

XXX

Bourdin, Ph.-A., Bingert, S., & Peter, H. 2013 Observationally driven 3D magnetohydrodynamics model of the solar corona above an active region. *Astron. Astrophys.* **555**, A123.

Bourdin, Ph.-A., Singh, N. K., & Brandenburg, A. 2018 "Magnetic helicity reversal in the corona at small plasma beta," *Astrophys. J.* (submitted, arXiv:1804.04153).

Boyarsky, A., Fröhlich, J., & Ruchayskiy, O. 2012 Self-consistent evolution of magnetic fields and chiral asymmetry in the early Universe. *Phys. Rev. Lett.* **108**, 031301.

Boyarsky, A., Fröhlich, J., & Ruchayskiy, O. 2015 Magnetohydrodynamics of chiral relativistic fluids. *Phys. Rev. D***92**, 043004.

Brandenburg, A. 1998a Disc Turbulence and Viscosity. In *Theory of Black Hole Accretion Discs* (ed. M. A. Abramowicz, G. Björnsson, J. E. Pringle), pp. 61–86. Cambridge University Press.

Brandenburg, A. 1998b Theoretical Basis of Stellar Activity Cycles. In *Tenth Cambridge Workshop on Cool Stars, Stellar Systems, and the Sun* (ed. R. Donahue & J. Bookbinder), pp. 173–191. Astron. Soc. Pac. Conf. Ser., Col. **154**.

Brandenburg, A. 2001 The inverse cascade and nonlinear alpha-effect in simulations of isotropic helical hydromagnetic turbulence. *Astrophys. J.* **550**, 824–840.

Brandenburg, A. 2005a The case for a distributed solar dynamo shaped by near-surface shear. *Astrophys. J.* **625**, 539–547.

Brandenburg, A. 2005b Turbulence and its parameterization in accretion discs. *Astron. Nachr.* **326**, 787–797.

Brandenburg, A. 2008 The dual role of shear in large-scale dynamos. *Astron. Nachr.* **329**, 725–731.

Brandenburg, A. 2016 Stellar mixing length theory with entropy rain. *Astrophys. J.* **832**, 6.

Brandenburg, A. 2017 Analytic solution of an oscillatory migratory α^2 stellar dynamo. *Astron. Astrophys.* **598**, A117.

Brandenburg, A., Ashurova, M. B., & Jabbari, S. 2017a Compensating Faraday depolarization by magnetic helicity in the solar corona. *Astrophys. J. Lett.* **845**, L15.

Brandenburg, A., & Campbell, C. G. 1997 Modelling magnetized accretion discs. In *H. Spruit, & E. Meyer-Hofmeister* (ed. Accretion disks – New aspects), pp. 109–124. Springer-Verlag.

Brandenburg, A., Candelaresi, S., & Chatterjee, P. 2009 Small-scale magnetic helicity losses from a mean-field dynamo. *Month. Not. Roy. Astron. Soc.* **398**, 1414–1422.

Brandenburg, A., & Chatterjee, P. 2018 "Strong nonlocality variations in a spherical mean-field dynamo," *Astron. Nachr.* DOI:10.1002/asna.201813472 (arXiv:1802.04231).

Brandenburg, A., & Dobler, W. 2001 Large scale dynamos with helicity loss through boundaries. *Astron. Astrophys.* **369**, 329–338.

Brandenburg, A., & Giampapa, M. S. 2018 Enhanced stellar activity for slow antisolar differential rotation? *Astrophys. J. Lett.* **855**, L22.

Brandenburg, A., & Kahniashvili, T. 2017 Classes of hydrodynamic and magnetohydrodynamic turbulent decay. *Phys. Rev. Lett.* **118**, 055102.

Brandenburg, A., & Nordlund, Å. 2011 Astrophysical turbulence modeling. *Rep. Prog. Phys.* **74**, 046901.

Brandenburg, A., & Rädler, K.-H. 2013 Yoshizawa's cross-helicity effect and its quenching. *Geophys. Astrophys. Fluid Dyn.* **107**, 207–217.

Brandenburg, A., & Sokoloff, D. 2002 Local and nonlocal magnetic diffusion and alpha-effect tensors in shear flow turbulence. *Geophys. Astrophys. Fluid Dyn.* **96**, 319–344.

Brandenburg, A., & Stepanov, R. 2014 Faraday signature of magnetic helicity from reduced depolarization. *Astrophys. J.* **786**, 91.

Brandenburg, A., & Subramanian, K. 2000 Large scale dynamos with ambipolar diffusion nonlinearity. *Astron. Astrophys.* **361**, L33–L36.

Brandenburg, A., & Subramanian, K. 2005a Astrophysical magnetic fields and nonlinear dynamo theory. *Phys. Rep.* **417**, 1–209.

Brandenburg, A., & Subramanian, K. 2005b Strong mean field dynamos require supercritical helicity fluxes. *Astron. Nachr.* **326**, 400–408.

Brandenburg, A., & Tuominen, I. 1991 The solar dynamo. In *The Sun and cool stars: activity, magnetism, dynamos, IAU Coll. 130* (ed. I. Tuominen, D. Moss, & G. Rüdiger), pp. 223–233. Lecture Notes in Physics **380**, Springer-Verlag.

Brandenburg, A., & Urpin, V. 1998 Magnetic fields in young galaxies due to the cross-helicity effect. *Astron. Astrophys.* **332**, L41–L44.

Brandenburg, A., Chatterjee, P., Del Sordo, F., Hubbard, A., Käpylä, P. J., & Rheinhardt, M. 2010 Turbulent transport in hydromagnetic flows. *Phys. Scr.* **T142**, 014028.

Brandenburg, A., Donner, K. J., Moss, D., Shukurov, A., Sokoloff, D. D., & Tuominen, I. 1992 Dynamos in discs and halos of galaxies. *Astron. Astrophys.* **259**, 453–461.

Brandenburg, A., Donner, K. J., Moss, D., Shukurov, A., Sokoloff, D. D., & Tuominen, I. 1993 Vertical magnetic fields above the discs of spiral galaxies. *Astron. Astrophys.* **271**, 36–50.

Brandenburg, A., Enqvist, K., & Olesen, P. 1996 Large-scale magnetic fields from hydromagnetic turbulence in the very early universe. *Phys. Rev. D***54**, 1291–1300.

Brandenburg, A., Gressel, O., Käpylä, P. J., Kleeorin, N., Mantere, M. J., & Rogachevskii, I. 2013 New scaling for the alpha effect in slowly rotating turbulence. *Astrophys. J.* **762**, 127.

Brandenburg, A., Jennings, R. L., Nordlund, Å., Rieutord, M., Stein, R. F., & Tuominen, I. 1996 Magnetic structures in a dynamo simulation. *J. Fluid Mech.* **306**, 325–352.

Brandenburg, A., Kahniashvili, T., & Tevzadze, A. G. 2015 Nonhelical inverse transfer of a decaying turbulent magnetic field. *Phys. Rev. Lett.* **114**, 075001.

Brandenburg, A., Käpylä, P. J., & Mohammed, A. 2004 Non-Fickian diffusion and tau-approximation from numerical turbulence. *Phys. Fluids* **16**, 1020–1027.

Brandenburg, A., Kemel, K., Kleeorin, N., Mitra, D., & Rogachevskii, I. 2011a Detection of negative effective magnetic pressure instability in turbulence simulations. *Astrophys. J. Lett.* **740**, L50.

Brandenburg, A., Kemel, K., Kleeorin, N., & Rogachevskii, I. 2012a The negative effective magnetic pressure in stratified forced turbulence. *Astrophys. J.* **749**, 179.

Brandenburg, A., Kleeorin, N., & Rogachevskii, I. 2010 Large-scale magnetic flux concentrations from turbulent stresses. *Astron. Nachr.* **331**, 5–13.

Brandenburg, A., Krause, F., Meinel, R., Moss, D., & Tuominen, I. 1989 The stability of nonlinear dynamos and the limited role of kinematic growth rates. *Astron. Astrophys.* **213**, 411–422.

Brandenburg, A., Mathur, S., & Metcalfe, T. S. 2017b Evolution of coexisting long and short period stellar activity cycles. *Astrophys. J.* **845**, 79.

Brandenburg, A., Moss, D., & Shukurov, A. 1995 Galactic fountains as magnetic pumps. *Month. Not. Roy. Astron. Soc.* **276**, 651–662.

Brandenburg, A., Moss, D., & Tuominen, I. 1992a Stratification and thermodynamics in mean-field dynamos. *Astron. Astrophys.* **265**, 328–344.

Brandenburg, A., Moss, D., & Tuominen, I. 1992b Turbulent pumping in the solar dynamo. In *The Solar Cycle* (ed. K. L. Harvey), pp. 536–542. ASP Conference Series, **27**.

Brandenburg, A., Nordlund, Å., Pulkkinen, P., Stein, R.F., & Tuominen, I. 1990 3-D Simulation of turbulent cyclonic magneto-convection. *Astron. Astrophys.* **232**, 277–291.

Brandenburg, A., Nordlund, Å., Stein, R. F., & Torkelsson, U. 1995 Dynamo generated turbulence and large scale magnetic fields in a Keplerian shear flow. *Astrophys. J.* **446**, 741–754.

Brandenburg, A., Petrie, G. J. D., & Singh, N. K. 2017c Two-scale analysis of solar magnetic helicity. *Astrophys. J.* **836**, 21.

Brandenburg, A., Procaccia, I., & Segel, D. 1995 The size and dynamics of magnetic flux structures in MHD turbulence. *Phys. Plasmas* **2**, 1148–1156.

Brandenburg, A., Rädler, K.-H., & Kemel, K. 2012b Mean-field transport in stratified and/or rotating turbulence. *Astron. Astrophys.* **539**, A35.

Brandenburg, A., Rädler, K.-H., Rheinhardt, M., & Käpylä, P. J. 2008a Magnetic diffusivity tensor and dynamo effects in rotating and shearing turbulence. *Astrophys. J.* **676**, 740–751.

Brandenburg, A., Rädler, K.-H., Rheinhardt, M., & Subramanian, K. 2008b Magnetic quenching of alpha and diffusivity tensors in helical turbulence. *Astrophys. J. Lett.* **687**, L49–L52.

Brandenburg, A., Rädler, K.-H., & Schrinner, M. 2008c Scale dependence of alpha effect and turbulent diffusivity. *Astron. Astrophys.* **482**, 739–746.

Brandenburg, A., Rogachevskii, I., & Kleeorin, N. 2016 Magnetic concentrations in stratified turbulence: the negative effective magnetic pressure instability. *New J. Phys.* **18**, 125011.

Brandenburg, A., Saar, S. H., & Turpin, C. R. 1998 Time evolution of the magnetic activity cycle period. *Astrophys. J. Lett.* **498**, L51–L54.

Brandenburg, A., Schober, J., & Rogachevskii, I. 2017d The contribution of kinetic helicity to turbulent magnetic diffusivity. *Astron. Nachr.* **338**, 790–793.

Brandenburg, A., Schober, J., Rogachevskii, I., Kahniashvili, T., Boyarsky, A., Fröhlich, J.,

Ruchayskiy, O., & Kleeorin, N. 2017e The turbulent chiral magnetic cascade in the early universe. *Astrophys. J. Lett.* **845**, L21.

Brandenburg, A., Subramanian, K., Balogh, A., & Goldstein, M. L. 2011b Scale-dependence of magnetic helicity in the solar wind. *Astrophys. J.* **734**, 9.

Brown, B. P., Miesch, M. S., Browning, M. K., Brun, A. S., & Toomre, J. 2011 Magnetic cycles in a convective dynamo simulation of a young solar-type star. *Astrophys. J.* **731**, 69.

Browning, M. K. 2008 Simulations of dynamo action in fully convective stars. *Astrophys. J.* **676**, 1262–1280.

Cameron, R., & Schüssler, M. 2015 The crucial role of surface magnetic fields for the solar dynamo. *Science* **347**, 1333–1335.

Cameron, R., & Schüssler, M. 2017 An update of Leighton's solar dynamo model. *Astron. Astrophys.* **599**, A52.

Cameron, R. H., Duvall, T. L., Schüssler, M., & Schunker, H. 2018 Observing and modeling the poloidal and toroidal fields of the solar dynamo. *Astron. Astrophys.* **609**, A56.

Campanelli, L. 2007 Evolution of magnetic fields in freely decaying magnetohydrodynamic turbulence. *Phys. Rev. Lett.* **98**, 251302.

Candelaresi, S., & Brandenburg, A. 2013 How much helicity is needed to drive large-scale dynamos? *Phys. Rev. E***87**, 043104.

Candelaresi, S., Hubbard, A., Brandenburg, A., & Mitra, D. 2011 Magnetic helicity transport in the advective gauge family. *Phys. Plasmas* **18**, 012903.

Cattaneo, F., & Hughes, D. W. 1996 Nonlinear saturation of the turbulent alpha effect. *Phys. Rev. E***54**, R4532–R4535.

Cattaneo, F., Hughes, D. W. 2009 Problems with kinematic mean field electrodynamics at high magnetic Reynolds numbers. *Month. Not. Roy. Astron. Soc.* **395**, L48–L51.

Cattaneo, F., & Tobias, S. M. 2009 Dynamo properties of the turbulent velocity field of a saturated dynamo. *J. Fluid Mech.* **621**, 205–214.

Chamandy, L., Subramanian, K., & Shukurov, A. 2013 Galactic spiral patterns and dynamo action - I. A new twist on magnetic arms. *Month. Not. Roy. Astron. Soc.* **428**, 3569–3589.

Charbonneau, P. 2010 Dynamo models of the solar cycle. *Liv. Rev. Solar Phys.* **7**, 3.

Chatterjee, P., Mitra, D., Brandenburg, A., & Rheinhardt, M. 2011 Spontaneous chiral symmetry breaking by hydromagnetic buoyancy. *Phys. Rev. E***84**, 025403R.

Chatterjee, P., Mitra, D., Rheinhardt, M., & Brandenburg, A. 2011 Alpha effect due to buoyancy instability of a magnetic layer. *Astron. Astrophys.* **534**, A46.

Choudhuri, A. R., Schüssler, M., & Dikpati, M. 1995 The solar dynamo with meridional circulation. *Astron. Astrophys.* **303**, L29–L32.

Christensson, M., Hindmarsh, M., & Brandenburg, A. 2001 Inverse cascade in decaying 3D magnetohydrodynamic turbulence. *Phys. Rev. E***64**, 056405–6.

Cole, E., Brandenburg, A., Käpylä, P. J., & Käpylä, M. J. 2016 Robustness of oscillatory α^2 dynamos in spherical wedges. *Astron. Astrophys.* **593**, A134.

Cooper, C. M., Wallace, J., Brookhart, M., Clark, M., Collins, C., Ding, W. X., Flanagan, K., Khalzov, I., Li, Y., Milhone, J., Nornberg, M., Nonn, P., Weisberg, D., Whyte, D. G., Zweibel, E., & Forest, C. B. 2014 The Madison plasma dynamo experiment: A facility for studying laboratory plasma astrophysics. *Phys. Plasmas* **21**, 013505.

Courvoisier A., Hughes D. W., & Proctor M. R. E. 2010 Self-consistent mean-field magnetohydrodynamics. *Proc. Roy. Soc. Lond.* **466**, 583–601.

Cossette, J.-F., & Rast, M. P. 2016 Supergranulation as the largest buoyantly driven convective scale of the Sun. *Astrophys. J. Lett.* **829**, L17.

Courvoisier, A., Hughes, D. W., & Tobias, S. M. 2006 α-effect in a family of chaotic flows. *Phys. Rev. Lett.* **96**, 034503.

Deardorff, J. W. 1966 The counter-gradient heat flux in the lower atmosphere and in the laboratory. *J. Atmosph. Sci.* **23**, 503–506.

Deardorff, J. W. 1972 Theoretical expression for the countergradient vertical heat flux. *J. Geophys. Res.* **77**, 5900–5904.

Del Sordo, F., Guerrero, G., & Brandenburg, A. 2013 Turbulent dynamo with advective magnetic helicity flux. *Month. Not. Roy. Astron. Soc.* **429**, 1686–1694.

Dermer, C. D., Cavadini, M., Razzaque, S., Finke, J. D., Chiang, J., & Lott, B. 2011 Time delay

of cascade radiation for TeV blazars and the measurement of the intergalactic magnetic field. *Astrophys. J. Lett.* **733**, L21.

Devlen, E., Brandenburg, A., & Mitra, D. 2013 A mean field dynamo from negative eddy diffusivity. *Month. Not. Roy. Astron. Soc.* **432**, 1651–1657.

Dikpati, M., & Charbonneau, P. 1999 A Babcock-Leighton flux transport dynamo with solar-like differential rotation. *Astrophys. J.* **518**, 508–520.

Dobler, W., Stix, M., & Brandenburg, A. 2006 Convection and magnetic field generation in fully convective spheres. *Astrophys. J.* **638**, 336–347.

Donner, K.J., & Brandenburg, A. 1990 Generation and interpretation of galactic magnetic fields. *Astron. Astrophys.* **240**, 289–298.

Drobyshevskij, E. M. & Yuferev, V. S. 1974 Topological pumping of magnetic flux by three-dimensional convection. *J. Fluid Mech.* **65**, 33–44.

Durrer, R., & Caprini, C. 2003 Primordial magnetic fields and causality. *JCAP* **0311**, 010.

Dvornikov, M., & Semikoz, V. B. 2017 Influence of the turbulent motion on the chiral magnetic effect in the early universe. *Phys. Rev. D***95**, 043538.

Eberhard, G., & Schwarzschild, K. 1913 On the reversal of the calcium lines H and K in stellar spectra. *Astrophys. J.* **38**, 292–295.

Fan, Y. 2001 The emergence of a twisted Ω-tube into the solar atmosphere. *Astrophys. J.* **554**, L111–L114.

Fan, Y. 2008 The three-dimensional evolution of buoyant magnetic flux tubes in a model solar convective envelope. *Astrophys. J.* **676**, 680–697.

Fan, Y. 2009 Magnetic Fields in the Solar Convection Zone. *Liv. Rev. Solar Phys.* **6**, 4.

Featherstone, N. A., & Hindman, B. W. 2016 The spectral amplitude of stellar convection and its scaling in the high-Rayleigh-number regime. *Astrophys. J.* **818**, 32.

Ferrière, K. 1992a Effect of an ensemble of explosions on the galactic dynamo. I. General formulation. *Astrophys. J.* **389**, 286–296.

Ferrière, K. 1992b Effect of the explosion of supernovae and superbubbles on the galactic dynamo. *Astrophys. J.* **391**, 188–198.

Ferrière, K. 1993a The full alpha-tensor due to supernova explosions and superbubbles in the galactic disk. *Astrophys. J.* **404**, 162–184.

Ferrière, K. 1993b Magnetic diffusion due to supernova explosions and superbubbles in the galactic disk. *Astrophys. J.* **409**, 248–261.

Field, G. B., & Blackman, E. G. 2002 Dynamical quenching of the α^2 dynamo. *Astrophys. J.* **572**, 685–692.

Field, G. B., & Carroll, S. M. 2000 Cosmological magnetic fields from primordial helicity. *Phys. Rev. D***62**, 103008.

Finn, J. M., & Antonsen, T. M. 1985 Magnetic helicity: What it is and what is it good for? *Comm. Plasma Phys. Contr. Fusion* **9**, 111–123.

Forest, C. B., Bayliss, R. A., Kendrick, R. D., Nornberg, M. D., O'Donnell, R., & Spence, E. J. 2002 Hydrodynamic and numerical modeling of a spherical homogeneous dynamo experiment. *Magnetohydrodynamics* **38**, 107–120.

Forest, C. B., Flanagan, K., Brookhart, M., Clark, M., Cooper, C. M., Désangles, V., Egedal, J., Endrizzi, D., Khalzov, I. V., Li, H., Miesch, M., Milhone, J., Nornberg, M., Olson, J., Peterson, E., Roesler, F., Schekochihin, A., Schmitz, O., Siller, R., Spitkovsky, A., Stemo, A., Wallace, J., Weisberg, D., Zweibel, E. 2015 The Wisconsin Plasma Astrophysics Laboratory. *J. Plasma Phys.* **81**, 345810501.

Frank, F. C. 1953 On spontaneous asymmetric synthesis. *Biochim. Biophys. Acta* **11**, 459–464.

Galloway, D. J., & Proctor, M. R. E. 1992 Numerical calculations of fast dynamos in smooth velocity fields with realistic diffusion. *Nature* **356**, 691–693.

Gastine, T., Yadav, R. K., Morin, J., Reiners, A., & Wicht, J. 2014 From solar-like to antisolar differential rotation in cool stars. *Month. Not. Roy. Astron. Soc.* **438**, L76–L80.

Gellert, M., Rüdiger, G., & Hollerbach, R. 2011 Helicity and alpha-effect by current-driven instabilities of helical magnetic fields. *Month. Not. Roy. Astron. Soc.* **414**, 2696–2701.

Gent, F. A., Shukurov, A., Fletcher, A., Sarson, G. R., & Mantere, M. J. 2013a The supernova-regulated ISM - I. The multiphase structure. *Month. Not. Roy. Astron. Soc.* **432**, 1396–1423.

Gent, F. A., Shukurov, A., Sarson, G. R., Fletcher, A., & Mantere, M. J. 2013b The supernova-regulated ISM - II. The mean magnetic field. *Month. Not. Roy. Astron. Soc.* **430**, L40–L44.

Ghizaru, M., Charbonneau, P., & Smolarkiewicz, P. K. 2010 Magnetic cycles in global large-eddy simulations of solar convection. *Astrophys. J.* **715**, L133–L137.

Giampapa, M. S., Brandenburg, A., Cody, A. M., Skiff, B. A., & Hall, J. C. 2017 "The rotation and chromospheric activity of the solar-type stars in the open cluster M67," *Astrophys. J.* (submitted, arXiv:https://www.nordita.org/preprints, no. 2017-121).

Gilman, P. A. 1977 Nonlinear dynamics of Boussinesq convection in a deep rotating shell. I. *Geophys. Astrophys. Fluid Dyn.* **8**, 93–135.

Gilman, P. A. 1983 Dynamically consistent nonlinear dynamos driven by convection in a rotating spherical shell. II. Dynamos with cycles and strong feedbacks. *Astrophys. J. Suppl.* **53**, 243–268.

Glatzmaier, G. A. 1985 Numerical simulations of stellar convective dynamos. II. Field propagation in the convection zone. *Astrophys. J.* **291**, 300–307.

Goldreich, P., & Sridhar, S. 1995 Toward a theory of interstellar turbulence. 2: Strong alfvenic turbulence. *Astrophys. J.* **438**, 763–775.

Greer, B. J., Hindman, B. W., Featherstone, N. A., & Toomre, J. 2015 . *Astrophys. J. Lett.* **803**, L17–Helioseismic imaging of fast convective flows throughout the near-surface shear layer.

Gressel, O. 2013 Dynamo effects in magnetorotational turbulence with finite thermal diffusivity. *Astrophys. J.* **770**, 100.

Gressel, O., Ziegler, U., Elstner, D., & Rüdiger, G. 2008a Dynamo coefficients from local simulations of the turbulent ISM. *Astron. Nachr.* **329**, 619–624.

Gressel, O., Elstner, D., Ziegler, U., & Rüdiger, G. 2008b Direct simulations of a supernova-driven galactic dynamo. *Astron. Astrophys.* **486**, L35–L38.

Gressel, O., Elstner, D., & Ziegler, U. 2013 Towards a hybrid dynamo model for the Milky Way. *Astron. Astrophys.* **560**, A93.

Gressel, O., & Pessah, M. E. 2015 Characterizing the mean-field dynamo in turbulent accretion disks. *Astrophys. J.* **810**, 59.

Gruzinov, A. V., & Diamond, P. H. 1994 Self-consistent theory of mean-field electrodynamics. *Phys. Rev. Lett.* **72**, 1651–1653.

Gruzinov, A. V., & Diamond, P. H. 1995 Self-consistent mean field electrodynamics of turbulent dynamos. *Phys. Plasmas* **2**, 1941–1947.

Gruzinov, A. V., & Diamond, P. H. 1996 Nonlinear mean field electrodynamics of turbulent dynamos. *Phys. Plasmas* **3**, 1853–1857.

Guerrero, G., & Käpylä, P. J. 2011 Dynamo action and magnetic buoyancy in convection simulations with vertical shear. *Astron. Astrophys.* **533**, A40.

Hanasoge, S. M., Duvall, T. L., Jr., & DeRosa, M. L. 2010 Seismic constraints on interior solar convection. *Astrophys. J. Lett.* **712**, L98–L102.

Hanasoge, S. M., Duvall, T. L., & Sreenivasan, K. R. 2012 Anomalously weak solar convection. *Proc. Natl. Acad. Sci.* **109**, 11928–11932.

Hanasoge, S., Gizon, L., & Sreenivasan, K. R. 2016 Seismic sounding of convection in the Sun. *Ann. Rev. Fluid Dyn.* **48**, 191–217.

Hanasz, M., Otmianowska-Mazur, K., Kowal, G., & Lesch, H. 2009a Cosmic-ray-driven dynamo in galactic disks. A parameter study. *Astron. Astrophys.* **498**, 335–346.

Hanasz, M., Kowal, G., Otmianowska-Mazur, K., & Lesch, H. 2004 Amplification of galactic magnetic fields by the cosmic-ray-driven dynamo. *Astrophys. J.* **605**, L33–L36.

Hanasz, M., Wóltański, D., & Kowalik, K. 2009b Global galactic dynamo driven by cosmic rays and exploding magnetized stars. *Astrophys. J. Lett.* **706**, L155–L159.

Harutyunyan, G., Strassmeier, K. G., Künstler, A., Carroll, T. A., & Weber, M. 2016 Anti-solar differential rotation on the active sub-giant HU Virginis. *Astron. Astrophys.* **592**, A117.

Heinemann, T., McWilliams, J. C., & Schekochihin, A. A. 2011 Magnetic-field generation by randomly forced shearing waves. *Phys. Rev. Lett.* **107**, 255004.

Hickmann, K. S., Godinez, H. C., Henney, C. J., & Arge, C. N. 2015 Data assimilation in the ADAPT photospheric flux transport model. *Solar Phys.* **290**, 1105–1118.

Hood, A. W., Archontis, V., Galsgaard, K., & Moreno-Insertis, F. 2009 The emergence of toroidal flux tubes from beneath the solar photosphere. *Astron. Astrophys.* **503**, 999–1011.

Hotta, H., Rempel, M., & Yokoyama, T. 2014 High-resolution Calculations of the Solar Global Convection with the Reduced Speed of Sound Technique. I. The Structure of the Convection and the Magnetic Field without the Rotation. *Astrophys. J.* **786**, 24.

Hotta, H., Rempel, M., & Yokoyama, T. 2015 Efficient Small-scale Dynamo in the Solar Convection Zone. *Astrophys. J.* **803**, 42.

Hotta, H., Rempel, M., & Yokoyama, T. 2016 Large-scale magnetic fields at high Reynolds numbers in magnetohydrodynamic simulations. *Science* **351**, 1427–1430.

Hoyng, P. 1988 Turbulent transport of magnetic fields. III. Stochastic excitation of global magnetic field modes. *Astrophys. J.* **332**, 857–871.

Hubbard, A., Del Sordo, F., Käpylä, P. J., & Brandenburg, A. 2009 The α effect with imposed and dynamo-generated magnetic fields. *Month. Not. Roy. Astron. Soc.* **398**, 1891–1899.

Hubbard, A., & Brandenburg, A. 2009 Memory effects in turbulent transport. *Astrophys. J.* **706**, 712–726.

Hubbard, A., & Brandenburg, A. 2010 Magnetic helicity fluxes in an α^2 dynamo embedded in a halo. *Geophys. Astrophys. Fluid Dyn.* **104**, 577–590.

Hubbard, A., & Brandenburg, A. 2011 Magnetic helicity flux in the presence of shear. *Astrophys. J.* **727**, 11.

Hubbard, A., & Brandenburg, A. 2012 Catastrophic quenching in $\alpha\Omega$ dynamos revisited. *Astrophys. J.* **748**, 51.

Jabbari, S., Brandenburg, A., Kleeorin, N., & Rogachevskii, I. 2017 Sharp magnetic structures from dynamos with density stratification. *Month. Not. Roy. Astron. Soc.* **467**, 2753–2765.

Jing, J., Park, S.-H., Liu, C., Lee, J., Wiegelmann, T., Xu, Y., Deng, N., & Wang, H. 2012 Evolution of Relative Magnetic Helicity and Current Helicity in NOAA Active Region 11158. *Astrophys. J.* **752**, L9.

Jouve, L., Brown, B. P., & Brun, A. S. 2010 Exploring the $P_{\rm cyc}$ vs. $P_{\rm rot}$ relation with flux transport dynamo models of solar-like stars. *Astron. Astrophys.* **509**, A32.

Joyce, M., & Shaposhnikov, M. 1997 Primordial magnetic fields, right electrons, and the Abelian anomaly. *Phys. Rev. Lett.* **79**, 1193–1196.

Kahniashvili, T., Tevzadze, A. G., Brandenburg, A., & Neronov, A. 2013 Evolution of primordial magnetic fields from phase transitions. *Phys. Rev. D***87**, 083007.

Käpylä, M. J., Käpylä, P. J., Olspert, N., Brandenburg, A., Warnecke, J., Karak, B. B., & Pelt, J. 2016 Multiple dynamo modes as a mechanism for long-term solar activity variations. *Astron. Astrophys.* **589**, A56.

Käpylä, P. J., Brandenburg, A., Kleeorin, N., Käpylä, M. J., & Rogachevskii, I. 2016 Magnetic flux concentrations from turbulent stratified convection. *Astron. Astrophys.* **588**, A150.

Käpylä, P. J., Korpi, M. J., Brandenburg, A., Mitra, D., & Tavakol, R. 2010 Convective dynamos in spherical wedge geometry. *Astron. Nachr.* **331**, 73–81.

Käpylä, P. J., Mantere, M. J., & Brandenburg, A. 2012 Cyclic magnetic activity due to turbulent convection in spherical wedge geometry. *Astrophys. J. Lett.* **755**, L22.

Käpylä, P. J., Mantere, M. J., Cole, E., Warnecke, J., & Brandenburg, A. 2013 Effects of strong stratification on equatorward dynamo wave propagation. *Astrophys. J.* **778**, 41.

Käpylä, P. J., Käpylä, M. J., & Brandenburg, A. 2014 Confirmation of bistable stellar differential rotation profiles. *Astron. Astrophys.* **570**, A43.

Käpylä, P. J., Käpylä, M. J., Olspert, N., Warnecke, J., & Brandenburg, A. 2017a Convection-driven spherical shell dynamos at varying Prandtl numbers. *Astron. Astrophys.* **599**, A4.

Käpylä, P. J., Rheinhardt, M., Brandenburg, A., Arlt, R., Käpylä, M. J., Lagg, A., Olspert, N., & Warnecke, J. 2017b Extended subadiabatic layer in simulations of overshooting convection. *Astrophys. J. Lett.* **845**, L23.

Käpylä, P. J., Viviani, M., Käpylä, M. J., & Brandenburg, A. 2018 "Effects of a subadiabatic layer on convection and dynamos in spherical wedge simulations," *Geophys. Astrophys. Fluid Dyn.* (submitted). 1803.05898

Karak, B. B., Rheinhardt, M., Brandenburg, A., Käpylä, P. J., & Käpylä, M. J. 2014 Quenching and anisotropy of hydromagnetic turbulent transport. *Astrophys. J.* **795**, 16.

Karak, B. B., Käpylä, M. J., Käpylä, P. J., Brandenburg, A., Olspert, N., & Pelt, J. 2015 Magnetically controlled stellar differential rotation near the transition from solar to anti-solar profiles. *Astron. Astrophys.* **576**, A26.

Karak, B. B., Kitchatinov, L. L., & Choudhuri, A. R. 2014 A dynamo model of magnetic activity in solar-like stars with different rotational velocities. *Astrophys. J.* **791**, 59.

Kazantsev, A. P. 1968 Enhancement of a magnetic field by a conducting fluid. *Sov. Phys. JETP* **26**, 1031–1034.

Kemel, K., Brandenburg, A., Kleeorin, N., & Rogachevskii, I. 2012 Properties of the negative effective magnetic pressure instability. *Astron. Nachr.* **333**, 95–100.

Kemel, K., Brandenburg, A., Kleeorin, N., Mitra, D., & Rogachevskii, I. 2012 Spontaneous formation of magnetic flux concentrations in stratified turbulence. *Solar Phys.* **280**, 321–333.

Kemel, K., Brandenburg, A., Kleeorin, N., Mitra, D., & Rogachevskii, I. 2013 Active region formation through the negative effective magnetic pressure instability. *Solar Phys.* **287**, 293–313.

Kitchatinov, L. L. 1991 Turbulent transport of magnetic fields in a highly conducting rotating fluid and the solar cycle. *Astron. Astrophys.* **243**, 483–491.

Kitchatinov, L. L., & Mazur, M. V. 2000 Stability and equilibrium of emerged magnetic flux. *Solar Phys.* **191**, 325–340.

Kitchatinov, L. L. & Rüdiger, G. 2004 Anti-solar differential rotation. *Astron. Nachr.* **325**, 496–500.

Kleeorin, N., Mond, M., & Rogachevskii, I. 1993 Magnetohydrodynamic instabilities in developed small-scale turbulence. *Phys. Fluids* **5**, 4128–4134.

Kleeorin, N., Mond, M., & Rogachevskii, I. 1996 Magnetohydrodynamic turbulence in the solar convective zone as a source of oscillations and sunspots formation. *Astron. Astrophys.* **307**, 293–309.

Kleeorin, N., Moss, D., Rogachevskii, I., & Sokoloff, D. 2000 Helicity balance and steady-state strength of the dynamo generated galactic magnetic field. *Astron. Astrophys.* **361**, L5–L8.

Kleeorin, N., Moss, D., Rogachevskii, I., & Sokoloff, D. 2002 The role of magnetic helicity transport in nonlinear galactic dynamos. *Astron. Astrophys.* **387**, 453–462.

Kleeorin, N., Moss, D., Rogachevskii, I., & Sokoloff, D. 2003 Nonlinear magnetic diffusion and magnetic helicity transport in galactic dynamos. *Astron. Astrophys.* **400**, 9–18.

Kleeorin, N., & Rogachevskii, I. 1994 Effective Ampère force in developed magnetohydrodynamic turbulence. *Phys. Rev. E***50**, 2716–2730.

Kleeorin, N. I., Rogachevskii, I. V., & Ruzmaikin, A. A. 1989 Negative magnetic pressure as a trigger of large-scale magnetic instability in the solar convective zone. *Pis. Astron. Zh.* **15**, 639–645.

Kleeorin, N. I., Rogachevskii, I. V., Ruzmaikin, A. A. 1990 Magnetic force reversal and instability in a plasma with advanced magnetohydrodynamic turbulence. *Sov. Phys. JETP* **70**, 878–883.

Kleeorin, N., Rogachevskii, I., & Ruzmaikin, A. 1995 Magnitude of the dynamo-generated magnetic field in solar-type convective zones. *Astron. Astrophys.* **297**, 159–167.

Kleeorin, N. I., & Ruzmaikin, A. A. 1982 Dynamics of the average turbulent helicity in a magnetic field. *Magnetohydrodynamics* **18**, 116–122. Translation from Magnitnaya Gidrodinamika, 2, pp. 17–24 (1982)

Kleeorin, N. I., Ruzmaikin, A. A., & Sokoloff, D. D. 1983 Activity cycle periods in late-type stars. *Astrophys. Spa. Sci.* **95**, 131–136.

Kochukhov, O., Makaganiuk, V., Piskunov, N., Snik, F., Jeffers, S. V., Johns-Krull, C. M., Keller, C. U., Rodenhuis, M., & Valenti, J. A. 2011 First detection of linear polarization in the line profiles of active cool stars. *Astrophys. J. Lett.* **732**, L19.

Korpi, M. J., Brandenburg, A., Shukurov, A., Tuominen, I., & Nordlund, Å. 1999 A supernova regulated interstellar medium: simulations of the turbulent multiphase medium. *Astrophys. J. Lett.* **514**, L99–L102.

Korpi, M. J. 2004 Modelling the turbulent magnetized ISM. *Astrophys. Spa. Sci.* **289**, 449–457.

Kővári, Z., Kriskovics, L., Künstler, A., Carroll, T. A., Strassmeier, K. G., Vida, K., Oláh, K., Bartus, J., Weber, M. 2015 A. *Astron. Astrophys.* **573**, A98.ntisolar differential rotation of the K1-giant σ Geminorum revisited

Kővári, Z., Strassmeier, K. G., Carroll, T. A., Oláh, K., Kriskovics, L., Kővári, E., Kovács, O., Vida, K., Granzer, T., & Weber, M. 2017 Antisolar differential rotation with surface lithium enrichment on the single K-giant V1192 Orionis. *Astron. Astrophys.* **606**, A42.

Kowal, G., Otmianowska-Mazur, K., & Hanasz, M. 2006 Dynamo coefficients in Parker unstable disks with cosmic rays and shear. The new methods of estimation. *Astron. Astrophys.* **445**, 915–929.

Krause, F., & Rädler, K.-H. 1980 *Mean-field Magnetohydrodynamics and Dynamo Theory.* Oxford: Pergamon Press.

Krivodubskii, V. N. 1984 Magnetic field transfer in the turbulent solar envelope. *Sov. Astron.* **28**, 205–211.

Lanotte, A., Noullez, A., Vergassola, M., & Wirth, A. 1999 Large-scale dynamo produced by negative magnetic eddy diffusivities. *Geophys. Astrophys. Fluid Dyn.* **91**, 131–146.

Lehtinen, J., Jetsu, L., Hackman, T., Kajatkari, P., & Henry, G. W. 2016 Activity trends in young solar-type stars. *Astron. Astrophys.* **588**, A38.

Leighton, R. B. 1969 A magneto-kinematic model of the solar cycle. *Astrophys. J.* **156**, 1–26.

Lim, E.-K., Yurchyshyn, V., & Goode, P. 2012 First simultaneous detection of moving magnetic features in photospheric intensity and magnetic field data. *Astrophys. J.* **753**, 89.

Liu, Y., & Schuck, P. W. 2012 Magnetic energy and helicity in two emerging active regions in the sun. *Astrophys. J.* **761**, 105.

Lord, J. W., Cameron, R. H., Rast, M. P., Rempel, M., & Roudier, T. 2014 The role of subsurface flows in solar surface convection: modeling the spectrum of supergranular and larger scale flows. *Astrophys. J.* **793**, 24.

Losada, I. R., Brandenburg, A., Kleeorin, N., Mitra, D., & Rogachevskii, I. 2012 Rotational effects on the negative magnetic pressure instability. *Astron. Astrophys.* **548**, A49.

Losada, I. R., Brandenburg, A., Kleeorin, N., & Rogachevskii, I. 2013 Competition of rotation and stratification in flux concentrations. *Astron. Astrophys.* **556**, A83.

Machida, M., Nakamura, K. E., Kudoh, T., Akahori, T., Sofue, Y., & Matsumoto, R. 2013 Dynamo activities driven by magnetorotational instability and the Parker instability in galactic gaseous disks. *Astrophys. J.* **764**, 81.

Masada, Y., & Sano, T. 2014 Mean-field modeling of an α^2 dynamo coupled with direct numerical simulations of rigidly rotating convection. *Astrophys. J. Lett.* **794**, L6.

Matthaeus, W. H., & Goldstein, M. L. 1982 Measurement of the rugged invariants of magnetohydrodynamics in the solar wind. *J. Geophys. Res.* **87**, 6011–6028.

Mestel, L., & Subramanian, K. 1991 Galactic dynamos and density wave theory. *Month. Not. Roy. Astron. Soc.* **248**, 677–687.

Miesch, M. S., Brun, A. S., De Rosa, M. L., & Toomre, J. 2008 Structure and evolution of giant cells in global models of solar convection. *Astrophys. J.* **673**, 557–575.

Miesch, M., Matthaeus, W., Brandenburg, A., Petrosyan, A., Pouquet, A., Cambon, C., Jenko, F., Uzdensky, D., Stone, J., Tobias, S., Toomre, J., & Velli, M. 2015 Large-eddy simulations of magnetohydrodynamic turbulence in space and astrophysics. *Spa. Sci. Rev.* **194**, 97–137.

Miesch, M. S., & Toomre, J. 2009 Turbulence, magnetism, and shear in stellar interiors. *Ann. Rev. Fluid Dyn.* **41**, 317–345.

Mitra, D., Tavakol, R., Brandenburg, A., & Moss, D. 2009 Turbulent dynamos in spherical shell segments of varying geometrical extent. *Astrophys. J.* **697**, 923–933.

Mitra, D., Tavakol, R., Käpylä, P. J., & Brandenburg, A. 2010a Oscillatory migrating magnetic fields in helical turbulence in spherical domains. *Astrophys. J. Lett.* **719**, L1–L4.

Mitra, D., Candelaresi, S., Chatterjee, P., Tavakol, R., & Brandenburg, A. 2010b Equatorial magnetic helicity flux in simulations with different gauges. *Astron. Nachr.* **331**, 130–135.

Mitra, D., & Brandenburg, A. 2012 Scaling and intermittency in incoherent α–shear dynamo. *Month. Not. Roy. Astron. Soc.* **420**, 2170–2177.

Moffatt, H. K. 1970 Turbulent dynamo action at low magnetic Reynolds number. *J. Fluid Mech.* **41**, 435–452.

Moffatt, H. K. 1972 An approach to a dynamic theory of dynamo action in a rotating conducting fluid. *J. Fluid Mech.* **53**, 385–399.

Moffatt, H. K. 1978 *Magnetic Field Generation in Electrically Conducting Fluids.* Cambridge: Cambridge Univ. Press.

Morgenthaler, A., Petit, P., Morin, J., Aurière, M., Dintrans, B., Konstantinova-Antova, R., & Marsden, S. 2011 Direct observation of magnetic cycles in Sun-like stars. *Astron. Nachr.* **332**, 866–871.

Moss, D., Tuominen, I., & Brandenburg, A. 1990 Nonlinear dynamos with magnetic buoyancy in spherical geometry. *Astron. Astrophys.* **228**, 284–294.

Moss, D., Brandenburg, A., & Tuominen, I. 1991 Properties of mean field dynamos with nonaxisymmetric α-effect. *Astron. Astrophys.* **247**, 576–579.

Moss, D., & Brandenburg, A. 1995 The generation of nonaxisymmetric magnetic fields in the giant planets. *Geophys. Astrophys. Fluid Dyn.* **80**, 229–240.

Nelson, N. J., Brown, B. P., Brun, A. S., Miesch, M. S., & Toomre, J. 2013 Magnetic wreaths and cycles in convective dynamos. *Astrophys. J.* **762**, 73.

Nelson, N. J., Brown, B. P., Brun, A. S., Miesch, M. S., & Toomre, J. 2014 Buoyant magnetic loops generated by global convective dynamo action. *Solar Phys.* **289**, 441–458.

Nelson, N. J., & Miesch, M. S. 2014 Generating buoyant magnetic flux ropes in solar-like convective dynamos. *Plasm. Phys. Control. Fusion* **56**, 064004.

Nordlund, Å., Brandenburg, A., Jennings, R. L., Rieutord, M., Ruokolainen, J., Stein, R. F., & Tuominen, I. 1992 Dynamo action in stratified convection with overshoot. *Astrophys. J.* **392**, 647–652.

Noyes, R. W., Hartmann, L., Baliunas, S. L., Duncan, D. K., & Vaughan, A. H. 1984 Rotation, convection, and magnetic activity in lower main-sequence stars. *Astrophys. J.* **279**, 763–777.

Noyes, R. W., Weiss, N. O., & Vaughan, A. H. 1984 The relation between stellar rotation rate and activity cycle periods. *Astrophys. J.* **287**, 769–773.

Olesen, P. 1997 Inverse cascades and primordial magnetic fields. *Phys. Lett. B* **398**, 321–325.

Olspert, N., Lehtinen, J. J., Käpylä, M. J., Pelt, J., & Grigorievskiy, A. 2018 Estimating activity cycles with probabilistic methods II. The Mount Wilson Ca H&K data, *Astron. Astrophys.* (submitted, arXiv:1712.08240).

O'Mara, B., Miesch, M. S., Featherstone, N. A., & Augustson, K. C. 2016 i. *Adv. Spa. Res.* **58**, 1475–t.tle = " 1489Velocity amplitudes in global convection simulations: The role of the Prandtl number and near-surface driving

Park, K., & Blackman, E. G. 2012a Comparison between turbulent helical dynamo simulations and a non-linear three-scale theory. *Month. Not. Roy. Astron. Soc.* **419**, 913–924.

Park, K., & Blackman, E. G. 2012b Simulations of a magnetic fluctuation driven large-scale dynamo and comparison with a two-scale model. *Month. Not. Roy. Astron. Soc.* **423**, 2120–2131.

Parker, E. N. 1955a Hydromagnetic dynamo models. *Astrophys. J.* **122**, 293–314.

Parker, E. N. 1955b The formation of sunspots from the solar toroidal field. *Astrophys. J.* **121**, 491–507.

Parker, E. N. 1971a The generation of magnetic fields in astrophysical bodies. II. The galactic field. *Astrophys. J.* **163**, 255–278.

Parker, E. N. 1971b The Generation of Magnetic Fields in Astrophysical Bodies.IV. The Solar and Terrestrial Dynamos. *Astrophys. J.* **164**, 491–509.

Parker, E. N. 1975 The generation of magnetic fields in astrophysical bodies. X. Magnetic buoyancy and the solar dynamo. *Astrophys. J.* **198**, 205–209.

Parker, E. N. 1979 *Cosmical magnetic fields*. Clarendon Press, Oxford.

Parker, E. N. 1987 The dynamo dilemma. *Solar Phys.* **110**, 11–21.

Parker, E. N. 1992 Fast dynamos, cosmic rays, and the galactic magnetic field. *Astrophys. J.* **401**, 137–145.

Pavlović, P., Leite, N., & Sigl, G. 2017 Chiral magnetohydrodynamic turbulence. *Phys. Rev. D***96**, 023504.

Perri, B., & Brandenburg, A. 2018 Spontaneous flux concentrations from the negative effective magnetic pressure instability beneath a radiative stellar surface. *Astron. Astrophys.* **609**, A99.

Pipin, V. V. 2008 The mean electro-motive force and current helicity under the influence of rotation, magnetic field and shear. *Geophys. Astrophys. Fluid Dyn.* **102**, 21–49.

Pipin, V. V. 2015 Dependence of magnetic cycle parameters on period of rotation in non-linear solar-type dynamos. *Month. Not. Roy. Astron. Soc.* **451**, 1528–1539.

Pipin, V. V. 2017 Non-linear regimes in mean-field full-sphere dynamo. *Month. Not. Roy. Astron. Soc.* **466**, 3007–3020.

Pipin, V. V., & Kosovichev, A. G. 2011 The subsurface-shear-shaped solar $\alpha\Omega$ dynamo. *Astrophys. J.* **727**, L45.

Pipin, V. V., & Kosovichev, A. G. 2013 The mean-field solar dynamo with a double cell meridional circulation pattern. *Astrophys. J.* **776**, 36.

Pipin, V. V., & Kosovichev, A. G. 2016 Dependence of stellar magnetic activity cycles on rotational period in a nonlinear solar-type dynamo. *Astrophys. J.* **823**, 133.

Pipin, V. V., & Pevtsov, A. A. 2014 Magnetic helicity of the global field in solar cycles 23 and 24. *Astrophys. J.* **789**, 21.

Pipin, V. V., Kuzanyan, K. M., Zhang, H., & Kosovichev, A. G. 2011
. *Astrophys. J.* **743**, 160–Turbulent cross-helicity in the mean-field solar dynamo problem.

Pipin, V. V., Sokoloff, D. D., Zhang, H., & Kuzanyan, K. M. 2013a Helicity conservation in nonlinear mean-field solar dynamo. *Astrophys. J.* **768**, 46.

Pipin, V. V., Zhang, H., Sokoloff, D. D., Kuzanyan, K. M., & Gao, Y. 2013b The origin of the helicity hemispheric sign rule reversals in the mean-field solar-type dynamo. *Month. Not. Roy. Astron. Soc.* **435**, 2581–2588.

Pouquet, A., Frisch, U., & Léorat, J. 1976 Strong MHD helical turbulence and the nonlinear dynamo effect. *J. Fluid Mech.* **77**, 321–354.

Proctor, M. R. E. 2007 Effects of fluctuation on alpha-omega dynamo models. *Month. Not. Roy. Astron. Soc.* **382**, L39–L42.

Racine, É., Charbonneau, P., Ghizaru, M., Bouchat, A., & Smolarkiewicz, P. K. 2011 On the mode of dynamo action in a global large-eddy simulation of solar convection. *Astrophys. J.* **735**, 46.

Rädler, K.-H. 1969 On some electromagnetic phenomena in electrically conducting turbulently moving matter, especially in the presence of Coriolis forces. *Geod. Geophys. Veröff., Reihe II* **13**, 131–135.

Rädler, K.-H. 1973 Zur Dynamotheorie kosmischer Magnetfelder. I. Gleichungen für sphärische Dynamomodelle. *Astron. Nachr.* **294**, 213–223.

Rädler, K.-H. 1976 Mean-Field Magnetohydrodynamics as a Basis of Solar Dynamo Theory. In *Basic Mechanisms of Solar Activity, Proceedings from IAU Symposium No.* **71** *held in Prague, Czechoslovakia* (ed. V. Bumba and J. Kleczek), pp. 323–344. D. Reidel Publishing Company Dordrecht.

Rädler, K.-H. 1986a Investigations of spherical kinematic mean-field dynamo models. *Astron. Nachr.* **307**, 89–113.

Rädler, K.-H. 1986b On the effect of differential rotation on axisymmetric and non-axisymmetric magnetic fields of cosmical bodies. *Plasma Physics* **ESA SP-251**, 569–574.

Rädler, K.-H., & Brandenburg, A. 2009 Mean-field effects in the Galloway-Proctor flow. *Month. Not. Roy. Astron. Soc.* **393**, 113–125.

Rädler, K.-H., Brandenburg, A., Del Sordo, F., & Rheinhardt, M. 2011 Mean-field diffusivities in passive scalar and magnetic transport in irrotational flows. *Phys. Rev. E***84**, 4.

Rädler, K.-H., Kleeorin, N., & Rogachevskii, I. 2003 The mean electromotive force for MHD turbulence: the case of a weak mean magnetic field and slow rotation. *Geophys. Astrophys. Fluid Dyn.* **97**, 249–274.

Rädler, K.-H., & Ness, N. F. 1990 The symmetry properties of planetary magnetic fields. *J. Geophys. Res.* **95**, 2311–2318.

Rädler K.-H., & Rheinhardt M. 2007 Mean-field electrodynamics: critical analysis of various analytical approaches to the mean electromotive force. *Geophys. Astrophys. Fluid Dyn.* **101**, 11–48.

Rädler, K.-H., Rheinhardt, M., Apstein, E., & Fuchs, H. 2002a On the mean-field theory of the Karlsruhe dynamo experiment I. Kinematic theory. *Magnetohydrodynamics* **38**, 41–71.

Rädler, K.-H., Rheinhardt, M., Apstein, E., & Fuchs, H. 2002b On the mean-field theory of the Karlsruhe dynamo experiment II. Back-reaction of the magnetic field on the fluid flow. *Magnetohydrodynamics* **38**, 73–94.

Rädler, K.-H., Rheinhardt, M., Apstein, E., & Fuchs, H. 2002c On the mean-field theory of the Karlsruhe dynamo experiment. *Nonl. Processes Geophys.* **38**, 171–187.

Rädler, K.-H., & Stepanov, R. 2006 Mean electromotive force due to turbulence of a conducting fluid in the presence of mean flow. *Phys. Rev. E***73**, 056311.

Rädler, K.-H., & Wiedemann, E. 1989 Numerical experiments with a simple nonlinear mean-field dynamo model. *Geophys. Astrophys. Fluid Dyn.* **49**, 71–80.

Rädler, K.-H., Wiedemann, E., Brandenburg, A., Meinel, R., & Tuominen, I. 1990 Nonlinear

mean-field dynamo models: Stability and evolution of three-dimensional magnetic field configurations. *Astron. Astrophys.* **239**, 413–423.

Reinhold, T., & Arlt, R. 2015 Discriminating solar and antisolar differential rotation in high-precision light curves. *Astron. Astrophys.* **576**, A15.

Rempel, M. 2005 Solar differential rotation and meridional flow: the role of a subadiabatic tachocline for the Taylor-Proudman balance. *Astrophys. J.* **622**, 1320–1332.

Rempel, M. 2017 Extension of the MURaM radiative MHD code for coronal simulations. *Astrophys. J.* **834**, 10.

Rempel, M., & Cheung, M. C. M. 2014 Numerical simulations of active region scale flux emergence: From spot formation to decay. *Astrophys. J.* **785**, 90.

Rheinhardt, M., & Brandenburg, A. 2010 Test-field method for mean-field coefficients with MHD background. *Astron. Astrophys.* **520**, A28.

Rheinhardt, M., & Brandenburg, A. 2012 Modeling spatio-temporal nonlocality in mean-field dynamos. *Astron. Nachr.* **333**, 71–77.

Rheinhardt, M., Devlen, E., Rädler, K.-H., & Brandenburg, A. 2014 Mean-field dynamo action from delayed transport. *Month. Not. Roy. Astron. Soc.* **441**, 116–126.

Rieutord, M., Brandenburg, A., Mangeney, A., & Drossart, P. 1994 Reynolds stress and differential rotation in Boussinesq convection in a rotating spherical shell. *Astron. Astrophys.* **286**, 471–480.

Roberts, G. O. 1972 Dynamo action of fluid motions with two-dimensional periodicity. *Phil. Trans. Roy. Soc.* **A 271**, 411–454.

Roberts, P. H. 1972 Kinematic dynamo models. *Phil. Trans. Roy. Soc.* **A272**, 663–698.

Roberts, P. H., & Soward, A. M. 1975 A unified approach to mean field electrodynamics. *Astron. Nachr.* **296**, 49–64.

Roberts, P. H., & Soward, A. M. 1992 Dynamo theory. *Ann. Rev. Fluid Dyn.* **24**, 459–512.

Roberts, P. H. 1993 Dynamo Theory. In *Astrophysical Fluid Dynamics* (ed. J.-P. Zahn & J. Zinn-Justin), pp. 229–323. North-Holland, Amsterdam.

Rogachevskii, I., & Kleeorin, N. 1997 Intermittency and anomalous scaling for magnetic fluctuations. *Phys. Rev. E***56**, 417–426.

Rogachevskii, I., & Kleeorin, N. 2003 Electromotive force and large-scale magnetic dynamo in a turbulent flow with a mean shear. *Phys. Rev. E***68**, 036301.

Rogachevskii, I., & Kleeorin, N. 2004 Nonlinear theory of a 'shear–current' effect and mean-field magnetic dynamos. *Phys. Rev. E***70**, 046310.

Rogachevskii, I., & Kleeorin, N. 2007 Magnetic fluctuations and formation of large-scale inhomogeneous magnetic structures in a turbulent convection. *Phys. Rev. E***76**, 056307.

Rogachevskii, I., Kleeorin, N., Brandenburg, A., & Eichler, D. 2012 Cosmic-ray current-driven turbulence and mean-field dynamo effect. *Astrophys. J.* **753**, 6.

Rogachevskii, I., Ruchayskiy, O., Boyarsky, A., Fröhlich, J., Kleeorin, N., Brandenburg, A., & Schober, J. 2017 Laminar and turbulent dynamos in chiral magnetohydrodynamics. I. Theory. *Astrophys. J.* **846**, 153.

Rosén, L., Kochukhov, O., Hackman, T., & Lehtinen, J. 2016 Magnetic fields of young solar twins. *Astron. Astrophys.* **593**, A35.

Rüdiger, G. 1978 On the α-effect for slow and fast rotation. *Astron. Nachr.* **299**, 217–222.

Rüdiger, G. 1980 Reynolds stresses and differential rotation I. On recent calculations of zonal fluxes in slowly rotating stars. *Geophys. Astrophys. Fluid Dyn.* **16**, 239–261.

Rüdiger, G. 1989 *Differential rotation and stellar convection: Sun and solar-type stars*. Gordon & Breach, New York.

Rüdiger, G., & Hollerbach, R. 2004 *The magnetic universe*. New York: Wiley-VCH, Weinheim.

Rüdiger, G., & Kitchatinov, L. L. 1993 Alpha-effect and alpha-quenching. *Astron. Astrophys.* **269**, 581–588.

Rüdiger, G., & Kitchatinov, L. L. 2006 Do mean-field dynamos in nonrotating turbulent shear-flows exist?. *Astron. Nachr.* **327**, 298–303.

Rüdiger, G., & Pipin, V. V. 2000 Viscosity-alpha and dynamo-alpha for magnetically driven compressible turbulence in Kepler disks. *Astron. Astrophys.* **362**, 756–761.

Rüdiger, G., & Spahn, F. 1992 On the stability of mean-field models of the solar convection zone. *Solar Phys.* **138**, 1–9.

Rüdiger, G., Kitchatinov, L. L., & Brandenburg, A. 2011 Cross helicity and turbulent magnetic diffusivity in the solar convection zone. *Solar Phys.* **269**, 3–12.

Rüdiger, G., Pipin, V. V., & Belvedère, G. 2001 Alpha-effect, helicity and angular momentum transport for a magnetically driven turbulence in the solar convection zone. *Solar Phys.* **198**, 241–251.

Ruzmaikin, A. A., Sokoloff, D. D. & Shukurov, A. M. 1988 *Magnetic Fields of Galaxies*. Kluwer, Dordrecht.

Salvesen, G., Simon, J. B., Armitage, P. J., & Begelman, M. C. 2016 Accretion disc dynamo activity in local simulations spanning weak-to-strong net vertical magnetic flux regimes. *Month. Not. Roy. Astron. Soc.* **457**, 857–874.

Schmitt, D. & Schüssler, M. 1989 Non-linear dynamos. I. One-dimensional model of a thin layer dynamo. *Astron. Astrophys.* **223**, 343–351.

Schober, J., Rogachevskii, I., Brandenburg, A., Boyarsky, A., Fröhlich, J., Ruchayskiy, O., & Kleeorin, N. 2017 "Laminar and turbulent dynamos in chiral magnetohydrodynamics-II: Simulations," *Astrophys. J.* (submitted, arXiv:1711.09733).

Schou, J., Antia, H. M., Basu, S., Bogart, R. S., Bush, R. I., Chitre, S. M., Christensen-Dalsgaard, J., di Mauro, M. P., Dziembowski, W. A., Eff-Darwich, A., Gough, D. O., Haber, D. A., Hoeksema, J. T., Howe, R., Korzennik, S. G., Kosovichev, A. G., Larsen, R. M., Pijpers, F. P., Scherrer, P. H., Sekii, T., Tarbell, T. D., Title, A. M., Thompson, M. J., & Toomre, J. 1998 Helioseismic Studies of Differential Rotation in the Solar Envelope by the Solar Oscillations Investigation Using the Michelson Doppler Imager. *Astrophys. J.* **505**, 390–417.

Schrijver, C. J. 1983 Coronal activity in F-, G-, and K-type stars. I - Relations between parameters characterizing stellar structure and activity. *Astron. Astrophys.* **127**, 289–296.

Schrijver, C. J., Cote, J, Zwaan, C., Saar, S. H. 1989 Relations between the photospheric magnetic field and the emission from the outer atmospheres of cool stars. I. The solar Ca II K line core emission. *Astrophys. J.* **337**, 964–976.

Schrinner, M., Rädler, K.-H., Schmitt, D., Rheinhardt, M., & Christensen, U. 2005 Mean-field view on rotating magnetoconvection and a geodynamo model. *Astron. Nachr.* **326**, 245–249.

Schrinner, M., Rädler, K.-H., Schmitt, D., Rheinhardt, M., & Christensen, U. R. 2007 Mean-field concept and direct numerical simulations of rotating magnetoconvection and the geodynamo. *Geophys. Astrophys. Fluid Dyn.* **101**, 81–116.

See, V., Jardine, M., Vidotto, A. A., Donati, J.-F., Boro Saikia, S., Bouvier, J., Fares, R., Folsom, C. P., Gregory, S. G., Hussain, G., Jeffers, S. V., Marsden, S. C., Morin, J., Moutou, C., do Nascimento, J. D., Petit, P., & Waite, I. A. 2016 The connection between stellar activity cycles and magnetic field topology. *Month. Not. Roy. Astron. Soc.* **462**, 4442–4450.

She, Z.-S., Jackson, E., & Orszag, S. A. 1990 Intermittent vortex structures in homogeneous isotropic turbulence. *Nature* **344**, 226–228.

Shukurov, A. 1998 Magnetic spiral arms in galaxies. *Month. Not. Roy. Astron. Soc.* **299**, L21–L24.

Simard, C., Charbonneau, P., Dubé, C. 2016 Characterization of the turbulent electromotive force and its magnetically-mediated quenching in a global EULAG-MHD simulation of solar convection. *Astrophys. Spa. Sci.* **58**, 1522–1537.

Singh, N. K., Käpylä, M. J., Brandenburg, A., Käpylä, P. J., Lagg, A., & Virtanen, I. 2018 "Bihelical spectrum of solar magnetic helicity and its evolution," *Astrophys. J.* (submitted, arXiv:1804.04994).

Sokoloff, D. D., & Shukurov, A. M. 1990 Regular magnetic fields in coronae of spiral galaxies. *Nature* **347**, 51–53.

Solanki, S. K., Inhester, B., Schüssler, M. 2006 The solar magnetic field. *Rep. Prog. Phys.* **69**, 563–668.

Snodin, A. P., Brandenburg, A., Mee, A. J., & Shukurov, A. 2006 Simulating field-aligned diffusion of a cosmic ray gas. *Month. Not. Roy. Astron. Soc.* **373**, 643–652.

Squire, J., & Bhattacharjee, A. 2016 The magnetic shear-current effect: generation of large-scale magnetic fields by the small-scale dynamo. *J. Plasma Phys.* **82**, 535820201.

Spruit, H. 1997 Convection in stellar envelopes: a changing paradigm. *Mem. Soc. Astron. Ital.* **68**, 397–413.

Sridhar, S. & Subramanian, K. 2009 Nonperturbative quasilinear approach to the shear dynamo problem. *Phys. Rev. E* **80**, 066315.

Steenbeck, M., & Krause, F. 1969a Zur Dynamotheorie stellarer und planetarer Magnetfelder I. Berechnung sonnenähnlicher Wechselfeldgeneratoren. *Astron. Nachr.* **291**, 49–84.

Steenbeck, M., & Krause, F. 1969b Zur Dynamotheorie stellarer und planetarer Magnetfelder II. Berechnung planetenähnlicher Gleichfeldgeneratoren. *Astron. Nachr.* **291**, 271–286.

Steenbeck, M., Krause, F., & Rädler, K.-H. 1966 Berechnung der mittleren Lorentz-Feldstärke $\overline{\boldsymbol{v}\times\boldsymbol{B}}$ für ein elektrisch leitendes Medium in turbulenter, durch Coriolis-Kräfte beeinflußter Bewegung. *Z. Naturforsch.* **21a**, 369–376. See also the translation in Roberts & Stix, The turbulent dynamo, Tech. Note 60, NCAR, Boulder, Colorado (1971).

Stefani, F., & Gerbeth, G. 2003 Oscillatory mean-field dynamos with a spherically symmetric, isotropic helical turbulence parameter α. *Phys. Rev. E* **67**, 027302.

Stix, M. 1974 Comments on the solar dynamo. *Astron. Astrophys.* **37**, 121–133.

Strassmeier, K. G., Kratzwald, L., & Weber, M. 2003 Doppler imaging of stellar surface structure. XX. The rapidly-rotating single K2-giant HD 31993 = V1192 Orionis. *Astron. Astrophys.* **408**, 1103–1113.

Strugarek, A., Beaudoin, P., Charbonneau, P., Brun, A. S., & do Nascimento, J.-D. 2017 Reconciling solar and stellar magnetic cycles with nonlinear dynamo simulations. *Science* **357**, 185–187.

Subramanian, K. 1999 Unified treatment of small- and large-scale dynamos in helical turbulence. *Phys. Rev. Lett.* **83**, 2957–2960.

Subramanian, K. 2002 Magnetic helicity in galactic dynamos. *Bull. Astr. Soc. India* **30**, 715–721.

Subramanian, K., & Brandenburg, A. 2006 Magnetic helicity density and its flux in weakly inhomogeneous turbulence. *Astrophys. J.* **648**, L71–L74.

Subramanian, K., & Brandenburg, A. 2014 Traces of large-scale dynamo action in the kinematic stage. *Month. Not. Roy. Astron. Soc.* **445**, 2930–2940.

Sur, S., Brandenburg, A., & Subramanian, K. 2008 Kinematic alpha effect in isotropic turbulence simulations. *Month. Not. Roy. Astron. Soc.* **385**, L15–L19.

Syntelis, P., Archontis, V., Gontikakis, C., & Tsinganos, K. 2015 Emergence of non-twisted magnetic fields in the Sun: Jets and atmospheric response. *Astron. Astrophys.* **584**, A10.

Taylor, A. M., Vovk, I., & Neronov, A. 2011 Extragalactic magnetic fields constraints from simultaneous GeV-TeV observations of blazars. *Astron. Astrophys.* **529**, A144.

Thompson, M. J., Christensen-Dalsgaard, J., Miesch, M. S., & Toomre, J. 2003 The internal rotation of the sun. *Ann. Rev. Astron. Astrophys.* **41**, 599–643.

Tilgner, A., & Brandenburg, A. 2008 A growing dynamo from a saturated Roberts flow dynamo. *Month. Not. Roy. Astron. Soc.* **391**, 1477–1481.

Tobias, S. M., Proctor, M. R. E., & Knobloch, E. 1997 The Role of absolute instability in the solar dynamo. *Astron. Astrophys.* **318**, L55–L58.

Tobias, S. M., Proctor, M. R. E., & Knobloch, E. 1998a Convective and absolute instabilities of fluid flows in finite geometry. *Physica D* **113**, 43–72.

Tobias, S. M., Brummell, N. H., Clune, T. L., & Toomre, J. 1998b Pumping of magnetic fields by turbulent penetrative convection. *Astrophys. J. Lett.* **502**, L177–L177.

Tobias, S. M., Brummell, N. H., Clune, T. L., & Toomre, J. 2001 Transport and storage of magnetic field by overshooting turbulent compressible convection. *Astrophys. J.* **549**, 1183–1203.

Tuominen, I., & Rüdiger, G. 1989 Solar differential rotation as a multiparameter turbulence problem. *Astron. Astrophys.* **217**, 217–228.

Tuominen, I., Brandenburg, A., Moss, D., & Rieutord, M. 1994 Does solar differential rotation arise from a large scale instability?. *Astron. Astrophys. Suppl.* **284**, 259–264.

Tziotziou, K., Georgoulis, M. K., & Liu, Y. 2013 Interpreting eruptive behavior in NOAA AR 11158 via the region's magnetic energy and relative-helicity budgets. *Astrophys. J.* **772**, 115.

Vainshtein, S. I., & Cattaneo, F. 1992 Nonlinear restrictions on dynamo action. *Astrophys. J.* **393**, 165–171.

Vainshtein, S. I., & Ruzmaikin, A. A. 1971 Generation of the large-scale Galactic magnetic field. *Astron. Zh.* **48**, 902–909.

van Ballegooijen, A. A. 1984 The effect of reynolds stress in the solar convective zone on the vertical structure of flux tubes, and on their convective instability. In *Small-Scale Dynamical Processes in Quiet Stellar Atmospheres, Proceedings of the Conference held in Sunspot* (ed. Stephen L. Keil), pp. 260–264. Aura.

Vemareddy, P., Ambastha, A., Maurya, R. A., & Chae, J. 2012 On the injection of helicity by the shearing motion of fluxes in relation to flares and coronal mass ejections. *Astrophys. J.* **761**, 86.

Vilhu, O. 1984 The nature of magnetic activity in lower main sequence stars. *Astron. Astrophys.* **133**, 117–126.

Vishniac, E. T., & Brandenburg, A. 1997 An incoherent α-Ω dynamo in accretion disks. *Astrophys. J.* **475**, 263–274.

Vitense, E. 1953 Die Wasserstoffkonvektionszone der Sonne. *Z. Astrophys.* **32**, 135–164.

Viviani, M., Warnecke, J., Käpylä, M. J., Käpylä, P. J., Olspert, N., Cole-Kodikara, E. M., Lehtinen, J. J., & Brandenburg, A. 2017 "Transition from axi- to nonaxisymmetric dynamo modes in spherical convection models of solar-like stars," *Astron. Astrophys.* (in press). 1710.10222

Wang, H., Liu, C., Deng, N., Zeng, Z., Xu, Y., Jing, J., & Cao, W. 2014 Study of two successive three-ribbon solar flares on 2012 July 6. *Astrophys. J. Lett.* **781**, L23.

Warnecke, J. 2017 Dynamo cycles in global convection simulations of solar-like stars, *Astron. Astrophys.* (submitted, arXiv:1712.01248).

Warnecke, J., Brandenburg, A., & Mitra, D. 2011 Dynamo-driven plasmoid ejections above a spherical surface. *Astron. Astrophys.* **534**, A11.

Warnecke, J., Brandenburg, A., & Mitra, D. 2012 Magnetic twist: a source and property of space weather. *J. Spa. Weather Spa. Clim.* **2**, A11.

Warnecke, J., Käpylä, P. J., Käpylä, M. J., & Brandenburg, A. 2014 On the cause of solar-like equatorward migration in global convective dynamo simulations. *Astrophys. J. Lett.* **796**, L12.

Warnecke, J., Losada, I. R., Brandenburg, A., Kleeorin, N., & Rogachevskii, I. 2013 Bipolar magnetic structures driven by stratified turbulence with a coronal envelope. *Astrophys. J. Lett.* **777**, L37.

Warnecke, J., Losada, I. R., Brandenburg, A., Kleeorin, N., & Rogachevskii, I. 2016 Bipolar region formation in stratified two-layer turbulence. *Astron. Astrophys.* **589**, A125.

Warnecke, J., Rheinhardt, M., Käpylä, P. J., Käpylä, M. J., & Brandenburg, A. 2018 Turbulent transport coefficients in spherical wedge dynamo simulations of solar-like stars. *Astron. Astrophys.* **609**, A51.

Weber, M., Strassmeier, K. G., & Washuettl, A. 2005 Indications for anti-solar differential rotation of giant stars. *Astron. Nachr.* **326**, 287–291.

Wilson, O. C. 1978 Chromospheric variations in main-sequence stars. *Astrophys. J.* **266**, 379–396.

Worledge, D., Knobloch, E., Tobias, S., & Proctor, M. 1997 Dynamo Waves in Semi-Infinite and Finite Domains. *RSPSA* **453**, 119–143.

Yokoi, N. 2013 Cross helicity and related dynamo. *Geophys. Astrophys. Fluid Dyn.* **107**, 114–184.

Yokoi, N., Schmitt, D., Pipin, V., & Hamba, F. 2016 A new simple dynamo model for stellar activity cycle. *Astrophys. J.* **824**, 67.

Yoshizawa, A., & Yokoi, N. 1993 Turbulent magnetohydrodynamic dynamo effect for accretion disks using the cross-helicity effect. *Astrophys. J.* **407**, 540–548.

Yoshimura, H. 1975 A model of the solar cycle driven by the dynamo action of the global convection in the solar convection zone. *Astrophys. J. Suppl.* **29**, 467–494.

Yousef, T. A., Heinemann, T., Schekochihin, A. A., Kleeorin, N., Rogachevskii, I., Iskakov, A. B., Cowley, S. C., & McWilliams, J. C. 2008a Generation of magnetic field by combined action of turbulence and shear. *Phys. Rev. Lett.* **100**, 184501.

Yousef, T. A., Heinemann, T., Rincon, F., et al. 2008b o. *Astron. Nachr.* **329**, 737–Y.usef, T. A., Heinemann, T., Rincon, F., Schekochihin, A. A., Kleeorin, N., Rogachevskii, I., Cowley, S. C., & McWilliams, J. C. 2008b Numerical experiments on dynamo action in sheared and rotating turbulence. *Astron. Nachr.* **329**, 737–749.

Zeldovich, Ya. B. 1957 The magnetic field in the two-dimensional motion of a conducting turbulent liquid. *Sov. Phys. JETP* **4**, 460–462.

Zeldovich, Ya. B., Ruzmaikin, A. A., Sokoloff, D. D. 1983 *Magnetic fields in astrophysics*. Gordon & Breach, New York.

Zhao, J., Bogart, R. S., Kosovichev, A. G., Duvall, T. L., Jr., & Hartlep, T. 2013 Detection of equatorward meridional flow and evidence of double-cell meridional circulation inside the Sun. *Astrophys. J.* **774**, L29.

Zhang, H., Brandenburg, A., & Sokoloff, D. D. 2014 Magnetic helicity and energy spectra of a solar active region. *Astrophys. J. Lett.* **784**, L45.

Zhang, H., Brandenburg, A., & Sokoloff, D. D. 2016 Evolution of magnetic helicity and energy spectra of solar active regions. *Astrophys. J.* **819**, 146.

Ziegler, U., & Rüdiger, G. 2000 Angular momentum transport and dynamo-effect in stratified, weakly magnetic disks. *Astron. Astrophys.* **356**, 1141–1148.

Zrake, J. 2014 Inverse cascade of nonhelical magnetic turbulence in a relativistic fluid. *Astrophys. J.* **794**, L26.